# A Liquid-in-Glass Thermometer with Sub-MicroKelvin Resolution, and its Application for Calorimetry

by

Robert David

B.Sc., Applied Mathematics (1998)
McGill University

S.M., Mechanical Engineering (2000)
Massachusetts Institute of Technology

Submitted to the Department of Mechanical Engineering
in Partial Fulfillment of the Requirements for the Degree of
Doctor of Philosophy in Mechanical Engineering

at the

Massachusetts Institute of Technology

September 2006



Signature of Author……
Department of Mechanical Engineering
July 3, 2006

Certified by……
Ian Hunter
Professor of Mechanical Engineering
Thesis Supervisor

Accepted by……...
Lallit Anand
Chairman, Department Committee on Graduate Students

A LIQUID-IN-GLASS THERMOMETER WITH SUB-MICROKELVIN RESOLUTION, AND ITS APPLICATION FOR CALORIMETRY

by

ROBERT DAVID

Submitted to the Department of Mechanical Engineering
on July 3, 2006 in partial fulfillment of the
requirements for the degree of Doctor of Philosophy in
Mechanical Engineering

ABSTRACT

Labeling methods with optical readout are widely used to implement high throughput screens for drug discovery. However, labeling requires assay customization and does not allow examination of the reactants in their native state. The most direct and universal non-labeling method is calorimetry, but current calorimetric techniques are limited in resolution and throughput for pharmaceutical applications. In this thesis, a novel single-reaction microcalorimeter with optical readout, based on liquid expansion, was designed and built.

The instrument was first constructed as a miniature liquid-in-glass thermometer in which the meniscus level was read by a Michelson interferometer. Contact angle hysteresis was limited by a wetting film and the low meniscus velocity. The sub-microKelvin resolution achieved was the lowest known for any thermometer above cryogenic temperatures.

The thermometer was modified for use as a batch analysis microcalorimeter. Special attention was paid to minimize evaporation of the 1 μL reaction drops. Resolution of approximately 10 μJ was achieved for an acid dilution.

Thesis Supervisor: Ian Hunter

Title: Professor of Mechanical Engineering and Professor of Bioengineering

# Acknowledgments

I would like to first thank my advisor, Prof. Ian Hunter, for the opportunity to work in his unique lab. The combination of talented researchers, cutting-edge equipment, and his own vast expertise have impressed and inspired me from the day I arrived.

I also thank the other members of my thesis committee, Prof. John Lienhard and Dr. Leonard Lerman, for their time and wisdom.

There are many people to thank within the lab. Bryan Crane's helpfulness and good humor made him as good a lab roommate as I could have hoped for. Craig Forest's encouragement and upbeat attitude cheered me up when work was difficult. Tim Fofonoff, Andrew Taberner, Hsin-Ni Ho, Cathy Hogan, Mike Garcia-Webb, and John Madden not only helped my research but also made the lab a friendlier place, as did many others over the years, including Patrick Anquetil, Peter Madden, James Tangorra, Mealani Nakamura, and James Celestino.

Whenever an administrative issue came up, Kate Melvin in Prof. Hunter's office and Leslie Regan in the department office were helpful and accommodating.

Steve Buerger's visits to our room in the lab and the good-natured rants that inevitably followed were always a welcome break from work. I also enjoyed getting to know Max Berniker, Justin Verdirame, Ben Paxton, and Matt Spenko outside the lab.

Many of my warmest memories from MIT will involve the friends I made in Ashdown House: Chi Nguyen and Hsiang-Wei Lu, Juan Zheng and Josh Vaughan, An Nguyen, and Sandip Roy. Life is empty without hockey, and hockey would have been empty without Todd Stefanik, Dinh-Yen Tran, Eric Wu, and Alvin Fu (not to mention the Neanderthals). Wai Ling Yee also left me many good memories and made me a better person.

I appreciate the support I've always had from my uncle Michael. Finally, finishing this thesis was the hardest thing I've ever done. I would not have made it without the love and support of all my family, especially my Mom and Dad, my brother Daniel, and my cousin David.

# Table of Contents

# List of Figures

# List of Tables

# Chapter 1.
# Introduction

## 1.1 Drug Development

This thesis describes the design and construction of a miniature liquid-in-glass thermometer, and its use in a microcalorimeter. These results form the first steps in a project to build a sensitive, high throughput microcalorimeter for use in drug discovery.

Over the last several decades, medical drug development has been instrumental in reducing mortality and improving quality-of-life for patients with heart disease, cancer, AIDS, ulcer, osteoporosis, arthritis, influenza, asthma, and many other conditions [1].

Drugs are developed primarily by the pharmaceutical industry [2,3]. The process begins with the identification, based on biochemical research, of a target molecule implicated in a disease (discussed in [4]). The target is usually a protein [5]. The desired drug will bind to the target and produce a therapeutic effect either by triggering a beneficial cell process (agonist drug), or by blocking a different molecule from binding to the target, thereby preventing a harmful cell process (antagonist drug). For example, the breast cancer drug tamoxifen (Nolvadex, AstraZeneca) is an antagonist that binds to estrogen receptors, its target molecules. Tamoxifen prevents estrogen from binding to estrogen receptors and thereby promoting tumor growth.

After a target has been identified, the next step is the search for potential drugs. While rational drug design methods, such as virtual screening, have seen some success, the dominant method remains physical screening [6]. A library of compounds that are considered likely to bind to the target is designed (discussed in [7]). The library is created by combinatorial chemistry and may contain millions of compounds[1],

[1] In this thesis, the compound and target will often be called the ligand and protein, respectively. This is common practice in the literature, even though some drugs are not small molecules and some targets are not proteins.

necessitating a high throughput screening method. The compounds are arrayed in a series of multi-well plates, and target molecules are then added to each well. A variety of techniques are used to determine which of the compounds have successfully bound to the target (see Section 1.2). All of these techniques produce an optical signal, allowing an entire multi-well plate to be imaged at once for high throughput.

The hits recorded by high throughput screening are each subject to further testing to weed out unpromising compounds and generate leads for animal studies. Properties considered include binding affinity, ADME (absorption, distribution, metabolism, and excretion), toxicity, and others. With the high throughput screen possibly generating thousands of hits, the hit-to-lead process is also becoming increasingly high throughput.

Successful animal testing concludes the preclinical process and results in the authorization of an Investigational New Drug by the Food and Drug Administration (FDA), allowing human testing to begin. A drug that passes through the three clinical phases is then approved by the FDA to enter the market.

On average, a pharmaceutical company spends 12 years and $802 million to bring a drug from discovery to market [3]. Each month by which preclinical testing can be shortened saves $1.5 million [8]; the economic repercussions may, in fact, be much higher if the time saved results in the drug being brought to market before competing drugs. Thus, cheaper and more efficient screening methods in the early stages of preclinical research not only benefit public health by bringing medicines to patients sooner, but are very valuable to pharmaceutical companies.

## 1.2 High Throughput Screening

As described above, high throughput screening (HTS) is an important component of pre-clinical drug development. There is continual pressure in the industry to screen larger and larger libraries, and to minimize consumption of expensive reagents. HTS is carried out in standard 96-, 384-, 1536-, or 3456-well plates, with robots loading the reagents and automated data collection. Current throughput capability is on the order of 100,000 samples per day.

Screening assays are classified as homogeneous or heterogeneous. A homogeneous assay is one that does not require additional steps beyond mixing,

incubation, and reading. A heterogeneous assay requires additional steps, such as separation of the products from leftover reactants. Indeed, the lack of a separation step results in higher background levels for homogeneous assays [7]. Despite this, over the last decade, the trend in HTS has been toward homogeneous assays, since they are more easily automated.

HTS is dominated by labeling assays based on radioactivity and fluorescence. Among the most common assays are scintillation proximity assay (SPA), time-resolved fluorescence (TRF), fluorescence polarization (FP), and enzyme-linked immunosorbent assay (ELISA). In SPA, for example, the ligand is radiolabeled and the protein is attached to a scintillant bead. Binding of the ligand to the protein brings the radiolabel and the scintillant into close proximity; the beta particles being released by the radiolabel are then able to excite the scintillant, causing it to emit light seen by the detector.

Recent developments in HTS include nuclear magnetic resonance (NMR) screening [9] and high content screening of cells [10]. As well, quantum dots have been proposed as alternative labels to fluorophores [11,12]; however, despite superior spectroscopic properties, a number of other issues have prevented their use in drug screening [13].

About 100 pmol of ligand is typically used in HTS assays [14]. The plate readers have very high resolution, in the attomole to femtomole range of label, depending on the assay[2].

Labeling methods do, however, carry several drawbacks [15,16]: (*i*) use of radiolabels entails special safety procedures; (*ii*) labeling may interfere with the natural biological activity of the target [17]; (*iii*) extra reagents add cost; (*iv*) assays must be specially designed for each target, a process that consumes 4-12 months [18]. These issues have prompted intense interest in development of non-labeling assays [19].

## 1.3 Non-labeling Methods

A plethora of non-labeling methods exists. Some of these methods still require immobilization of protein to a solid surface, while others do not.

[2] Throughout this thesis, noise sources and detection limits will be specified using three standard deviations. The terms “detection limit” and “resolution” will be used interchangeably.

The most prominent among the methods requiring immobilization is surface plasmon resonance (SPR), reviewed in [20]. An SPR measurement uses a glass slide with a gold film deposited on one face. Protein is immobilized on the gold, and a solution containing the ligand flows over the protein. Light shone through the opposite face of the glass induces a surface plasmon wave that travels through the gold, and an evanescent field that penetrates a short distance into the solution. At a certain incident angle of light, the surface plasmon resonates, resulting in a dip in the intensity of reflected light. Since the angle at which this occurs depends on the solution refractive index, which in turn is affected by the surface coating, SPR can track binding of the ligand to the immobilized protein in real time. In the pharmaceutical industry, SPR is mainly used in a variety of applications for validating hits from high throughput screens [21].

Rapid progress has been made in the last few years on increasing the throughput of SPR instruments. In one approach, SPR was performed using proteins immobilized on colloidal gold nanoparticles [22]. Polarization optics have also been used to convert the SPR signal to an intensity change, allowing an array of 108 sensing spots to be monitored in parallel [23]. Similar methods are reviewed in [24]. Biacore sells one conventional SPR instrument (A100) with 20 sensing spots, and another (Flexchip) that uses grating-coupled SPR to image 400 spots at once (with limited resolution).

SPR surfaces are prepared using a variety of widely applicable techniques for protein immobilization [25]. However, extra assays are required to ensure that immobilization does not affect the protein's natural activity [26-28]. Another limitation of SPR is the proportionality of the signal to the mass of bound ligand, which makes detection more difficult for small ligands. As well, only a low density of protein can be immobilized to the sensing surface, causing the amount of protein (~1 fmol) to limit the extent of the reaction. One modern commercial SPR instrument (Biacore S51) has resolution of about 10 amol [29]; however, a few nanomoles [30] of ligand are typically consumed in each determination in order to ensure that all the protein is bound (i.e., to keep the ligand concentration above the affinity).

Other SPR-like techniques have been described. In one instance, an immobilization surface was etched to form a guided-mode resonant filter, rendering the

wavelength of reflected light sensitive to ligand binding [31]. In another, backscattering interferometry was used to measure changes in refractive index due to binding in PDMS microfluidic channels [32,33].

Two final non-labeling methods requiring protein immobilization will be mentioned. In one, protein is immobilized on a quartz crystal microbalance, and ligand binding is detected as a change in the crystal resonant frequency [16,25,34,35]. In [36], this technique was shown to achieve similar resolution to SPR. In the second, protein is immobilized on silicon nanowires, and ligand binding is detected as a change in the nanowire conductance [37]. The immobilization required in these methods still carries the same drawbacks mentioned above for SPR.

Other non-labeling methods exist that examine the reactants closer to their native state, with no immobilization required. The most widespread of these is mass spectrometry, a method for measuring the mass-to-charge ratio of molecules in the vapor phase. In pharmaceutical research, mass spectrometry is most often used in conjunction with liquid chromatography (together called LC-MS) for verifying the purity of compounds in chemical libraries (review in [38]). The interface between LC and MS is provided by nanoelectrospray ionization or atmospheric pressure chemical ionization.

MS can also be used to detect protein-ligand binding via the resulting change in mass-to-charge ratio of the protein [39]. However, covalent interactions cannot be studied, and due to non-specific binding, vapor-phase interactions may not always be representative of liquid-phase interactions [40].

Increased throughput has been achieved in an LC-MS system developed by Novartis called SpeedScreen [41]. Here, proteins are mixed with 400 ligands at a time and size exclusion chromatography is employed to separate protein-ligand complexes from the remaining mixture. The pooling of ligands introduces limitations, as ligands with identical mass-to-charge ratios cannot be distinguished, and non-specific interactions are possible.

A second labeling- and immobilization-free method is thermal shift assay, or ThermoFluor, originally developed and patented by 3-Dimensional Pharmaceuticals [42] (now part of Johnson & Johnson). In this assay, protein and ligand are mixed and the protein melting temperature is measured. If exothermic binding has occurred, the

protein-ligand complex will be more stable than the protein alone, and will consequently melt at a higher temperature (likewise, a lower temperature for endothermic binding). A high throughput version of this method has been implemented in 384-well plates, by detecting the melting of protein using an environmentally-sensitive dye [43]. Aberrant signals can occur in thermal shift assay due to ligands that fluoresce [44], ligands with affinity for the unfolded protein, and certain ligands that destabilize the protein [45]. As well, affinity is measured at the melting temperature and cannot be accurately extrapolated to physiological temperature without knowledge of the enthalpy of reaction, which is normally measured calorimetrically.

Ultrasonic spectroscopy is another non-labeling, non-immobilization technology that has been used to examine binding reactions. In this method, piezoelectric transducers generate resonant acoustic waves in the reaction cell, and the attenuation and velocity of the waves is measured (review in [46]). These properties are sensitive to changes in hydration and packing of a protein, which may be induced by ligand binding [47]. However, they are also sensitive to nonspecific interactions and aggregation, and correct interpretation of the data remains a subject of research. Ultrasonic spectroscopy has thus often been used in combination with other analytical methods to characterize protein-ligand binding (e.g., [48]). A commercial ultrasonic spectrometer with minimum cell volume of 30 μL and resolution down to 0.3 ng/L is available [49,50]. Parallel measurements have yet to be demonstrated.

The final method for examining binding without the use of labels or immobilization is calorimetry, which we overview now.

## 1.4 Calorimetry

The measurement of heat can be performed by several types of instruments. In the earliest ($18^{th}$ century) calorimeters, heat – at that time identified as caloric – was quantified by weighing the amount of ice it melted into water. While later instruments were more sophisticated, the last half century has seen an especially rapid improvement in resolution, and miniaturization of sample volume, in calorimeters that were mainly built for biochemical applications.

Calorimeters are either scanning or isothermal. In the former, measurements are made while the sample temperature is scanned (usually upwards). Typically, scanning calorimeters are used to measure specific heats or heats of fusion. In the pharmaceutical industry, one widely applied technique is differential scanning calorimetry (DSC). DSC is mainly used for physical characterization of materials [51] and has limited utility in binding studies [52]. Heats of reaction, which form our concern, are normally measured using isothermal calorimeters.

Isothermal calorimeters generally fall into three categories: heat conduction, power compensation, and adiabatic. In a heat conduction calorimeter, heat generated by a chemical reaction flows through a sensor, normally a thermopile, to the surroundings. In a power compensation calorimeter, the sample is kept precisely isothermal by active temperature control, usually employing a Peltier device. In an adiabatic calorimeter, heat is trapped inside the sample and the temperature change is measured, normally by a thermistor.

Some calorimeters also feature a twin, or differential, design, in which the calorimeter contains adjacent sample and reference cells for subtraction of common mode noise. Finally, in a titration calorimeter, one of the reactants is introduced into the other, one aliquot at a time.

Since temperature change is the measured quantity in a calorimeter, an adiabatic design generates the maximum signal. This would seem to obviate the use of thermopile temperature sensors, since the metallic thermopile arms allow heat to escape to the environment. However, thermopiles do not self-heat (as thermistors do), and are best for rejecting common mode noise, since they inherently measure a temperature difference. Thus, calorimeter design involves a trade-off between maximum signal and minimum noise.

The calorimeter built for this thesis used a liquid expansion thermometer, and therefore was designed to be adiabatic (see Section 4.5). More precisely, the calorimeter was isoperibolic, meaning that the environment around the reaction volume was kept at a constant temperature. (In a truly adiabatic calorimeter, the environment temperature must always match the reaction volume temperature.) While a second, reference reaction

volume was not included in the present calorimeter (see Section 5.1), in a future parallelized version control wells will be beneficial (see Section 6.2).

Modern calorimetry may be said to have begun in 1953, with the replacement of traditional mercury thermometers by thermistors [53], allowing automated measurement. In the following two decades, calorimeter resolution was significantly improved and the reaction volume was miniaturized to the milliliter range [54]. Calorimeters of several designs, reviewed in [55], were marketed by companies such as LKB (now Thermometric), Setaram, and Tronac. As designs were refined, thermopiles gradually replaced thermistors as temperature sensors. In 1983, a twin titration calorimeter with 0.2 mL sample volume and 6.1 μJ resolution was reported [56]. Finally, a landmark 1989 paper [57] described an isothermal titration calorimeter that is now commercialized by Microcal. This instrument and similar competitors have since found extensive application in the pharmaceutical industry (reviewed recently in [52]).

Isothermal titration calorimetry (ITC), in the standard design described in [57], is a power compensating, differential method. The instrument's sample cell contains buffer and protein, with only buffer in the reference cell. The ligand is injected simultaneously into each cell in aliquots (continuous injection has recently been introduced by Microcal). Cell volume is typically 1 to 5 mL, with each aliquot about 10 μL. A typical experiment lasts 1 to 2 hours. The power compensation required to keep the sample cell isothermal during the titration, minus the power compensation required for the reference cell, is the output signal. As the titration proceeds, the protein binding sites become occupied and the heat of reaction generated by each aliquot decreases. A reaction model fitted to the measured heats of reaction from each injection allows estimation of both the enthalpy and entropy of reaction by ITC. In the pharmaceutical industry, ITC is most commonly used for measuring binding affinities [51].

While a few newer ITC instruments have been described in the literature [58-60], the state-of-the-art has shifted from academia to industry. Table 1 summarizes the specifications for the top-of-the-line microcalorimeters offered by the three major manufacturers.

Calorimetry in general, and ITC in particular, have been referred to as the "gold standard" in drug discovery applications [25,61], and ITC is often used to confirm results

| Company | Microcal | CSC | Thermometric |
|---|---|---|---|
| WWW site | microcalorimetry.com | calscorp.com | thermometric.com |
| Model | VP-ITC | N-ITC III | 3201 |
| Sample Volume (mL) | 1.4 | 1 | 4 |
| Electrical Resolution (μJ) | -- | 0.1 | 1 |
| Chemical Resolution (μJ) | 1.9 | 3 | -- |

**Table 1.** Commercial ITC instruments. The specifications represent information available either on the web sites, or from sales staff. Data from different companies may not be equivalent. Electrical resolution is the limit of detection for Joule heating (and thus does not include mixing noise), and chemical resolution is the reproducibility of a standard reaction.

obtained using other techniques [44,45,52,62]. Calorimetry has unique advantages as an analytical method; it is universally applicable with no requirement for reaction-specific assay design, and, more than any other method, it provides direct thermodynamic information on the interaction of the ligand and target in their native state. However, high sample consumption (typically 0.5 mg of protein for ITC [63]) and low throughput have precluded its use in the earlier stages of drug development. In particular, this has prevented the realization of label-free high throughput screening via calorimetry [64].

Towards this and other ends, miniature calorimetric devices, with microliter-level sample volumes, have also been developed over the past few decades. The most successful design in the 1970's and 1980's was the enzyme thermistor, reviewed in [65]. In this device, which measured heat from enzyme-catalyzed reactions, the enzyme was immobilized on beads of controlled-pore glass. The beads were packed into a column, through which the reaction volume flowed. Matched thermistors measured the temperature difference between the inlet and outlet of the column. In one device, resolution of 9 μJ was achieved with a 1 μL reaction volume [66].

As in ITC, thermopiles have largely replaced thermistors in miniature calorimeters. Most recent devices are variations of a design called a chip calorimeter (reviewed in [67]). In a chip calorimeter, the chemical reaction takes place on top of a thin membrane suspended from a surrounding thick rim. A thermopile's hot junctions are deposited on the membrane, with the cold junctions on the rim, which acts as a heat sink. In some cases, an enzyme layer is immobilized to the membrane, under the reaction volume, in order to localize heat production. In flow injection analysis (FIA), the reaction volume flows continuously through the device, whereas in batch analysis (BA),

| Reference | Enzyme Immobilization | Format | Volume (μL) | Power Resolution (μW) | Energy Resolution (μJ) |
|---|---|---|---|---|---|
| [68] | yes | FIA | 50-100 | 0.2[a] | 4600 |
| [69] | yes | FIA | 1 | -- | 270 |
| [70] | no | FIA | 4 | -- | 240 |
| [71] | no | BA | 7 | 1 | 100 |
| [72] | no | PM | 0.00072 | 0.013[a] | -- |
| [73] | no | FIA | 20 | 0.3 | -- |
| [74] | no<br>yes | FIA<br>BA | 17<br>1 | 0.1<br>-- | 6000<br>400 |
| [64][b] | no | BA | 0.5 | -- | 0.5 |
| [75] | no | BA | 0.2 | 0.0015[a] | -- |
| [76] | no | FIA | 20 | 0.1 | 4 |

**Table 2.** Specifications for selected chip calorimeters in the literature, listed in chronological order. PM = physiometer. Volume = sample consumption (both reactants), which is often greater than the volume of the reaction chamber for FIA devices. [a] Electrical resolution. [b] Thermistor-based device.

single drops of the reactants are used. In both cases, reactions are typically complete in a few seconds. In contrast, in a physiometer, cells are placed on the membrane and chemically stimulated, and the change in their metabolism is measured over tens of minutes. Table 2 lists specifications for notable chip calorimeters in the literature.

Some progress has been made at building higher throughput calorimeters, in the realms of both ITC and chip calorimetry. In ITC, Microcal has introduced the AutoITC, with an autosampler that allows samples to be run unattended, sequentially. As well, a 4-channel nanocalorimeter is offered by Thermometric; similar instruments are discussed in [77]. Research towards parallelizing chip calorimeters has accelerated since this thesis was begun. Batch analysis is needed, since the FIA format used by many of the devices in Table 2 is not practical in an array [78]. Two research groups have envisioned [75,78], and a third has built [64], arrays of chip calorimeters, but so far measurements have been reported for only one device operated at a time. A commercial chip calorimeter array with robotic liquid handling is currently being developed by Vivactis [79]. The projected specifications are 10 to 20 μL sample volume, and resolutions of 50 nW and 3 μJ.

## 1.5 Overview

As seen in the foregoing, a high-throughput, sensitive microcalorimeter would have unique advantages for use in HTS, and would expand the range of applications for calorimetry to other medium-throughput assays in early drug development. It should be noted that important applications for high throughput calorimetry also exist in other industries, including enzyme discovery, identification of agrochemicals, and detection of bacteria in food and water [80].

Three desired specifications for the microcalorimeter to be built in this thesis were considered at the outset: its sample volume, the duration of monitored reactions, and its energy resolution.

The appropriate sample volume was one that would be compatible with robotic liquid handlers (i.e., 1 to 400 μL). A sample volume on the order of a few microliters would be suitable for use in either 384- or 1536-well plates. A 10 μL volume was originally planned, and this volume was used in the earlier iterations of the instrument (the thermometer). However, by the time of the final version of the calorimeter, a sample volume of 2 μL had proven more convenient. Either volume is typical of recent research in the area, as seen in Table 2. For the purposes of calculations below and in Chapter 2, a nominal sample volume of 5 μL will be assumed.

For reactions of interest to the pharmaceutical industry, the length of time over which the energy is released was expected to vary from 1 to 1800 s, depending on the class of reaction under study [14]. From a measurement perspective, the effective lower limit for the reaction duration was determined by the time constant for heat transfer from the reaction volume to the sensor. For a 5 μL volume, this time is on the order of 5 s.

With regard to the upper limit, measuring the same quantity of heat released over minutes rather than seconds is much more difficult due to drift arising from ambient temperature fluctuation. This increases the energy resolution of a calorimeter for slow reactions. In most cases in the literature, rapid reactions are used to characterize a calorimeter's energy resolution. The same was done in this thesis.

The original goal of the project for energy resolution was 0.1 μJ. Based on the heat capacity of the original planned volume of 10 μL, a temperature change of 2.4 μK

was expected. Thus, the first stage of the research was the selection of a temperature measurement method that was capable of microKelvin resolution and amenable to parallelization. Chapter 2 will present theoretical analysis of the methods that were considered.

The selected method was liquid expansion thermometry, which will be examined in depth in Chapter 3.

The instrument was built in two versions. The first version was a thermometer for verifying the required temperature resolution via Joule heating. In the second version, the capability of reactant mixing was added to the thermometer, forming a calorimeter. Chapter 4 will contain descriptions of the two versions of the instrument.

Chapter 5 will present the data collected from the instrument, consisting mainly of the temperature resolution of the thermometer and the energy resolution of the calorimeter.

Lastly, Chapter 6 will consist of the conclusions drawn from the research and suggestions for future work, including a preliminary design for a high throughput version of the calorimeter.

# Chapter 2.

# Temperature Measurement

## 2.1 Introduction

A number of techniques were considered for addressing the temperature measurement problem that was described in Section 1.5. In this chapter, approaches based on devices in the literature and other common temperature measurement methods will be evaluated. Both the temperature resolution and the scalability of each approach were important. Based on the discussion of reaction duration in Section 1.5, we will assume a measurement bandwidth of 0.05 to 1 Hz. While all methods can be used to measure heat either released or absorbed by a reaction, for simplicity of language, the reaction will be assumed to be exothermic throughout the thesis.

The sensing method that was chosen was liquid expansion. It was implemented as a miniature liquid-in-glass thermometer, with the meniscus level monitored by a Michelson interferometer. The liquid expansion approach in general will be discussed separately in Chapter 3, and the instrument itself in Chapters 4 to 5.

## 2.2 Thermopiles

A thermocouple relies on the coupling of thermal and electrical energy in certain metals (or semiconductors). Consider two arms of different conductors joined at junctions A and B, at respective temperatures $T_A$ and $T_B$, with, say, $T_A > T_B$ (see Figure 1). If the degree of coupling between thermal and electrical energy in each conductor is different, the isothermal condition at each junction results in a net flow of electrons across the junction. Additionally, within each arm, electrons diffuse from the hot

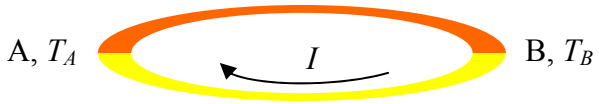


**Figure 1.** Thermoelectric effect with current $I$.

junction A to the cold junction B. These two phenomena are called the reverse Peltier effect and the Thomson effect, respectively (confusingly, just the first, or both together, are sometimes called the Seebeck effect). Together, for a small temperature difference, they result in a voltage

$$V_0 \approx (S_1 - S_2)(T_A - T_B),$$

where $S_1$ and $S_2$ are the Seebeck coefficients of the two conductors (derivation in [81]).

A thermopile is $n$ thermocouples connected in series, as shown in Figure 2. The voltage between each successive pair of junctions is still $V_0$, and thus the voltage between the first and last junctions is $nV_0$, making the thermopile $n$ times more sensitive than a single thermocouple.

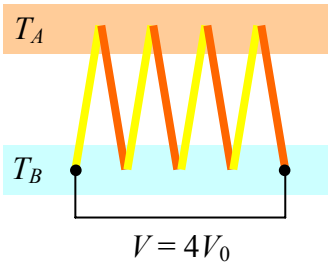


**Figure 2.** A 4-couple thermopile.

The dominant noise source in a thermopile is Johnson noise [82]. Thus, using our convention of three standard deviations, the minimum detectable temperature change for a thermopile is

$$\Delta T_{min} = \frac{3\sqrt{4k_B TRB}}{n \cdot (S_1 - S_2)}, \tag{1}$$

where $k_B$ is Boltzmann's constant ($1.38 \times 10^{-23}$ J/K), $T$ is the operating temperature (295 K), $R$ is the thermopile's electrical resistance, and $B$ is the measurement bandwidth (0.95 Hz).[3]

[3] All frequencies in this thesis will be expressed in Hertz.

The chip calorimeter, discussed in Section 1.4, is currently the dominant design for thermopile-based microcalorimetry of small volumes. The leading devices are manufactured by Xensor Integration [83]: for the LCM-2506, in Equation 1, $R$ = 150 kΩ and $S$ = 65 mV/K, giving $\Delta T_{min}$ = 2.2 μK; and for the NCM-9924, $R$ = 50 kΩ and $S$ = 50 mV/K, giving $\Delta T_{min}$ = 1.7 μK.

An example of an array of thermopile temperature sensors is reported in [84]. In such a device, the individual thermopiles are addressed sequentially, increasing the bandwidth by a factor of $N$, for $N$ wells. (Mixing each well sequentially would be time-consuming; individual measurements in this thesis using 1 μL volumes lasted about 100 s.) Using the best figure for the Xensor devices, this would result in an array resolution of at least 34 μK for $N$ = 384.

Material selection for the thermopile in a chip calorimeter is limited by compatibility with micromachining, and the requirement of a large difference in Seebeck coefficients. Thus, in order to improve the temperature resolution in Equation 1, we consider altering the thermopile dimensions so as to minimize $R$. Let $l$ be the length of the thermopile arms, $w$ their width, $h$ their height, and $\rho_1$ and $\rho_2$ the resistivities of the two materials. Then

$$\Delta T_{min} = \frac{6\sqrt{k_B T B(\rho_1 + \rho_2)}}{S_1 - S_2} \cdot \sqrt{\frac{l}{nwh}}.$$

If the diameter of the reaction volume is $d$, then for a radial thermopile $\pi d \approx 2nw$. Also, in [85], it was shown that the optimal value for $l$ is $d/4$. The resolution thus scales as $h^{-1/2}$. The value of $h$ is constrained by the fact that it represents a portion of the total membrane thickness, which must be thin enough to provide thermal isolation between the drop and the rim. A typical membrane thermal resistance is 200 K/W [67], which, for a 5 μL reaction volume, would result in a 4.2 s time constant. Since the thermal resistance scales as $h^{-1}$, thickening the thermopile arms to improve $\Delta T_{min}$ would result in unacceptable heat loss.

## 2.3 Resistance Temperature Detectors

Resistance temperature detectors (RTD's) exploit the dependence of resistivity on temperature in certain materials. They are predominantly made from either platinum or metal oxide semiconductors. Semiconductor RTD's are called thermistors.

Among the metals, platinum is most commonly used in RTD's due to its availability in high purity and its inertness. Platinum RTD's are used to define a large section of the International Temperature Scale. However, the sensitivity $S$ of platinum resistivity to temperature, at 0.00385 $K^{-1}$, is much lower than that of thermistors. For this reason, thermistors are preferred for microcalorimetry. Applications of thermistors in calorimetry were discussed in Section 1.4.

Thermistors exist in two varieties: negative temperature coefficient (NTC) and positive temperature coefficient (PTC). While in each case the resistance depends nonlinearly on temperature, for small temperature changes near ambient the sensitivity $S$ is approximately linear. For NTC and some PTC thermistors, typically $|S| \approx 0.05$ $K^{-1}$. Switching PTC thermistors are most sensitive in only a narrow range about their Curie temperature; for a Curie temperature of 120 °C, $S$ can reach 1 $K^{-1}$. However, for a Curie temperature near ambient, $S \approx 0.2$ $K^{-1}$ [86,87]. Therefore, we consider a switching PTC thermistor with $S = 0.2$ $K^{-1}$ as a potential microcalorimeter temperature sensor.

The fundamental noise source in any RTD is Johnson noise in the voltage:

$$\Delta V = 3\sqrt{4k_B TRB}\,,$$

where $k_B$ is Boltzmann's constant, $T$ is the operating temperature, $R$ is the electrical resistance of the sensor, and $B$ is the bandwidth.

A second noise source arises from thermistor self-heating. If unsteady fluid flow occurs within the reaction volume, as is required to mix reactants in a batch analysis format, convection of heat from the thermistor to the fluid will fluctuate. This places a limit on the power that can be dissipated by the thermistor [88,89].

Accounting for both these noise sources, Bowers and Carr [88] derived the following expression for a thermistor's temperature resolution when placed in an equal arm Wheatstone bridge[4]:

$$\Delta T_{min} = 16.4 \left( \frac{k_B TRB}{S^2} \right)^{1/3} C^{1/6} \ , \tag{2}$$

where $C$ is an empirical constant accounting for the convective noise. Bowers and Carr measured the lowest noise level, corresponding to $C = 5.7 \times 10^{-15}$ $K^2/V^4$, for a 100 kΩ thermistor. In a subsequent paper [91], they showed that the resolution in Equation 2 could be improved by a factor of at most 1.59 by measuring with unequal bridge arms.

Thus, for a single 100 kΩ PTC thermistor at 0.95 Hz bandwidth, $\Delta T_{min} = 0.93$ μK. However, in a parallel measurement of 384 thermistors, the bandwidth is increased to approximately 384 Hz, and $\Delta T_{min} = 6.9$ μK.

This calculated resolution is further limited by manufacturing considerations. Micromachined arrays of thermistors are common in bolometers, usually employing vanadium oxide or amorphous silicon thermistors with $S = 0.02$ to $0.05$ $K^{-1}$ [92], much lower than the value assumed above. An array of amorphous silicon thermistors has also been constructed for a microcalorimeter, with temperature resolution of 0.25 mK limited by 1/f noise in the thermistors [64].

## 2.4 Quartz Resonators

Piezoelectric quartz oscillators are widely used as timing references in electronic devices such as watches and computers. For these applications, the temperature dependence of the resonant frequency of the quartz plate is an undesirable source of drift. On the other hand, by maximizing the temperature dependence via judicious choice of the quartz cut, a highly sensitive temperature transducer can be created (reviewed in [93]). For certain cuts of the quartz crystal, the temperature sensitivity $S$ of the resonant frequency can reach $10^{-4}$ $K^{-1}$.

[4] The authors' analysis contains a number of mathematical errors. In Equation 10 of [88], $A^{2/3}/2$ should be $(A/2)^{2/3}$. The multiplying factor in Equation 11 should be 1.37, rather than 2.2. In the calculation of $E_B^{opt.}$ in Table 5, the factor of 2 in Equation 9 appears to have been neglected. In [90], the first of these errors is corrected, but the other two are reproduced. In [91], the second error is reproduced. Also in [91], in Equation 16, the square root should be a sixth root.

In the 1960's, using a quartz thermometer in a temperature-controlled oven, Smith and Spencer [94] measured noise of 3.8 μK over a 10 s period. Later, a quartz crystal laboratory thermometer was commercialized by Hewlett Packard (2804A) with resolution of 0.1 mK for a 10 s integration time.

Quartz resonators with a catalyst coating have been operated in air for gas calorimetry [95]; and in liquid, their application in quartz crystal microbalances (QCM's) was mentioned in Section 1.3. However, for high resolution thermometry, resonators must be sealed in evacuated packages, to minimize viscous losses to the surrounding medium.

Due to limitations in fabrication technology [96], precision quartz resonators typically have diameters of at least 5 mm [97]. This is too large for our application, since the heat capacity of the resonator and its package would dwarf that of the reaction volume.

Somewhat smaller quartz resonators can be made by photolithography and chemical etching. Thermometers in the shape of plates [98,99] and tuning forks [100] have been manufactured, but with an average dimension that is still typically 3 mm or larger. As well, the fabrication process severely degrades the quality factor $Q$ of the resonator, compromising its temperature resolution. A 1 × 5 × 10 mm sensor has been reported with 34 μK resolution [98].

Very small resonators, with diameters of 0.05 to 1 mm, have been defined by depositing electrodes of those diameters onto larger quartz plates (for a QCM application) [101]. However, the thermally conductive quartz separating the resonators would make them unsuitable as independent thermometers.

The fundamental limits on the resolution of quartz microresonators have been considered for an infrared sensor application [102]. In our application, the corresponding temperature resolution is

$$T_{min} = 3 \cdot \left[ \frac{\left(1.2 \times 10^{-19} f_0\right)^2}{2 \cdot \ln 2 \cdot S^2} \ln\left(\frac{f_2}{f_1}\right) + \frac{k_B T}{Q^2 P S^2} \cdot (f_2 - f_1) + \frac{k_B T^2}{C} \right]^{\frac{1}{2}},$$

where $f_0$ is the resonant frequency, $f_1$ and $f_2$ are the bandwidth limits, $k_B$ is Boltzmann's constant, $T$ is the operating temperature, $P$ is the power dissipated, and $C$ is the

resonator's heat capacity [102]. The three terms represent flicker noise, Johnson noise, and phonon noise, respectively (for simplicity, the phonon noise is written for an infinite bandwidth). For typical parameter values, the calculated resolution of a 1 mm diameter resonator is about 1 μK. As well, since the Johnson noise is small compared to the other terms, the resolution is not strongly bandwidth-dependent. Thus, at least in theory, if not for limitations in manufacturing technology, miniature quartz resonators could be useful in our application.

## 2.5 Gas Expansion

Gas thermometers rely on a change in volume and/or pressure of a gas to measure temperature change. The volumetric thermal expansion coefficient of an ideal gas at temperature $T$ is $1/T$; at room temperature, it is about 15 times larger than that of water. We might therefore imagine a calorimeter that measures the expansion of a volume of gas in thermal equilibrium with the liquid sample.

The most closely related devices found in the literature were Golay cell infrared radiation sensors. A Golay cell is a small, gas-filled chamber that contains a film of infrared-absorbing material. When infrared radiation is absorbed by the film, it heats the gas, which expands against a membrane in one of the chamber walls. The Golay cell may also be considered a radiation thermometer (see Section 2.9). A calorimeter based on the Golay cell design is illustrated in Figure 3.

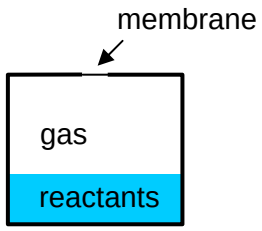


**Figure 3.** Design for a gas calorimeter.

Kenny et al. [103] built a Golay cell in which the membrane was a 0.7 μm thick silicon nitride film. The outer surface of the membrane was gold-coated to serve as an

electrode for a tunneling displacement sensor. The calculated sensitivity[5], defined as the displacement of the membrane's center point per unit change in the gas temperature, was $S = 15.5$ μm/K.

Two other groups have built Golay cells with capacitive displacement transducers. Chévrier et al. [104] calculated[5] $S = 0.3$ μm/K, but measured only 14 nm/K, with 5 mK resolution. They proposed using a more compliant membrane to improve results. Yamashita et al. [105] measured displacement noise of 20 nm, which, according to their calculations[6], corresponded to 3.5 mK resolution ($S = 5.7$ μm/K).

As seen in Chapters 4 to 5, the liquid expansion method adopted in this thesis achieved a much higher sensitivity ($S \sim 100$ to 500 μm/K) than these Golay cells. This was accomplished by forcing the liquid expansion through a narrow space of about 0.1 mm diameter, whereas the membrane diameter for all three Golay cells was on the order of 1 mm. Narrowing the membrane in a gas calorimeter would not necessarily amplify expansion though, because the membrane stiffness would increase. We will calculate the optimal membrane diameter to find the maximum sensitivity for a gas calorimeter like the one in Figure 3.

For an ideal gas, small changes in temperature ($\Delta T$), volume ($\Delta V$), and pressure ($\Delta P$) are related to their equilibrium values as follows [105]:

$$\frac{\Delta T}{T} = \frac{\Delta V}{V} + \frac{\Delta P}{P}. \tag{3}$$

To preserve the natural behavior of reagents, the experiment must be carried out at room temperature and pressure. The liquid expansion is small compared to the gas expansion, and can be neglected.

For an unstressed circular membrane clamped at the edges, the deflection under uniform pressure is

$$z(r) = \frac{\Delta P}{64D}\left(\left(\frac{d}{2}\right)^2 - r^2\right)^2, \tag{4}$$

[5] These authors calculated sensitivity using the average membrane displacement, resulting in values three times smaller than those given here. As well, in the case of Kenny et al., their calculation of $S = 1.3$ μm/K from Equations 14-15 in [103] was arrived at using an inaccurate membrane area.

[6] Equation 1 in [105] contains an error – 1/16 should be 8/9 – but Figure 3 is correct.

where $r$ is the radial coordinate, and $d$ is the membrane diameter [106]. $D$ is the membrane's bending stiffness, defined as

$$D = \frac{E t^3}{12(1-\nu^2)},$$

where $E$ is Young's modulus, $\nu$ is Poisson's ratio, and $t$ is the membrane thickness. Integrating Equation 4 gives the volume created by the membrane displacement:

$$\Delta V = \frac{\pi \Delta P}{12288 D} d^6 .$$

Substituting into Equation 3, and rearranging, now gives the sensitivity

$$S = \frac{z(0)}{\Delta T} = \frac{12 P V d^4}{\pi P T d^6 + 12288 D V T}. \tag{5}$$

Equation 5 is equivalent to Equation 1 in [104]. Differentiating with respect to $d$, the optimal membrane diameter is

$$d_{opt} = \sqrt[6]{\frac{24576 D V}{\pi P}} .$$

At ambient temperature and pressure, and $d = d_{opt}$, Equation 5 becomes $S = 0.020\ V^{2/3}\ D^{-1/3}$. For a gas volume of $V = 10$ μL, and $D = 5.4 \times 10^{-9}$ N·m [103], the sensitivity is 53 μm/K, still lower than the liquid expansion method. As well, Kenny et al. [103] found that, due to residual stress and other effects, the experimental stiffness of their membrane was 7 times higher than the calculated value, further lowering $S$. While increasing $V$ could gradually improve the sensitivity, it would also increase the heat capacity of the container holding the gas, thus lowering the temperature change being measured.

Despite the lower sensitivity, a potential advantage of a gas calorimeter over one based on liquid expansion was the possibility of using a capacitive or tunneling displacement sensor in place of an interferometer. A capacitive sensor, however, would have measured only an average membrane displacement, and has theoretically worse resolution than a Michelson interferometer [107].

A tunneling sensor was more promising, but suffers from a practical limitation. Kenny found that overly compliant membranes became stuck to the tunneling electrode due to attractive van der Waals forces [108]. His observation can be roughly translated

into a condition on the bending stiffness: $D \geq 0.04\, d^2$. Repeating the above calculations using the minimum value for $D$ results in $S = 0.17\, V^{1/2}$. Now, for $V$ = 10 μL, the sensitivity is only 17 μm/K, about an order of magnitude lower than the sensitivity using the liquid expansion method. The theoretical resolution of a tunneling sensor has been estimated to be 10 times better than a Michelson interferometer [107]. Thus, temperature resolution is expected to be similar using either method; however, the liquid expansion design was simpler, and preferable in case environmental noise proved dominant.

As a final note for comparison, the actual resolution of Kenny et al.'s tunneling transducer in the relevant (0.05 to 1 Hz) bandwidth may be calculated as 29 pm from their frequency response data [103]. This would produce temperature resolution of 1.7 μK, somewhat larger than was actually resolved in this thesis using liquid expansion (see Figure 30 in Chapter 5). A scanning tunneling microscope has also been built by a former student in the MIT Bioinstrumentation Lab, Peter Madden [109]. Its measured vertical resolution of 0.12 nm, comparable to the value for the Michelson interferometer in this work, was believed to be limited by building vibrations.

## 2.6 Speed of Sound

The speed of sound in water varies with temperature, having a value of 1488 m/s at room temperature. A polynomial has been fit to the most accurate data in water for temperatures of 273 to 368 K [110]; at 295 K, the sensitivity of the speed of sound to temperature is 2.91 m/s·K. A temperature change of a few microKelvins would therefore produce a change in the speed of sound on the order of 10 μm/s. This change is 10 to 100 times below the resolution of the most sensitive measurements reported in the literature [111,112], as well as the 0.2 mm/s resolution specified for the leading commercial ultrasonic spectrometers.[7] In fact, the compressibility change accompanying a reaction would affect the speed of sound much more strongly than the enthalpy change. Non-labeling detection based on this principle (i.e., ultrasonic spectroscopy) was discussed in Section 1.3.

[7] www.ultrasonic-scientific.com.

## 2.7 Refractive Index

Fiber optic temperature sensors are used mainly in applications requiring a rugged or remote sensor; for our application, they have poor resolution. Measurement is based on the optical fiber's thermal expansion, or the temperature sensitivity of its refractive index. A fiber optic coated with platinum catalyst, in an interferometric arrangement, has been used as a gas sensor with resolution of 0.1 mK [113]. In a similar experiment conducted in a liquid flow cell, antibody-antigen reaction was detected with resolution of 2.4 mK [114]. A fiber Bragg grating is a variation of refractive index written into the core of an optical fiber, which produces maximum reflectivity at the Bragg wavelength. Tsao et al. [115] measured the shifting of the Bragg wavelength to sense air temperature with resolution of 15 mK.

The refractive index of water itself can also be used to measure temperature. As described by the Lorentz-Lorenz law, it depends on temperature through the density [116], with a sensitivity of approximately $-9 \times 10^{-5}$ $K^{-1}$ near room temperature [117]. Interferometric methods have been used to measure liquid refractive index changes of $1.5 \times 10^{-8}$ in a 200 μL volume [118], and $7 \times 10^{-8}$ in a 40 nL volume [119]. The first of these would correspond to a temperature resolution of 0.17 mK in water.

We consider a design in which a Fabry-Pérot interferometer measures the change in refractive index due to a temperature change. (We assume no change in the refractive index due to the reaction itself; in the methods based on refractive index change that were discussed in Section 1.3, the reactants are greatly concentrated by immobilization to a surface.) Let $n$ be the refractive index, and $z$ the distance traveled by the light through the reaction volume. Then, the equivalent change in $z$ due to a temperature increase $\Delta T$ in the reaction volume is

$$\Delta z \approx \frac{z}{n} \cdot \frac{dn}{dT} \cdot \Delta T \cdot \tag{6}$$

As described in Chapters 4 to 5, the liquid expansion sensing method enabled a sensitivity of about 100 to 500 μm/K. According to Equation 6, achieving a similar sensitivity would require $z$ to be a few meters, an impractical value in a reaction volume of just a few microliters.

## 2.8 Bimetallic Cantilevers

A bimetallic cantilever temperature sensor is comprised of two metal layers with differing thermal expansion coefficients. It bends in response to a temperature change in order to accommodate the unequal strains in the two layers. Bimetallic cantilevers are commonly used in thermostats, being cheap and rugged, but have very poor (~1 K) resolution.

Bimetallic microcantilevers with greatly enhanced sensitivity were created by Gimzewski et al. [120], by coating silicon atomic force microscope tips with aluminum. They used the cantilevers, with an additional catalytic coating of platinum, to monitor heat released by the reaction of $H_2$ and $O_2$ gases. The deflection of the cantilever was measured with an optical lever – a laser beam reflecting from the cantilever tip to a position-sensitive photodiode.

The same group has also applied the microcantilevers to photothermal spectroscopy [121] and scanning calorimetry of solid samples [122]. In a liquid environment, they have coated microcantilevers with DNA segments or proteins to act as biosensors [123]. In the latter type of devices, the principal cause of cantilever bending is actually stress due to the binding of molecules, rather than heat of reaction [124].

In keeping with the goal of this thesis (see Chapter 1), we consider a microcantilever-based calorimeter design in which both reactants remain in solution and not immobilized to the cantilever surface. The cantilever is immersed in the reaction volume, and, due to its small size, experiences the same temperature change as the liquid when a reaction occurs.

The sensitivity of the cantilever, i.e., the deflection of the tip per unit temperature change, is given by [121]

$$S = 3(\alpha_1 - \alpha_2)\frac{t_1 + t_2}{{t_2}^2 K} L^2, \tag{7}$$

where $L$ is the cantilever length, $\alpha_1$ and $\alpha_2$ are the linear thermal expansion coefficients of the two layers, $t_1$ and $t_2$ are their thicknesses, and

$$K = 4 + 6n + 4n^2 + \frac{E_1}{E_2} n^3 + \frac{E_2}{E_1}\frac{1}{n},$$

with $E_1$ and $E_2$ the Young's moduli, and $n = t_1 / t_2$. For the typical parameter values listed in Table 3, the sensitivity is only 0.14 μm/K, about three orders of magnitude less than the sensitivity of the liquid expansion method (see Chapters 4 to 5). As well, the displacement resolution of the optical lever offers no theoretical advantage in resolution over the Michelson interferometer that was used with the liquid expansion method [107]. In fact, in practice, similar resolution of 0.1 to 0.2 nm has been achieved with both types of displacement sensor ([123,125] and Figure 30 in Chapter 5).

| | | | | |
|---|---|---|---|---|
| $L$ = 200 μm | $t_1$ = 0.05 μm | $\alpha_1 = 23.9 \times 10^{-6}$ K$^{-1}$ | $E_1$ = 80 GPa | $\rho_1$ = 2700 kg/m$^3$ |
| $w$ = 40 μm | $t_2$ = 0.6 μm | $\alpha_2 = 3 \times 10^{-6}$ K$^{-1}$ | $E_2$ = 180 GPa | $\rho_2$ = 3400 kg/m$^3$ |

**Table 3.** Parameter values for Al-$Si_3N_4$ microcantilevers from [121].

We might still hope to improve the sensitivity of the cantilever, as expressed in Equation 7. Since material selection is constrained by the micromachining manufacturing method, we will seek to optimize the cantilever dimensions ($L$, $n$, $t_2$, and the width $w$). To begin, it was pointed out in [126] that several researchers had used a sub-optimal value for $n$. Figure 4 shows that, in our case, the sensitivity can be improved to 0.53 μm/K for $n = 0.71$.

The remaining possibilities for increasing $S$ are to increase $L$ or decrease $t_2$. However, we must also consider the thermal vibration of the cantilever, which is the dominant fundamental noise source [126]:

$$\Delta z = 3 \cdot \sqrt{\frac{4k_B TBL^5}{Qw}\left[\frac{31 \cdot (\rho_1 t_1 + \rho_2 t_2)}{(E_1 t_1^{\,3} + E_2 t_2^{\,3})^3}\right]^{1/4}},$$

where $k_B$ is Boltzmann's constant, $T$ is the temperature, $B$ is the bandwidth, $Q$ is the cantilever quality factor, and $\rho_1$ and $\rho_2$ are the densities of the two layers. Dividing the noise $\Delta z$ by the sensitivity $S$ gives the temperature resolution $T_{min}$, which can be simplified to

$$T_{min} = \frac{1}{\alpha_1 - \alpha_2}\sqrt{\frac{4k_B TBL}{Qw}}\frac{K}{n+1}\left[\frac{31 \cdot (\rho_1 n + \rho_2)}{(E_1 n^3 + E_2)^3}\right]^{1/4}\frac{1}{t_2}.$$

For a 0.05 to 1 Hz bandwidth, and $Q = 3$ in water [124], $T_{min}$ = 6.6 μK. Moreover, it is clear that increasing $L$ or decreasing $t_2$ would in fact be detrimental to $T_{min}$. Thus,

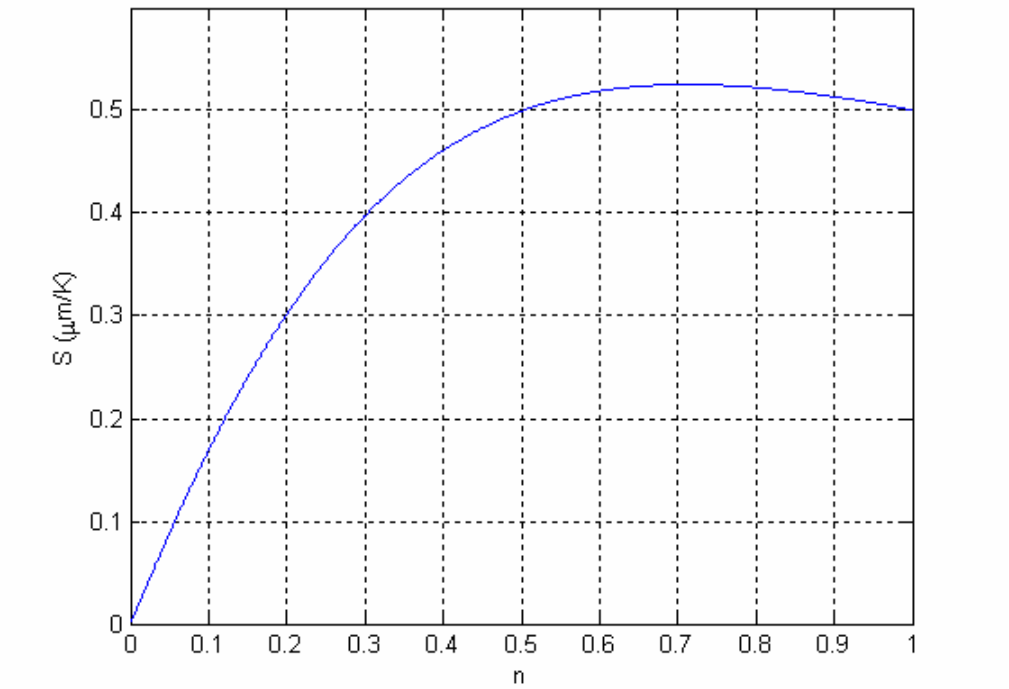


**Figure 4.** Optimization of the layer thickness ratio in a bimetallic microcantilever.

increasing the cantilever's sensitivity in order to make it less susceptible to environmental noise would result in insufficient temperature resolution.

Finally, two additional ideas for increasing the cantilever displacement were considered. A pair of adjacent cantilevers, bending in opposite directions, could double the signal as measured by an interferometer. However, this would still leave the sensitivity low. Alternatively, the cantilever could be attached to a second, twisted strip with an indicator [127] to amplify its displacement (Figure 5). This option was deemed too complex.

## 2.9 Radiation Thermometers

Radiation thermometers, reviewed in [128], determine the temperature of an object by measuring the radiation it emits according to Planck's Law:

$$J_\lambda = \frac{2\pi hc^2}{\lambda^5\left[\exp\left(\frac{hc}{\lambda k_B T}\right)-1\right]}, \tag{8}$$

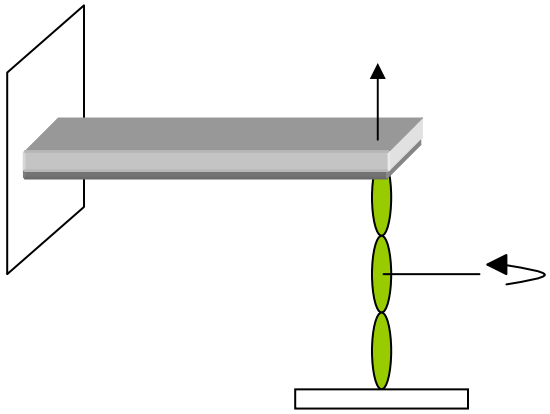

**Figure 5.** Mechanical amplifying mechanism attached to a bimetallic cantilever.

where $h$ is Planck's constant ($6.63 \times 10^{-34}$ J·s), $c$ is the speed of light ($3.00 \times 10^{8}$ m/s), $\lambda$ is wavelength, $k_B$ is Boltzmann's constant, and $T$ is the object's temperature (details in [129]). Radiation thermometers are mainly used for the measurement of very high temperatures, for non-contact measurements in harsh environments, and for observations in astronomy.

Two types of detectors are found in radiation thermometers. A thermal detector absorbs incoming radiation at all wavelengths and changes temperature. The detector is commonly a thermistor, in which case the device is called a bolometer. The radiation measured by a thermal detector, i.e., the integral of Equation 8 over $\lambda$, is $J = \sigma T^4$, where $\sigma$ is the Stefan-Boltzmann constant ($5.67 \times 10^{-8}$ W/m$^2$K$^4$).

The second type of detector, a photon detector, measures $J_\lambda$ in a narrow range of $\lambda$, in the vicinity of the wavelength of maximum emission $\lambda_{max} = 0.00290 / T$ (Wien's Law). The most common detector material, for measurements of temperatures near ambient, is HgCdTe. (Photomultiplier tubes are not available for wavelengths near $\lambda_{max} \approx$ 10 μm.)

Radiation thermometry has been parallelized in the form of thermal cameras (reviewed in [130]). A top-of-the-line thermal camera with an array of photon detectors can resolve 20 mK (FLIR Thermacam SC 3000); bolometer resolutions are similar [130]. Since radiation thermometers measure absolute temperature, high resolution requires an enormous dynamic range. For a thermal detector to measure a change in temperature of 1 μK about an ambient temperature of 295 K, $J$ must be measured with a resolution of 1 in 74 million. For a photon detector, the dynamic range in $J_\lambda$ depends on $\lambda$, but is also in the

tens of millions for infrared wavelengths near 10 μm. As will be seen in Chapters 4 to 5, using thermal expansion and interferometry a similar temperature resolution may be achieved by measuring an optical change on the order of 1 part in 1000.

# Chapter 3.
# Liquid-in-Glass Thermometry

## 3.1 Introduction

The calorimeter built for this thesis was based on a custom-built miniature liquid-in-glass thermometer, in which the meniscus level was measured by a Michelson interferometer. In this chapter, literature and issues related to liquid-in-glass thermometry will be discussed.

The liquid-in-glass thermometer was invented in the mid-1600's. In the twentieth century, it was largely superseded by the platinum resistance thermometer for precision measurements. There has thus been little recent research in the area.

Automated reading of the meniscus level in a mercury thermometer has been implemented using a video camera [131] and using a capacitive sensor [132]. A tiny gallium thermometer in which the bore was a carbon nanotube was constructed [133]. A thermometer design was patented in which the meniscus level was detected by the intensity of light reflected back into a fiber optic probe situated above it [134]. In a different design, an intensity-modulated light beam was reflected from the meniscus. Meniscus displacement changed the optical path length, and therefore the resonant frequency of the modulation [135].

The meniscus level in manometers has been measured interferometrically, but with modest resolution due to vibration problems [136]. Interferometry has also been used to measure thermal expansion of free drops of liquid crystals [137]. Finally, thermal expansion of a polymer has been measured with a Fabry-Pérot interferometer [138], with temperature resolution of 5 mK.

A liquid-in-glass thermometer read by an interferometer was a promising approach for the microcalorimeter. Unlike most other calorimetric methods, it incorporates optical detection, which is the basis of successfully parallelized fluorescent and radiological labeling assays.

The sensitivity was estimated beginning with the volumetric thermal expansion coefficient of water, which is $2.3 \times 10^{-4}$ $K^{-1}$ at room temperature. The addition of 0.1 μJ to 5 μL of water would therefore cause a volume expansion of $5.5 \times 10^{-18}$ $m^3$ (assuming no heat loss). If the solution was confined to a rigid container with a protruding capillary of diameter 1 μm, the water meniscus in the capillary would be expected to rise by 7 μm.

However, this neglected the effect of contact angle hysteresis, which has long been known to limit the resolution of mercury thermometers. The microcalorimeter resolution was expected to be similarly affected. In fact, contact angle hysteresis had only a minor effect on the thermometer and calorimeter data (shown in Chapter 5). In the remainder of this chapter, recent literature on contact angle hysteresis will be used to attempt to understand the discrepancy between the observations of the present instrument and the behavior of mercury thermometers.

## 3.2 Mercury Thermometers

In 1886, Pickering [139] alluded to the "well-known" phenomenon of irregular (jumping) meniscus motion in mercury thermometers, which he ascribed to "inertia of the bulb" – meaning that the mercury in the bulb did not expand at a constant rate due to a resistance in the thermometer bore to the advance of the meniscus. However, his main concern was that the reading of the thermometer at a given temperature was higher when approached from above, rather than from below. This problem was overcome by repeatedly tapping the thermometer prior to each reading, and by avoiding contamination of the bore walls via exposure to the open air during thermometer construction [140].

In his 1889 treatise on precision mercury thermometry, Guillaume [141] attributed both meniscus jumping and the temperature history effect to contact angle hysteresis (non-uniqueness of the contact angle). As the temperature rose slowly, the mercury meniscus in a thermometer bulged (the contact angle increased) before jumping to a higher level in the bore, where the process would be repeated. Guillaume showed

that the size of the jumps was expected to increase as the bore diameter decreased and as the bulb volume increased, thus negating any attempt to improve thermometer sensitivity beyond a certain level.

The balance of forces on the mercury column in a thermometer is

$$\left(p_1 - p_2\right)\cdot\frac{\pi d^2}{4} + \sigma\cos\theta\cdot\pi d - \frac{\pi d^2}{4}h\rho g = 0,$$

where $p_1$ is the pressure below the column, $p_2$ is the pressure above the column, $d$ is the bore diameter, $\sigma$ is the surface tension, $\theta$ is the contact angle, $h$ is the column height, $\rho$ is the density of mercury, and $g$ is the acceleration due to gravity. $\theta > 90°$ for mercury, which does not wet glass. If the temperature rises by $\Delta T$ and the meniscus bulges but does not advance, then the pressure in the mercury has increased by

$$\Delta p = \frac{4\sigma}{d}\left(\cos\theta_s - \cos\theta\right), \tag{9}$$

where $\theta_s$ is the static (previous) contact angle and $\theta$ is its value after the temperature increase.

$\Delta p$ can also be calculated from the compressibility of the mercury and the elasticity of the cylindrical thermometer bulb [141]:

$$\Delta p = \frac{\Delta\alpha\cdot\Delta T}{\dfrac{R_e^{\,2}}{R_e^{\,2} - R_i^{\,2}}\left(\dfrac{3}{3\lambda + 2\mu} + \dfrac{1}{\mu}\right) + \Delta\chi}, \tag{10}$$

where $\Delta\alpha$ is the difference of the volumetric thermal expansion coefficients of mercury and glass; $R_e$ and $R_i$ are the external and internal radii of the bulb, respectively; $\lambda$ and $\mu$ are the Lamé constants for the glass; and $\Delta\chi$ is the difference of the compressibilities of mercury and glass.

Guillaume neglected the volume created by the increase of $\theta$, which can be taken into account in Equation 10 by subtracting the following term from the numerator:

$$\frac{\pi d^3}{24V}\left[\frac{\cos\theta_s\cdot\left(2 + \sin\theta_s\right)}{\left(1 + \sin\theta_s\right)^2} - \frac{\cos\theta\cdot\left(2 + \sin\theta\right)}{\left(1 + \sin\theta\right)^2}\right], \tag{11}$$

where $V$ is the volume of mercury in the bulb.

The meniscus jumps when $\theta$ reaches its advancing value $\theta_a$ [141]. Equations 9 to 11 may be used to predict the size of the temperature jumps for a given thermometer; a

typical value for a precision mercury thermometer is a few milliKelvins. If the other thermometer dimensions are fixed, the value of $d$ that optimizes the temperature resolution can also be found (it is typically ~0.2 mm). However, in these calculations the assumption is made that $\theta_s$ and $\theta_a$ each have a unique, measurable value that is independent of both location in the bore and meniscus velocity. We will see in Section 3.4 that this is an oversimplification.

In 1959, Hall and Leaver [142] reported experiments measuring the size of meniscus jumps in various mercury thermometers, with results similar to the predictions of Guillaume's theory. They also found, as Pickering did, that vibration moved the meniscus closer to its equilibrium position. Later, Saarimaa and Wallin [132] made more precise observations by measuring the meniscus level capacitively, rather than by eye. This allowed them to increase the bore diameter and so reduce the jump size to below 0.3 mK.

## 3.3 Present Observations

In the present instrument, water expanded inside a glass capillary tube open at one end. At this end, the water was topped by a thin layer of mineral oil to prevent evaporation. An interferometer monitored the level of the oil/air interface (meniscus), which had a diameter of about 0.1 mm. Both water and mineral oil wet glass, producing $\theta < 90°$.

Based on the theory above, microKelvin-level temperature changes were expected to be insufficient to cause bulk motion or jumps of the meniscus. Instead, only changes in the contact angle were expected, which would cause nanometer-level displacements of the center point of the meniscus. However, this was not the case in practice.

The behavior of the meniscus was observed to vary strongly with its velocity. Viewed under a microscope at velocities of ~0.1 mm/s, a changing contact angle could at times be seen, as could a sidling motion of the meniscus up the capillary walls (for a rising temperature). Similar observations were made in [143]. At velocities of ~1 μm/s, the contact angle appeared constant and the meniscus moved smoothly, but there was an approximately 0.3 K discrepancy in its level depending on whether the temperature was rising or falling. Video recordings were made of the contact line at these velocities. A

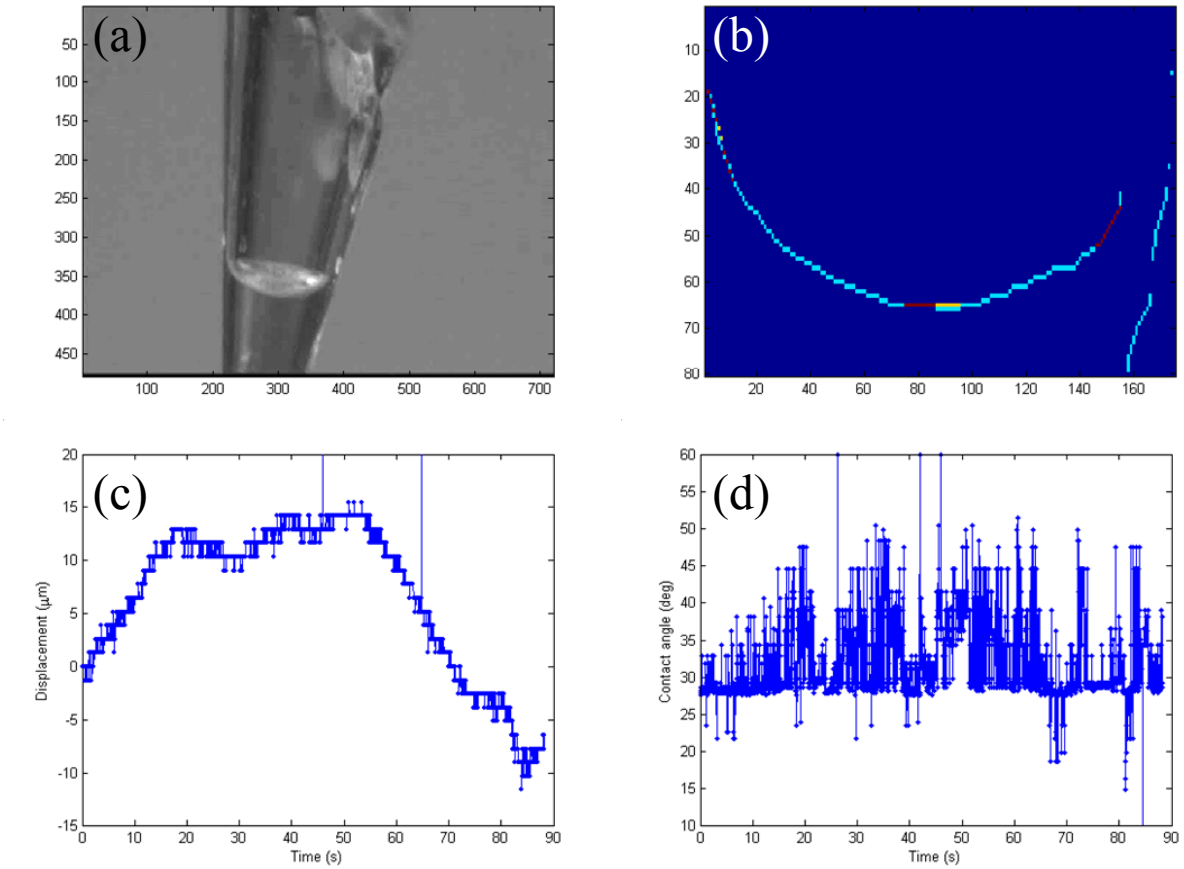


**Figure 6.** Video recording of meniscus: (a) Typical raw image of a single frame. (b) Result of image processing, showing meniscus level (center) and contact angles. (c) Meniscus motion. (d) Right side contact angle. In (c) and (d), a few points are visible where the image processing failed.

typical frame is shown in Figure 6, along with image processing results, which failed to discern any irregular meniscus motion or contact angle hysteresis. All of the microscope images appeared to show a permanent wetting film of oil on the capillary wall above the meniscus.

In the experiments (described fully in Chapter 5), meniscus velocity was ~1 nm/s, and irregular motion or hysteresis was rarely observed. The temperature history effect, which would have appeared as a stationary meniscus after a reversal in the direction of temperature drift, was absent or at most ~0.02 K.

The noise level in the data was similar whether the meniscus was rising or falling, and typically independent of its speed. Generally, abnormally high noise was corrected by realignment of the optics; however, in a few capillaries (out of dozens), the noise seemed to depend on the location of the meniscus on the capillary wall (i.e., the capillary

temperature). In these cases, noise was ascribed to contamination of the wall at that point. Most capillaries were not used for more than a few days due to design changes. Among capillaries that were used for a few months, in a couple of cases noise gradually increased (but in another it did not). This increased noise was also ascribed to contamination.

## 3.4 Contact Angle Hysteresis

Contact angle hysteresis is manifested as different values of the contact angle for advancing and receding contact lines. The contact angle may be thought of as the visible evidence of how much fluid pressure is needed to overcome the pinning forces experienced by the contact line. These pinning forces are due to inhomogeneities on the solid surface, which may be physical (i.e., roughness) or chemical. The advancing and receding contact angles are thus determined by the local condition of the surface on which they are measured, and are not fluid or material bulk properties; they also depend on fluid velocity [144].

Two regimes of surface inhomogeneity may be considered [145,146]: large-scale inhomogeneity, in which the entire contact line can be pinned; and small-scale inhomogeneity, in which sections of the contact line are pinned while the main part continues to move.

Large-scale inhomogeneity can cause meniscus jumps (also called stick-slip), as already described for mercury thermometers [141,142], and as observed in liquids advancing on thin glass fibers [145] and water advancing on a roughened glass surface [146].

Small-scale inhomogeneity can be modeled as the effect of a random pinning force acting on the contact line [146]. It was indirectly observed in [146] for water advancing in glass capillary tubes, where it was also shown that small-scale inhomogeneity can cause the meniscus level to depend on its history. As described above, this history dependence has been observed in both mercury thermometers and in the present instrument. In [147], the effect of small-scale inhomogeneity was observed directly in water advancing on a treated glass plate.

Inhomogeneities can be masked by a wetting film of the fluid on the wall surface above the meniscus, which acts as a lubricant [145,146,148,149]. For example, in everyday life, raindrops on a window pane are observed to descend erratically due to pinning forces [146], but to slide more easily along previously wet tracks. In experimental measurements of water advancing up vertical glass capillaries [146], it was shown that contact line dynamics were more strongly affected by surface inhomogeneity when the wetting film was given time to drain. The wetting film is effective only if the fluid advances slowly enough that the molecules in the film have time to self-organize in advance of the fluid [150]. An empirical expression was found for the required speed, for liquid polydimethylsiloxane (PDMS) on Pyrex:

$$u = \frac{8}{\eta}\sqrt[4]{\delta^6 \sigma \rho^3 g^3}\,, \tag{12}$$

where $\eta$ is viscosity and $\delta$ is the film thickness [150].

A receding meniscus always moves into already-wet regions of the surface, and should therefore be less affected by surface inhomogeneity. A non-wetting fluid such as mercury, however, is particularly sensitive to surface inhomogeneity; thus, meniscus jumps are seen for both rising and falling temperatures even in carefully cleaned thermometer bores.

In the present work, as described in the preceding section, the effect of wall inhomogeneity on the contact line progressively decreased as the velocity decreased, until little effect was seen at the experimental velocity. At this velocity, the observed wetting film of oil was apparently thick enough to allow self-organization of the fluid molecules ahead of the advancing meniscus. If 1 μm/s is taken as the nominal velocity at which contact angle hysteresis was largely absent in the capillary, then Equation 12 gives a wetting film thickness of 46 nm, not an unreasonable value.

As further evidence of the effect of the wetting film, the oil/water interface, for which no such film was visible, was generally observed (under the microscope) to move less smoothly than the oil/air interface. A few capillaries with insufficiently thick oil layers exhibited high noise due to pinning at the oil/water interface (because its diameter was too small; see Section 4.1 for the capillary geometry). Finally, on at least two

occasions, the smoothness of motion of the meniscus was markedly improved by raising and lowering the temperature in order to form an oil film on the capillary walls.

Vibration may be used to overcome either large-scale or small-scale inhomogeneity [139,142,147]. The extra energy allows the contact line to escape pinning and reach its equilibrium position. If the vibration then stops, the meniscus does not return to the previous position, but remains at the equilibrium position, as expected [142,147]. In [142], the vibration appears to have had sufficient energy to overcome the weaker pinning due to small-scale inhomogeneity but not the stronger pinning due to large-scale inhomogeneity.

No literature on meniscus motion in alcohol thermometers could be found. Since alcohol wets glass, it would be expected to behave similarly to the oil used in the microcalorimeter. Wetting liquids are not favored for precision liquid-in-glass thermometry because the film they leave on the bore walls can cause erroneous temperature readings if not drained. It is expected that compared to mercury, alcohol would offer better resolution at the cost of inferior accuracy.

# Chapter 4.
# Apparatus

## 4.1 Capillaries

In the first four sections of this chapter, the thermometer apparatus will be described. The modifications made to convert the instrument to a calorimeter will be the subject of the final section.

Capillaries were made from borosilicate glass capillary tubing purchased from Friedrich & Dimmock. The original tubes were 100 mm long, with an annular cross-section of 0.75 mm inner diameter (ID) and 1.5 mm outer diameter (OD). The capillary tubes were used as received, with no coatings or cleaning procedures applied. The manufacturing process is illustrated in Figure 7. Two necks were drawn in a capillary tube using a laser-based pipette puller (Sutter P-2000). The necks were 23 mm apart, so that the volume inside the capillary between them was 10 μL. The right neck, as seen in Figure 7, was drawn to an ID of about 0.1 mm, with a severe taper (see Figure 8). This could be achieved on the pipette puller by performing repeated pulls at the same point in the capillary. The proper pulling parameters were found by trial and error (see Table 4).

| Neck | Heat | Filament | Velocity | Delay | Pull | # Pulls |
|---|---|---|---|---|---|---|
| right | 450 | 4 | 45 | 120 | 0 | 1 |
| left | 450 | 4 | 19 | 120 | 0 | 4 |

**Table 4.** Parameters for the pipette puller (as entered; units arbitrary). The parameters had to be adjusted every few months, mainly by increasing the heat and modifying the velocity. This was perhaps due to aging of the puller's $CO_2$ laser. The values shown were used at the end of the thesis.

The capillary tube was then manually cut with a carbide saw slightly beyond the right neck. A syringe (with no needle) was sealed onto the left end of the tube using shrink wrap and a heat gun, and distilled water drawn into the tube, filling it. Tubes with

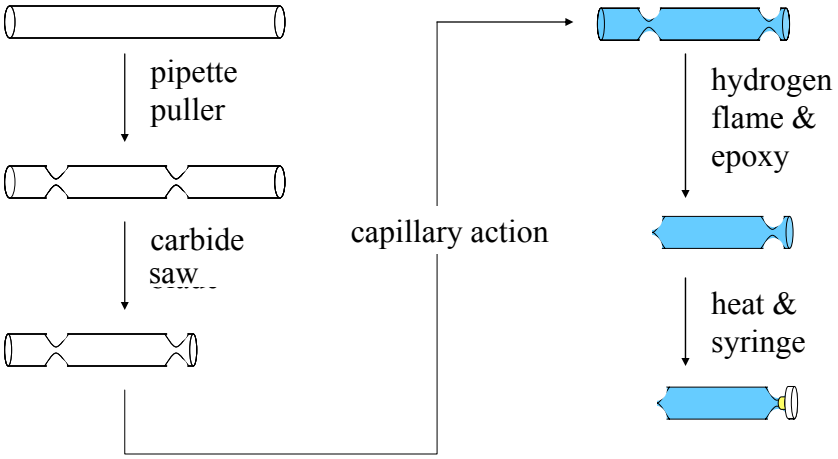


**Figure 7.** Capillary manufacturing process.

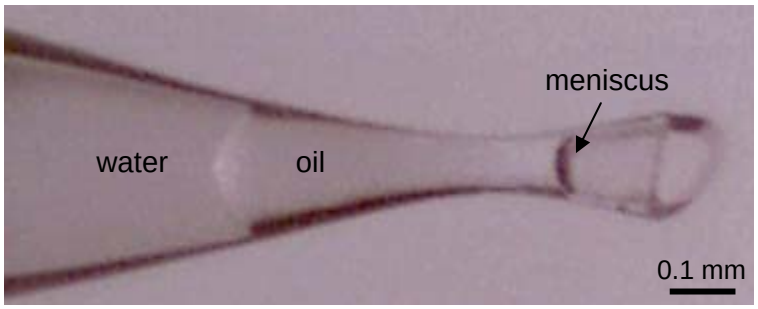


**Figure 8.** Capillary tip.

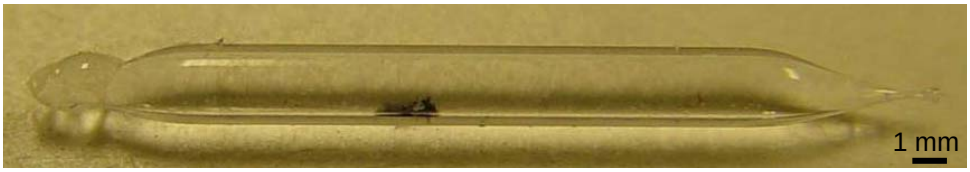


**Figure 9.** A completed capillary. The black mark was for identification.

slightly larger right necks could be filled by capillary action by simply inverting them in a vial of distilled water.

A hydrogen micro-torch (Arizona Hydrogen Hydroflame III) was used to bisect and seal the capillary at the left neck. The purpose of the left neck was to quicken the sealing and prevent air bubbles being formed in the interior next to the seal. (Filled capillaries containing air bubbles that were visible under a microscope were discarded.) The sealed (left) end was then dabbed in quick-dry epoxy to ensure an air-tight seal. A completed capillary is shown in Figure 9.

To prevent evaporation, a thin layer of mineral oil (Alfa Aesar) was added above the water at the open (right) end with a syringe. The oil/air interface (henceforth called the meniscus) was to be the reflecting surface for the interferometer (see Figure 8). Later, by applying heat to advance the meniscus to the rim of the open end, small amounts of oil could be added or removed until the meniscus had the desired diameter at the experimental temperature (24 to 28 °C).

Batches of capillaries were made in one continuous session so as to minimize the exposure of the interior capillary walls to the open air. Starting from about eight capillary tubes, usually about three acceptable capillaries could be produced in a few hours. The step with the lowest yield was the carbide saw cut, during which the capillary often broke at its neck.

The tapered and expanded shape of the capillary tips, shown in Figure 8, was necessary to allow the incident laser beam to reach the meniscus without passing through the glass capillary walls. If part of the beam passed through the walls, the non-uniform thickness of glass it encountered would degrade the interference pattern.

The tapered and expanded shape did not allow very thin necks to be fabricated, since below a certain diameter the capillary tube would separate into two pieces during pulling. After extensive testing in the pipette puller with capillary tubes made of both borosilicate glass and quartz, and of various ID and OD combinations, the tubes detailed above were found to produce the best results. Slightly thinner necks (to about 70 μm ID) could occasionally be made in these tubes, but they were extremely fragile.

A different strategy to allow access to the laser beam could have been to allow the pipette puller to separate the capillary tube, producing a tip with a taper but no expansion. In such a capillary, the meniscus would have had to reside very close to the rim of the open end to remain accessible to the beam. Very fine temperature control would be needed to keep the meniscus in this small region, and the temperature at which it resided there could be affected unpredictably by contact angle hysteresis (see Chapter 3), or evaporation. Positioning the meniscus exactly at the rim was not advantageous, as it was observed that the meniscus tended to become pinned at this location, causing irregular and greatly diminished motion under applied heat. Thus, the method described above for forming capillaries was the most practical.

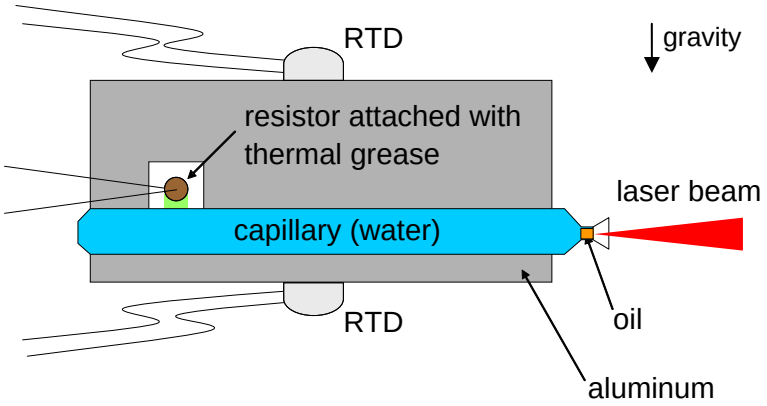


**Figure 10.** Schematic cross-section of the capillary mount for the thermometer.

Upon completion, capillaries were epoxied into an aluminum mount (Figure 10), which itself was mounted on three perpendicular translation stages for aligning to the laser beam focus. Two RTD's were located near the capillary for calibration of meniscus displacement to temperature change (see Section 5.2).

A heater was used to apply temperature changes to the capillary. In early versions of the thermometer, the heater was a length of nichrome wire wound around the capillary. However, much of the heat liberated in the wire did not enter the capillary, and thus this heater was later replaced by a laser (of known power) aimed at a black mark on the capillary. Since providing optical access to the laser through layers of thermal insulation was onerous, in the final iteration of the thermometer Joule heating was used again, in the form of a resistor mounted on the capillary with thermal grease (Figure 10).

## 4.2 Displacement Transducer

A number of displacement transducers could have been used to measure the meniscus level, including video recording [131], a capacitive sensor [132], a tunneling sensor, a confocal sensor [151], or an interferometer. An end-on transducer was favored for parallelization, which eliminated video recording. Both tunneling and capacitive measurements would have required the extra complexity of placing an electrode on the meniscus. These methods also suffered from limited range, since the signal depends on the separation between the electrodes exponentially (for tunneling) or as the inverse square (for capacitance). The limited range would have added the further complication of

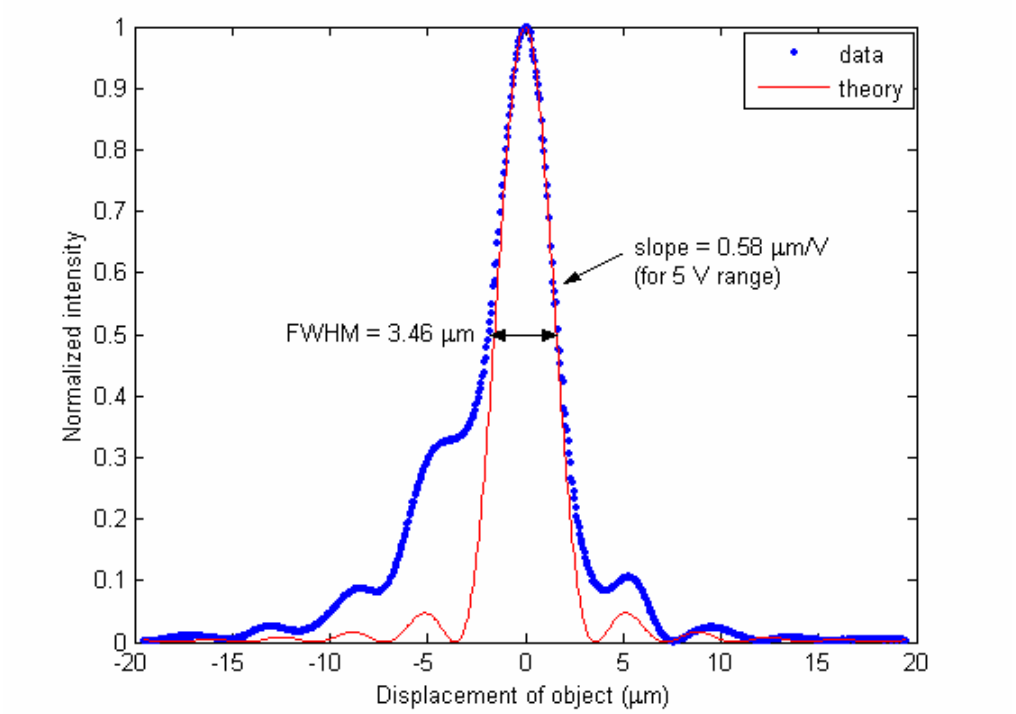


**Figure 11.** Axial response of the confocal sensor with a mirror object. The theoretical profile is from [152]. The interferometric sensor was about 28 times more sensitive.

creating highly isothermal conditions during alignment and data collection. Besides avoiding these difficulties, optical sensing had the added advantage that it lent itself to parallelization because of the availability of lens arrays and CCD and CMOS cameras. A confocal sensor was initially used as the displacement transducer, but it was replaced by an interferometer, which offered better depth of focus and higher sensitivity (see Figure 11). The interferometer also allowed the detected optical signal to be easily converted into units of displacement, via knowledge of the laser wavelength and refractive index of air.

An interferometric sensor could have been set up in either the Michelson, Mach-Zehnder, or Fabry-Pérot configuration. In the Michelson configuration (Figure 12a) the interferometer beam would have reflected off a surface of the reaction volume, whereas in the Mach-Zehnder configuration (Figure 12b) the beam would have passed through the volume. The Michelson configuration was preferable for three reasons: the solution did not have to be transparent; mixing of reactants inside the capillary (in a later calorimetric version of the instrument) was expected to cause less disturbance in the signal; and the reflection of the beam at the meniscus doubled the sensitivity.

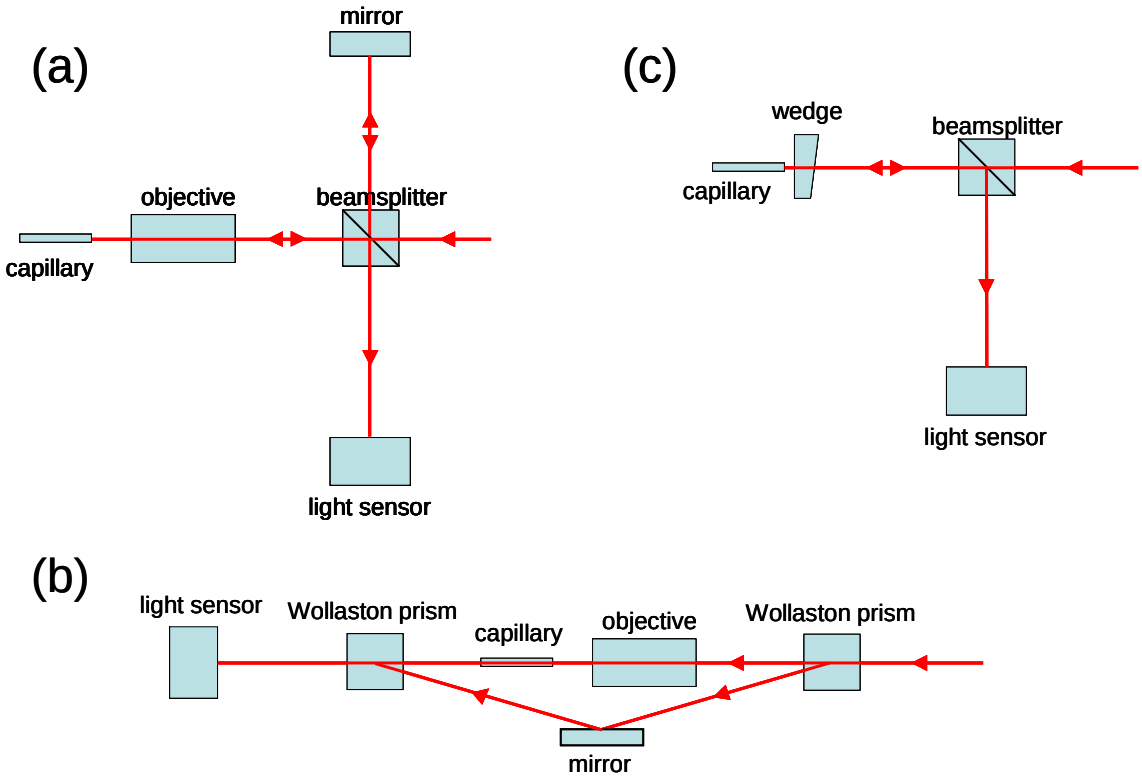


**Figure 12.** Interferometer schematics: (a) Michelson. (b) Mach-Zehnder. (c) Fabry-Pérot.

In the Fabry-Pérot configuration, a wedge-shaped piece of glass placed in front of the capillary would have formed an etalon with the meniscus (Figure 12c). The shared reference and object beam paths would have reduced noise compared to the Michelson configuration. However, the diameter of the beam incident on the meniscus could have been no more than a few micrometers due to the curvature of the ~0.1 mm diameter meniscus. Creating such a tightly collimated beam from a typical source laser beam diameter of about 1 mm would have required an impractically long optical path. A spot size of that dimension is easily produced, however, with appropriate optics (e.g., a microscope objective) in the Michelson configuration. Thus, the Michelson configuration was chosen for the interferometer.

## 4.3 Interferometer

The light source for the Michelson interferometer was a 656 nm fiber-coupled diode laser (Melles Griot 57ICS053). This laser was selected for its power stability and

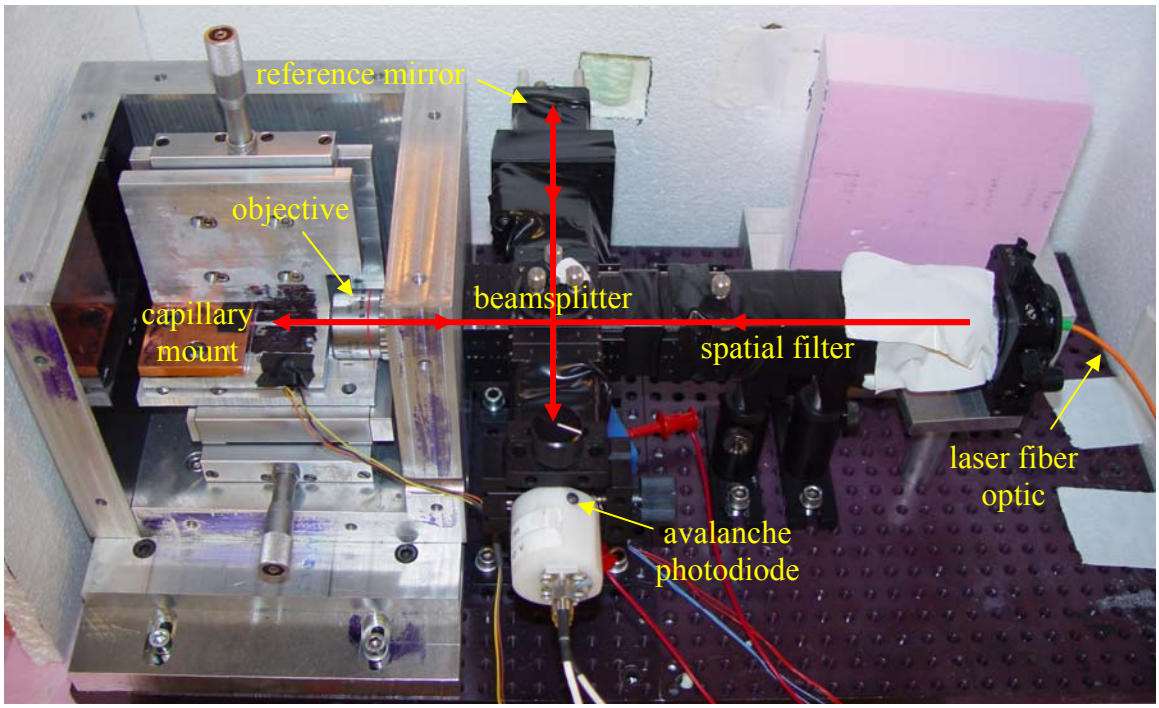


**Figure 13.** Optical path (red arrows). The top and front walls of the aluminum box have been removed.

because the fiber coupling simplified mounting the laser body (a heat source) far from the capillary. In earlier versions of the instrument, in which a free space (non-fiber-coupled) laser was used, windows had to be created in thermal insulation around the capillary. The free space laser also had to be mounted to the same support as the capillary to preserve alignment, which prevented thermal insulation of the capillary mount on its underside.

The laser beam path is illustrated in Figure 13. It was covered with black tape to eliminate stray reflections and disturbances in the beam caused by air currents. The beam path was made as compact as possible so as to minimize thermal expansion effects. The beam first passed through a spatial filter / beam expander consisting of an objective, pinhole, and lens. A beamsplitter divided the beam into the object and reference arms of the interferometer, which were each about 100 mm long and oriented 90° apart. In the object arm, the beam filled the back aperture of a 0.14 numerical aperture objective (Mitutoyo M Plan Apo 5X), which focused it on the meniscus. The long working distance of the objective (34 mm) minimized heat conduction from itself to the capillary. In the reference arm, the beam reflected from a mirror. A misaligned neutral density

filter in the reference arm attenuated the beam to approximately the intensity reflected from the capillary, for better fringe visibility at the detector.

The detector was an avalanche photodiode (EG&G C30916E). An iris placed in front of the detector passed only the central fringe of the interference pattern. The detector's output current was converted to a voltage and low pass filtered by a current amplifier (Stanford Research Systems SR570). The voltage was then read into a computer via a data acquisition card (DAQCard-1200 with BNC-2081 breakout board, National Instruments).

## 4.4 Thermal Isolation

Much effort was spent on isolating the thermometer from ambient temperature fluctuation. Room temperature changes of 1 to 2 K were commonly caused by the daily cycle of outdoor temperature, a change in the room air conditioner setting, or a change in the number of people in the room.

The thermal isolation design was conceptually aided by finite element modeling. However, accurate quantitative results could not be obtained from the models due to unknown and unpredictable thermal boundary conditions, the complex geometry of the setup, and the active temperature control in the setup (see below).

The basic strategy for thermal isolation was to construct a large heat capacity inside a large thermal resistance. The thermal resistance was an enclosure (Figure 14), about 0.9 m × 0.6 m × 0.6 m, and made of double layers of 50 mm thick vacuum insulation panels (Advantek Vaculok). The panels were attached to each other using caulking, with the top and front walls of the enclosure removable for access inside. Vacuum insulation panels were used after earlier nested Styrofoam enclosures proved inadequate.

The capillary, optics, and photodiode were located inside the enclosure, mounted on an optical breadboard. The oversized dimensions of the enclosure created a ~0.1 m air gap on all sides of the breadboard (other than below) for further thermal insulation. Below the optical breadboard were several slabs of plastic (chosen for its low thermal diffusivity) and a vibration-isolating breadboard (TMC). Thin sheets of white Styrofoam were mounted around the optical breadboard (see Figure 14) to block convective air

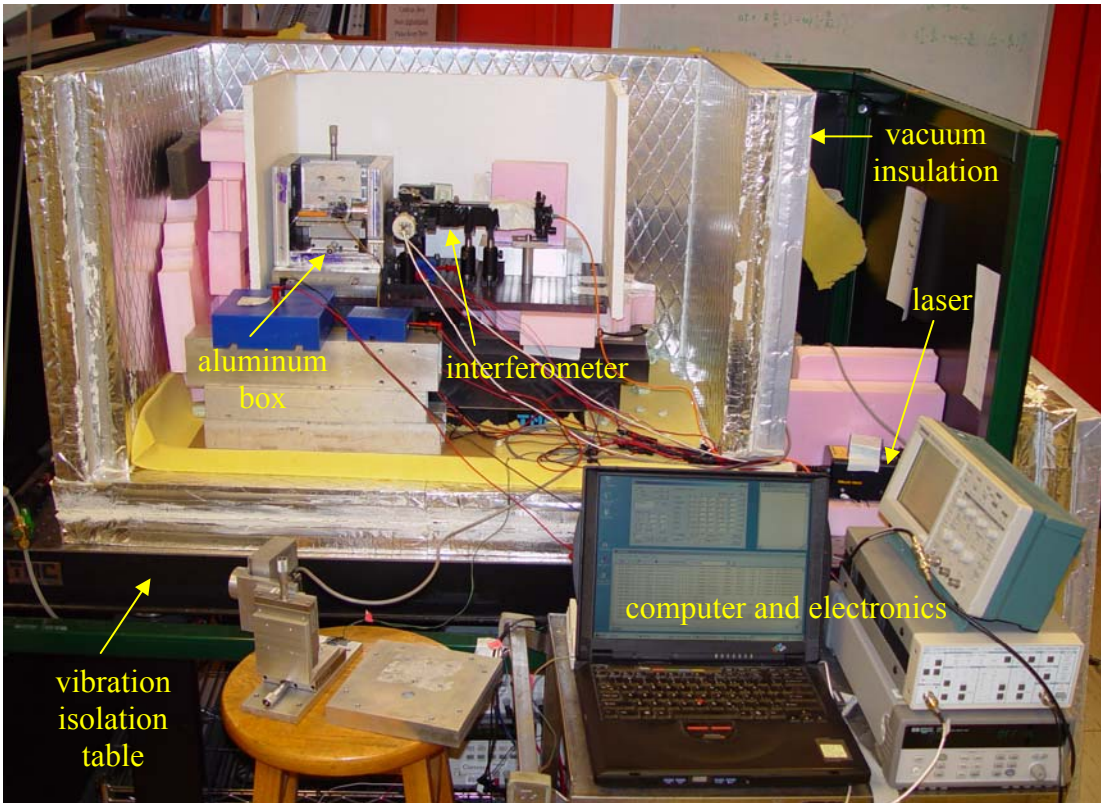


**Figure 14.** Entire setup.

currents. In an earlier version of the instrument, an inner enclosure was created in this way and filled with Styrofoam peanuts; however, removing the peanuts in order to gain access to the optics and capillary was too time-consuming.

The laser and electronics were outside the enclosure, with the laser fiber optic and other communicating wires running through a small opening in a corner of the enclosure. Since the laser output power was temperature-dependant, it was surrounded by slabs of Styrofoam insulation. To prevent overheating, two custom-built temperature controllers were mounted above and below the laser case (inside the Styrofoam). The top controller consisted of an RTD and a length of nichrome wire, and the bottom controller consisted of an RTD with a Peltier device (Marlow Industries DT6-6) for cooling. The vibration isolation table served as the heat sink for the Peltier device. The RTD measurements were read into a computer via a data acquisition box (Hewlett Packard 34970A), and the nichrome wire and Peltier device were connected to power supplies under computer command. PI control was implemented in a computer program (Figure 15), with the

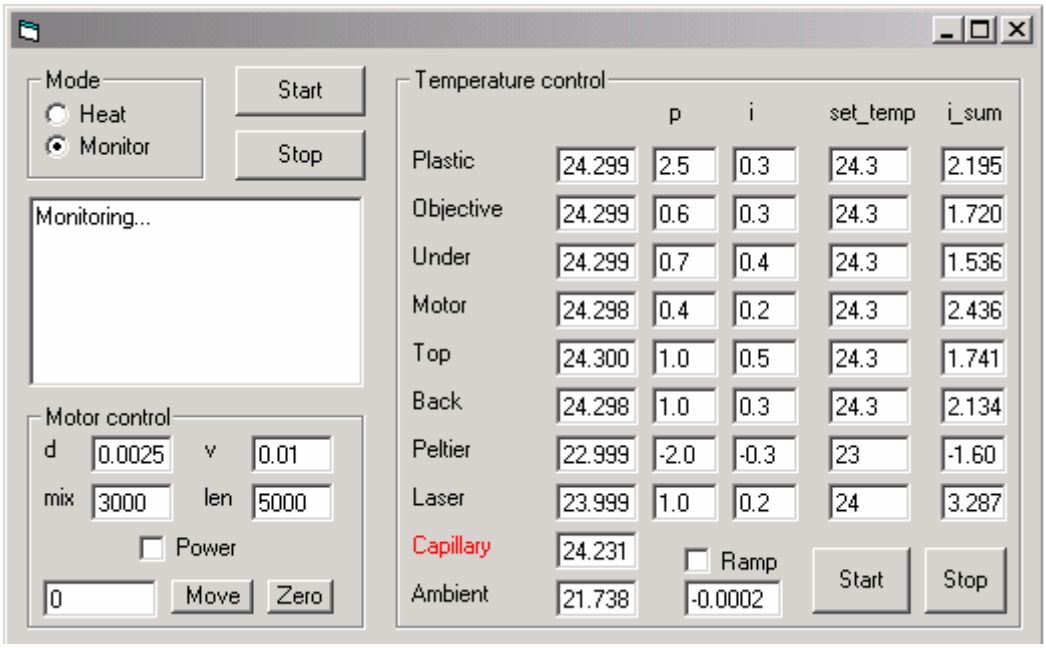


**Figure 15.** Screenshot of the computer program GUI. The program was written in Visual Basic 6.0 (code in Appendix). This revision controlled the calorimeter. In the temperature control section, the first column was the temperature (°C) measured by each RTD; the red label indicated the measurement underway. The i_sum column displayed the integrated errors (i.e., the I term multipliers). All control parameters could be adjusted at runtime. The heat mode temporarily overrode the temperature control in order to run an experiment. Data were saved to text files for later display and analysis in Matlab (The Mathworks).

parameters optimized by trial and error. This program also ran other temperature controllers (see below), as well as data collection and Joule heating of the capillary.

Inside the enclosure, the capillary and its three translation stages were mounted in an aluminum box with 25 mm thick walls, which formed a large heat capacity (see Figures 13-14). A hole machined into one of the box walls allowed access for the objective, and other holes allowed the stages to be translated from outside the box (so that temperature was constant during alignment). In an earlier version of the instrument, a heat sink was instead mounted on the translation stages, but this caused increased vibrational noise because of the large mass supported by the compliant stages.

Five additional temperature controllers were distributed on the equipment inside the enclosure. All used wire heaters since no heat sink was possible inside the enclosure. The heating wires were meandered so as to control the temperature over as large an area as possible. The set point for the controllers, which had to be above room temperature, could be varied within a range of about 24 to 28 °C to bring the meniscus to the desired

level. The controllers were repositioned occasionally, but generally one was located underneath the plastic slabs; a second above the aluminum box; a third on the objective outside the box; a fourth, upside down, under the optical breadboard, directly beneath the box; and a fifth either among the other optics or behind the box. No controllers were located inside the box so as to maintain a smoothly varying capillary temperature.

The RTD's used in all the controllers were wired in the Kelvin four wire configuration to eliminate the effect of lead resistance. The data acquisition box read the RTD's sequentially, using the maximum integration time (8 s). At these settings, temperature readings were returned with 1 mK resolution, but slightly better resolution (~0.5 mK) could be obtained by measuring resistance, and converting to temperature in the computer program using the Callendar-Van Dusen equation. Several times over the course of the instrument development, the RTD's were calibrated with respect to each other by mounting them close together inside the enclosure. The measured offsets for each RTD (typically about 0.05 K) were then included in the temperature calculation in the computer program.

The inability of the wire heaters to cool, and power supply current limits, both introduced nonlinearity that was not accounted for in the PI control. While the control was always stable, in order to speed convergence to the set temperature the accumulated error (for the I term) was occasionally adjusted manually in the program (Figure 15).

Temperature control was maintained within ±0.5 mK at the control RTD's; at the capillary, drift was limited to a few milliKelvins per hour (Figure 16). The controllers were also frequently used to ramp the temperature so as to cause a slow drift in capillary temperature.

Temperature control was also attempted using a water recirculator instead of wire heaters, with the water flowing through a tube meandering underneath the breadboard. However, this method was unsuccessful, probably because the measured temperature (of the water bath) was outside the enclosure.

As seen in Figure 14, the enclosure rested on a vibration isolation table (TMC) supported by compressed air from the building supply line. At one time, an inflated bicycle inner tube was inserted below the optical breadboard in an attempt to reduce vibrational noise; however, no improvement was seen.

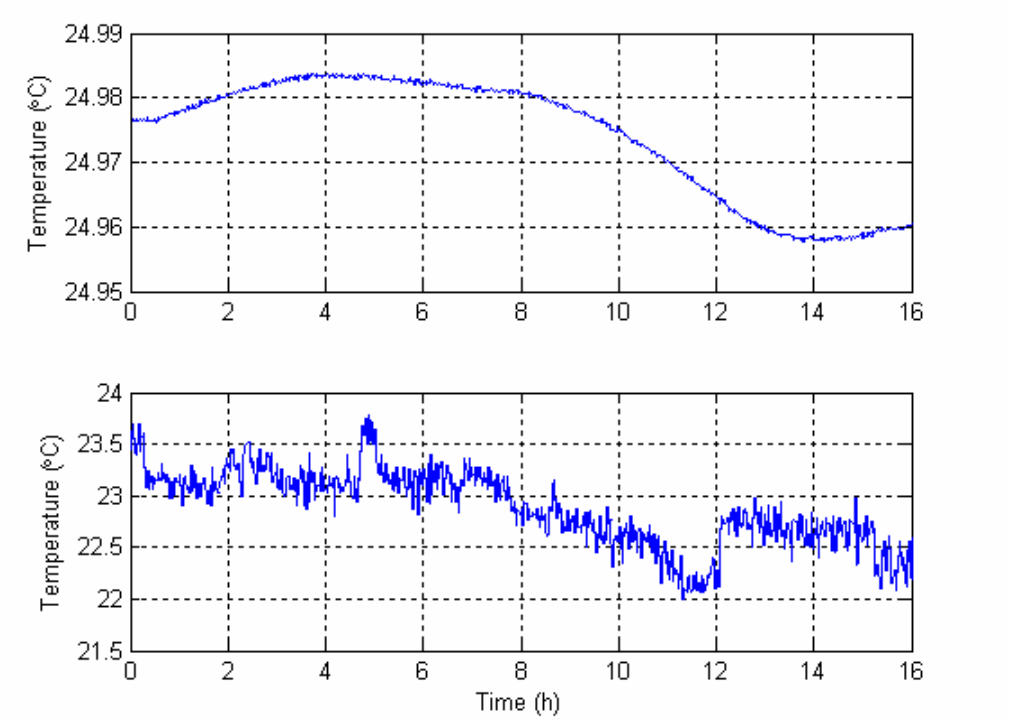


**Figure 16.** Typical behavior of ambient temperature outside the enclosure (bottom) and temperature near the capillary (top).

For minimum building vibrations, all experiments were run at night. The total time needed to align the interferometer signal and reach sufficiently stable temperature conditions inside the enclosure was as long as 24 hours in early experiments, and as short as 4 hours in later experiments (with the calorimeter) with the benefit of accumulated wisdom.

## 4.5 Calorimeter

For the calorimeter, the capillary mount was modified from the thermometer version shown in Figure 10. The new mount reduced heat loss from a chemical reaction at the capillary, and provided access from above for the mixing mechanism (Figure 17).

In the original design, the two reactants were loaded into the capillary, where only water had been present for the thermometer. By using the reactants themselves as the sensor, this design minimized both the heat capacity and time constant. The reactants were separated by a slug (a snippet of Teflon-coated steel wire) inside the capillary to delay diffusive mixing while the experiment came to thermal equilibrium. A magnet

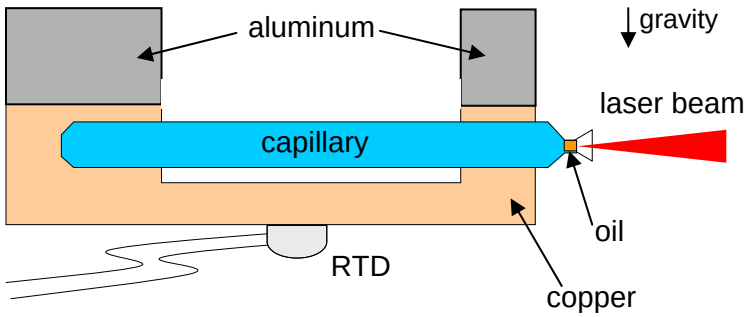


**Figure 17.** Schematic cross-section of the capillary mount for the calorimeter. Copper was used around the capillary instead of aluminum for a better heat sink. The RTD monitored the drift in capillary temperature.

mounted above the capillary was swung back and forth to actuate the slug and mix the reactants. The capillaries were shortened to a length of 14 mm (a volume of 6 μL) to speed mixing. However, the motion of the slug caused irreproducible disturbances in the meniscus level, probably via friction with the capillary walls or fluid viscosity, and this design was eventually abandoned.

A simpler design, in which the reactants were mixed outside the capillary, was implemented instead. Liquids other than water were considered for filling the capillary; however, none were identified that would provide a significant advantage (a much higher coefficient of thermal expansion; very low evaporation rate, or immiscibility with oil; non-toxicity; and non-flammability, because of the flame sealing of the bottom of the capillary).

In the new design, the two reaction drops were manually placed side-by-side on top of the capillary using a pipette. It was found that the wetting properties of the glass surface of the capillary changed over time, sometimes causing the drops to coalesce on their own. Thus, Teflon tape was wrapped around the capillary to provide a reproducible and disposable surface for each experiment. The distance between the drops was estimated to be about 0.5 mm; more closely spaced drops occasionally coalesced on their own. The same shorter capillary length (6 μL volume) continued to be used.

The drops were physically mixed by the end of a pipette tip that was swung from an arm mounted on a stepping motor (Figure 18). This configuration minimized the motor's motion. The motor was also mounted off the breadboard that supported the rest of the apparatus, since it otherwise produced significant vibrational noise. A small hole

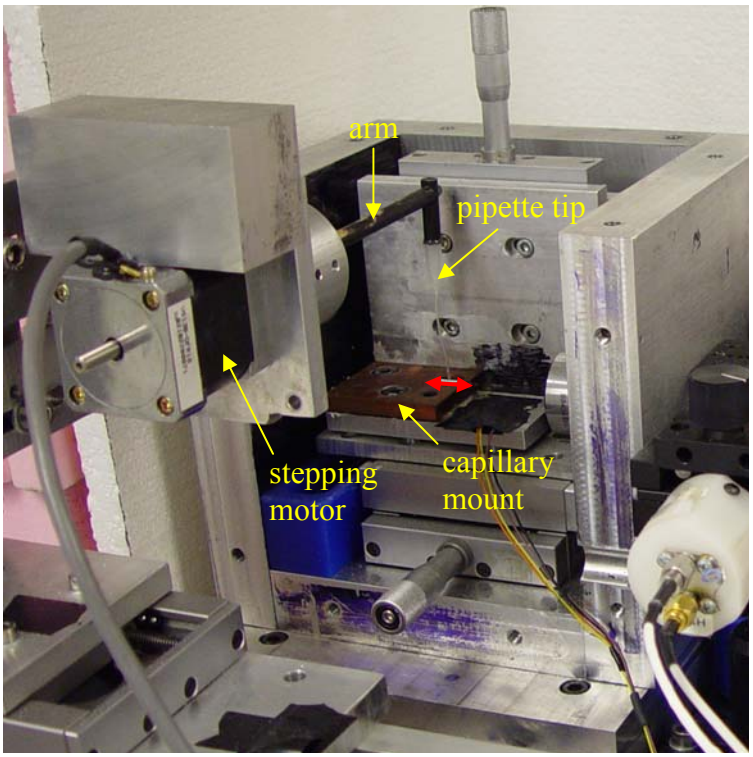


**Figure 18.** Drop mixing setup.

in the aluminum box allowed access to the arm. The motor was mounted on a vertical translation stage, at a height that left the pipette tip slightly above the surface of one drop. During the several hours it took for the temperature of the equipment to equilibrate, the drops evaporated, leaving them slightly lower. When data were collected, the motor was lowered between each run by about 0.1 mm, until the data showed that mixing had occurred. This was done in order to minimize contact between the pipette tip and the drop. In later experiments, the pipette tip was submerged in the drop from the beginning so that only a single run was required.

While different volumes, from 1 to 2.5 μL, were used for the drops, in the final experiments they were 1 μL. Manual coalescence of 1 μL drops of water and dye confirmed, visually, that mixing was instantaneous. The bottom of the pipette tip was melted shut to prevent capillary forces from drawing the drop(s) in.

The dilution of sulfuric acid (Sigma-Aldrich) in distilled water was used as a convenient test reaction; the reactants were readily available, sulfuric acid did not pose an evaporation problem, and the enthalpy of reaction was tabulated in the literature. For a starting sulfuric acid concentration of 0.01 M, the enthalpy was 30 μJ [153]. Since

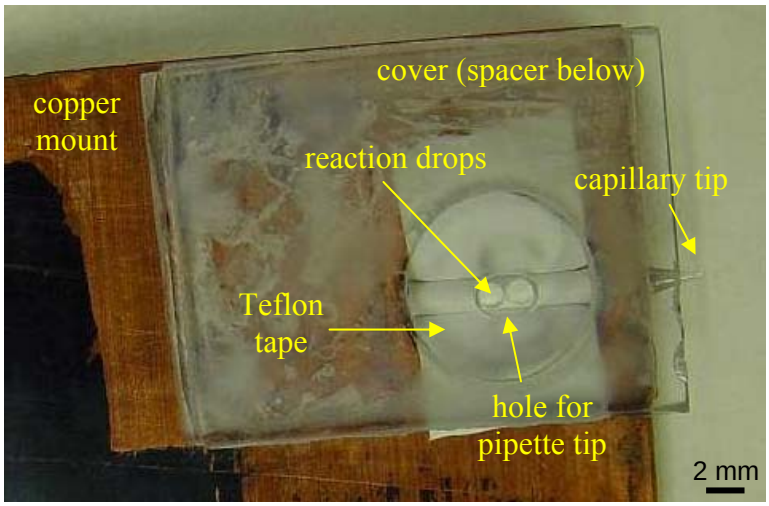


**Figure 19.** Evaporation seal for the calorimeter (top view). The hole is empty (of oil) for visibility.

evaporation of water probably increased the concentration of sulfuric acid at the time of mixing, the true enthalpy was estimated as 35 μJ.

Evaporation of the water in the reaction drops was a major obstacle. The heat of vaporization of the two drops was 4.5 J, which was six to seven orders of magnitude larger than the signal to be measured. (The surface energy change upon mixing was of order 0.1 μJ.) Drop coalescence caused a decrease in surface area, and a consequent reduction in evaporation rate, heating the drops. Moreover, heat generated by a reaction raised the vapor pressure of the drops, causing heat to be lost to evaporation without entering the capillary. To minimize evaporation, the drops were sealed into a small chamber by a cover and spacer (Figure 19), made of transparent plastic to aid alignment of the pipette tip. The pipette tip reached the drops through a hole in the cover filled with mineral oil. The cover and spacer were sealed in place using water (oil in later versions). To minimize condensation, the bottom of the cover was coated with oil, and Teflon tape was stretched between the capillary and mount. In later versions, to prevent oil wicking onto the capillary, the chamber around the capillary was lined with Teflon tape instead. Finally, to further limit evaporation, the temperature control in the enclosure was ramped downwards during the experiments, so that the drops were cooler than the cover, being thermally closer to the controllers.

# Chapter 5.
# Results

## 5.1 Noise

As discussed in Chapter 1, a significant advantage of calorimetry in drug screening is its universality – the sensor does not need to be customized to the reactants in the assay. The flip side of universality is non-specificity; since virtually all physical processes generate heat, there are many potential noise sources in a calorimeter, making the design and construction of instrumentation challenging.

The duration of experiments was typically about 100 s. The avalanche photodiode (APD) current was low pass filtered at 0.3 Hz by the amplifier, and the data were later detrended in Matlab. For the calorimeter, the low pass filter roll-off frequency was increased to 1 Hz to ensure that the signal followed the reaction dynamics. Thus, only noise in the bandwidth of approximately 0.01 to 1 Hz affected the data. Accurately predicting the magnitudes of various instrument and environmental noise sources in this bandwidth was often difficult and best done by measurement.

For example, the data sheet provided with the source laser specified power stability of 0.3% peak-to-peak in the 10 Hz to 2 MHz range, and 0.4% peak-to-peak over 2 hours, neither of which corresponded to the experimental bandwidth. In addition, these figures included neither the stabilizing effect of the temperature controller mounted on the laser, nor changes in the laser characteristics due to its aging.

Figure 20 shows a background noise measurement. The bottom trace indicated that dark current in the APD and noise generated in the subsequent electronics were insignificant. The middle traces showed that noise from laser stability and beam pointing, air currents drifting across the beam path, and thermal expansion of the optics contributed about half of the total seen in the interferometric signal (top traces).

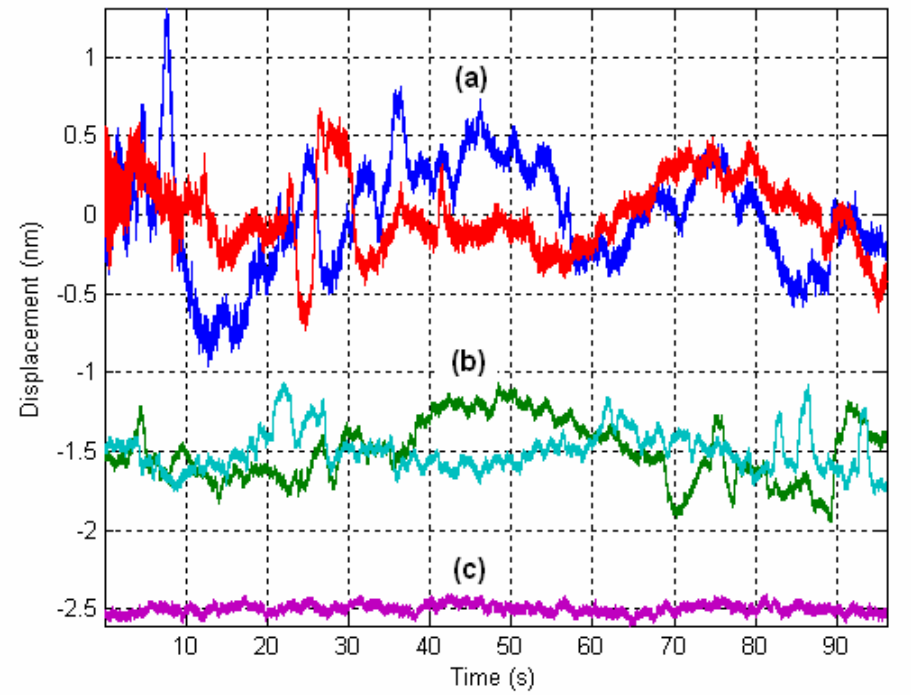


**Figure 20.** Background noise. (a) Interference signal with a capillary object. (b) Capillary intentionally misaligned so that only the reference beam was measured. (c) Spatial filter misaligned so that no light was incident on the detector. The traces are offset for clarity but were equally amplified; the displacement scale is meaningful only for the interference data.

The data in Figure 20 were collected near the end of the thesis, from the calorimeter setup. By this time, the output power of the laser had dropped significantly due to aging. Figure 21 shows an earlier background noise measurement made with the thermometer setup, in which the capillary was replaced as object by a mirror. The noise level was in fact lower than in the middle traces of Figure 20, which indicated that noise originating in the laser increased as the laser aged.

Comparison of Figure 21 with roughly contemporaneous thermometer data collected with a capillary in place (Figure 30 below) showed that noise inherent in the interferometer accounted for approximately 40% of the low frequency noise, and (not surprisingly) all of the high frequency noise.

Noise not inherent in the interferometer was due to environmental disturbances that caused actual motion of the meniscus. Of these, ambient temperature fluctuation was obviously the primary concern; efforts to mitigate its effect were discussed in Section 4.4.

A simple model of the setup gave an order-of-magnitude estimate of the effect ambient temperature fluctuations had on the capillary temperature. Let ambient

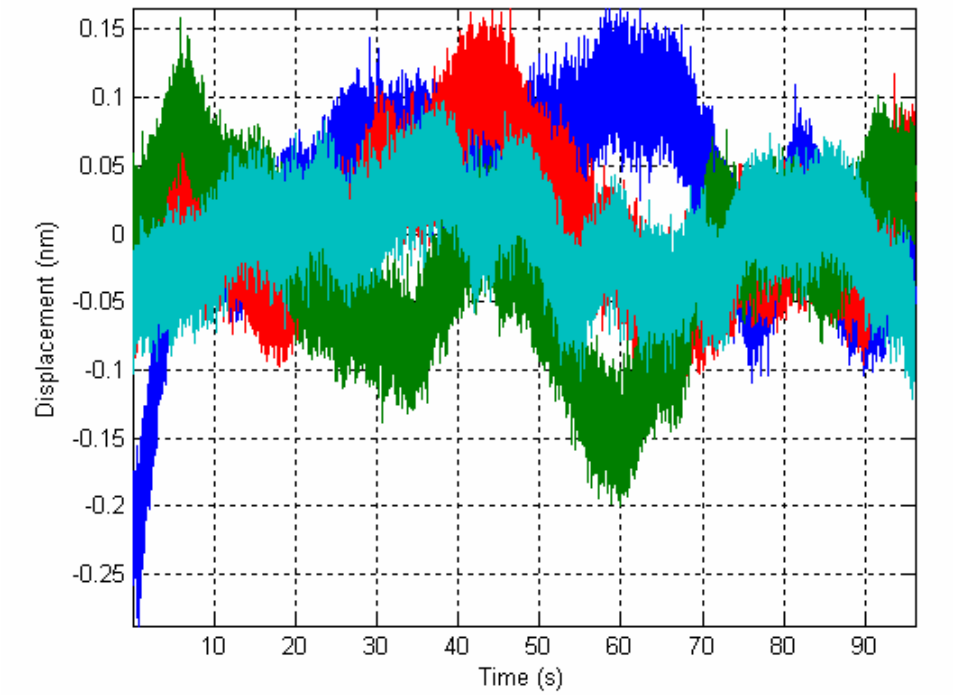


**Figure 21.** Four runs of measured noise with a mirror object replacing the capillary. A misaligned neutral density filter was placed in front of the mirror to approximate the reflectance of a capillary object.

temperature be represented by $T_\infty = T_0 + A\ \sin(\omega t)$, where the period of the sinusoid is the duration of one experiment (100 s). Since the temperature controllers inside the enclosure were each updated at 150 s intervals, we neglect their effect. Let $C$ represent the heat capacity of the apparatus, and $R$ the thermal resistance between the apparatus and the environment. If $T_0 + T$ is the capillary temperature, then

$$C\frac{dT}{dt} = \frac{A\sin(\omega t) - T}{R}. \tag{13}$$

The solution of Equation 13 is

$$T = \frac{A\left[\sin(\omega t) - RC\omega\cos(\omega t)\right]}{R^2C^2\omega^2 + 1}.$$

Since $RC \gg 1/\omega$, the environmental fluctuations are attenuated by a factor of approximately $RC\omega$. Calculated estimates for the experimental setup were $R \approx 7.1$ K/W for the vacuum insulation panels, and $C \approx 40$ kJ/K for the equipment inside the enclosure. $A$ was estimated as 0.039 K from ambient temperature readings, giving predicted fluctuations of order ± 2.2 μK at the capillary. In practice, the total measured fluctuations were somewhat smaller (see below), probably because the capillary was actually at the

center of a distributed capacity *C*. Still, the model indicated that ambient temperature fluctuations were likely a significant noise source.

Further evidence of this was obtained inadvertently when one of the two panels forming the top of the enclosure lost its vacuum. The temperature stability at the controllers deteriorated, and noise in the data increased, by a factor of approximately two. This occurred during the time that the setup was being transformed from a thermometer into a calorimeter. Since the most significant noise source in the calorimeter was due to evaporation of the reaction drops (see Section 4.5), increased temperature noise was tolerated, as were increased laser noise (discussed above) and vibration noise (from daytime experiments).

A second possible environmental noise source was ambient pressure fluctuation. The relationship between a change in pressure and the apparent temperature change measured by the capillary was expressed in Equation 10 in Section 3.2:

$$\Delta p = \frac{\Delta\alpha \cdot \Delta T}{\frac{R_e^{\,2}}{R_e^{\,2} - R_i^{\,2}}\left(\frac{3}{3\lambda + 2\mu} + \frac{1}{\mu}\right) + \Delta\chi}.$$

With $\Delta\alpha = 2.45 \times 10^{-4}$ K$^{-1}$, $R_e = 0.75$ mm, $R_i = 0.375$ mm, $\lambda = \mu = 26.1$ GPa, and $\Delta\chi = 4.35 \times 10^{-10}$ Pa$^{-1}$, the sensitivity was 2.1 μK/Pa. Pressure sensors available in the lab at the time had insufficient resolution to resolve ambient fluctuations; however, other researchers' data [154], collected in a similar setting and bandwidth, showed variation of ± 0.3 Pa, i.e. ± 0.64 μK. Thus, ambient pressure fluctuations may have been a significant noise source, depending on the attenuation provided by the enclosure and the aluminum box heat sink.

The effect of ambient acoustic noise was negligible, as loud noises did not noticeably affect the signal. Possible noise from contact angle hysteresis was discussed at length in Chapter 3.

With some capillaries, the meniscus level gradually descended over the course of weeks. This was attributed to evaporation of the top layer of mineral oil, or, possibly, evaporation of an invisible film of water between the mineral oil and the capillary wall, or a leak in the seal at the back of the capillary. The rate of evaporation was measured during calibration of the thermometer, as described below. In the worst cases, it could

amount to a few nanometers during a 100 s experiment. After detrending of the data, only a nonlinear effect would remain. Due to the stable temperature and still air in the vicinity of the capillary, nonlinear effects at this timescale were expected to be small.

Finally, building vibrations were a significant source of noise. Opening and closing of the room doors caused spikes of ~50 nm in the interferometer signal; opening and closing of other doors in the lab, or even down the hall, could cause ~10 nm disturbances. Footsteps in the room and vibrations from the adjacent machine shop also affected the data. Table 5 shows an example of noise measured in the thermometer at different times of day.

| Time | 6 a.m. | 6 p.m. | 11 p.m. | 6 a.m. | 10 p.m | 3 a.m. |
|---|---|---|---|---|---|---|
| Noise (nm) | 0.8 | 1.4 | 1.0 | 0.3 | 0.7 | 0.4 |

**Table 5.** Measured peak-to-peak value of low frequency noise at different times of day. The first four columns are from one 24-hour period; the last two are from a different day a month later, using a different capillary.

In an effort to potentially subtract vibrational noise from the data, measurements were made with an accelerometer (Brüel & Kjær model 86) mounted inside the enclosure. However, the accelerometer signal did not correlate with noise in the data, probably because it was too large to mount in rigid connection to the capillary and/or it had insufficient resolution.

A second, adjacent capillary was added to the thermometer setup in an effort to reduce common mode noise, which would include all the significant sources discussed above, other than contact angle hysteresis. The two capillaries (sample and reference) were identical, within the limits of the manufacturing process. The optical path was modified (Figure 22) in order to measure interference between beams reflecting from each of the capillaries. The reference capillary was mounted in a fixed position, and was aligned independently of the sample capillary via a new adjustable mount built for the objective. Ultimately, this setup was found to increase the noise level in the data. This was believed to be due to the two capillaries not being rigidly connected; the sensitivity of the reference capillary reflection to building vibrations in the lateral directions was consequently high compared to that of the mirror reference object in the single capillary setup.

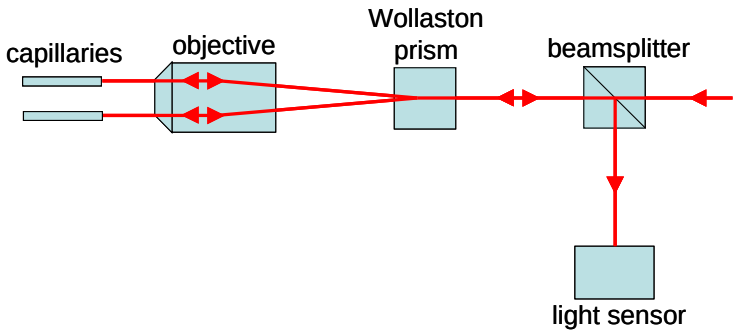


**Figure 22.** Optical path for twin capillary setup.

## 5.2 Thermometer

In the thermometer setup, meniscus displacement was calibrated to temperature change by allowing (or causing) the capillary temperature to drift, and comparing the readings of the nearby RTD's with the number of fringes crossed by the interferometer signal. Sometimes, a correction had to be made for evaporation, which caused the meniscus level to drop at constant temperature. If the meniscus displacement was $d_1$ during a temperature increase $\Delta T_1$ and time $t_1$, and $-d_2$ during a temperature decrease $-\Delta T_2$ and time $t_2$, then the sensitivity was calculated as

$$S = \left( d_1 + \frac{t_1}{t_2} d_2 \right) \Big/ \left( \Delta T_1 + \frac{t_1}{t_2} \Delta T_2 \right).$$

Calibration values were in the range expected from thermal expansion and the geometry (about 0.4 mm/K). Due to the taper of the capillary wall (Figure 8 in Section 4.1), the calibration value decreased as the capillary temperature increased.

Experiments were run while the temperature was slowly drifting either up or down. Heat was applied using the resistor (Figure 10 in Section 4.1) while the interferometer signal was in the linear, sensitive part of the sine wave (away from the peaks). The maximum and minimum values of the sine wave crossed immediately before and after data collection were then used to calculate the meniscus displacement from the known laser wavelength. (The range of the sine wave drifted slowly.)

Six sets of data are shown in Figures 23 to 28 (two others that were recorded in daytime are not included). The calibration values varied from 0.367 to 0.606 mm/K. The

right vertical axis shows the average temperature change of all the water in the capillary, whereas the resistor likely heated only a portion of the water by a larger amount. The data were detrended over the initial 40 s and final 20 s portions. The total deviation of the control signal over 105 s was typically below ±1.5 μK.

Figure 29 shows the linearity of the response as a function of heater power. The reproducibility appeared to worsen with greater applied heat; this was likely due to inaccurate calibration. The calibration accuracy was limited by the resolution of the RTD's and, possibly, by temperature differences between the RTD's and the capillary itself.

The thermometer could be used to measure larger temperature changes by fringe counting, with a resolution of 0.5 mK or better. The maximum range was about 0.5 K, limited by the meniscus moving out of focus.

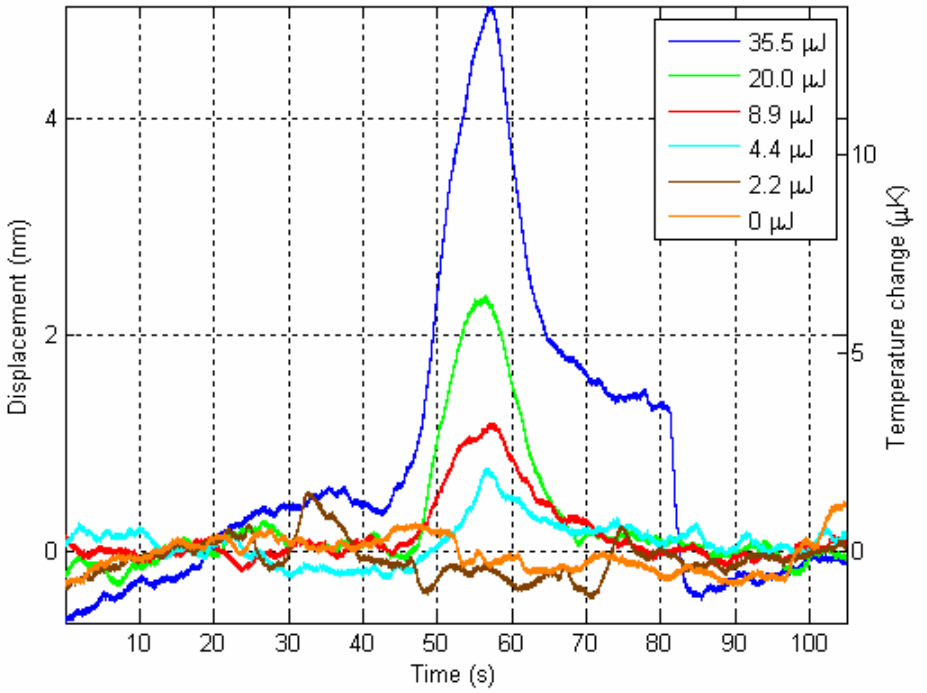


**Figure 23.** First set of thermometer data. The meniscus level is shown, with heat applied in the interval 46 to 56 s. The legend shows the energy released by the resistor; only about 4% apparently entered the capillary. The jump in the 0 μJ trace at 81 s was probably due to contact line pinning.

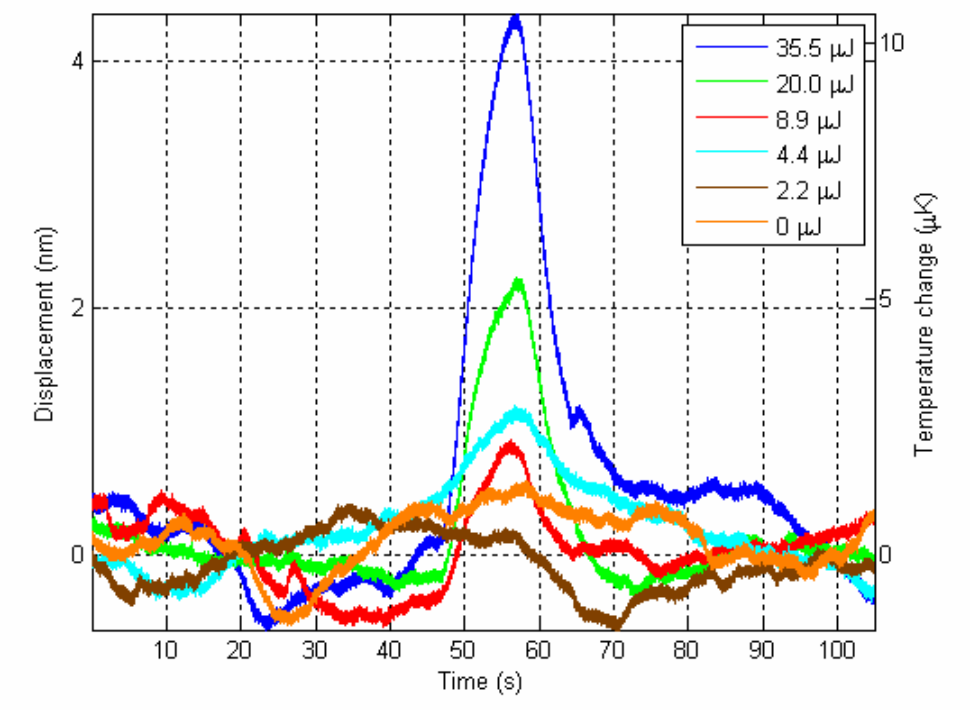


**Figure 24.** Second set of thermometer data.

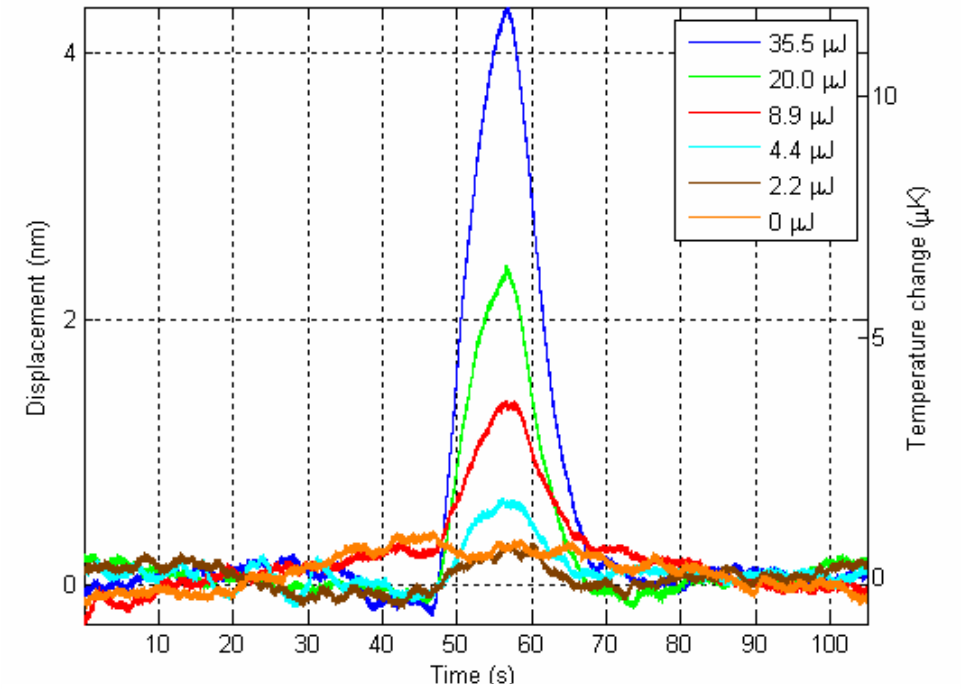


**Figure 25.** Third set of thermometer data.

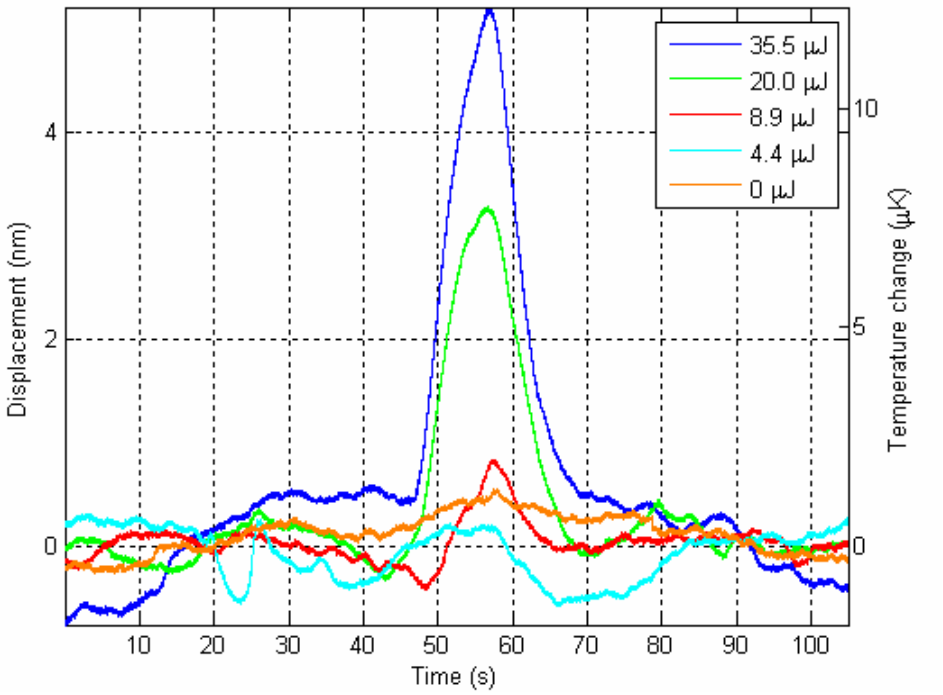


**Figure 26.** Fourth set of thermometer data.

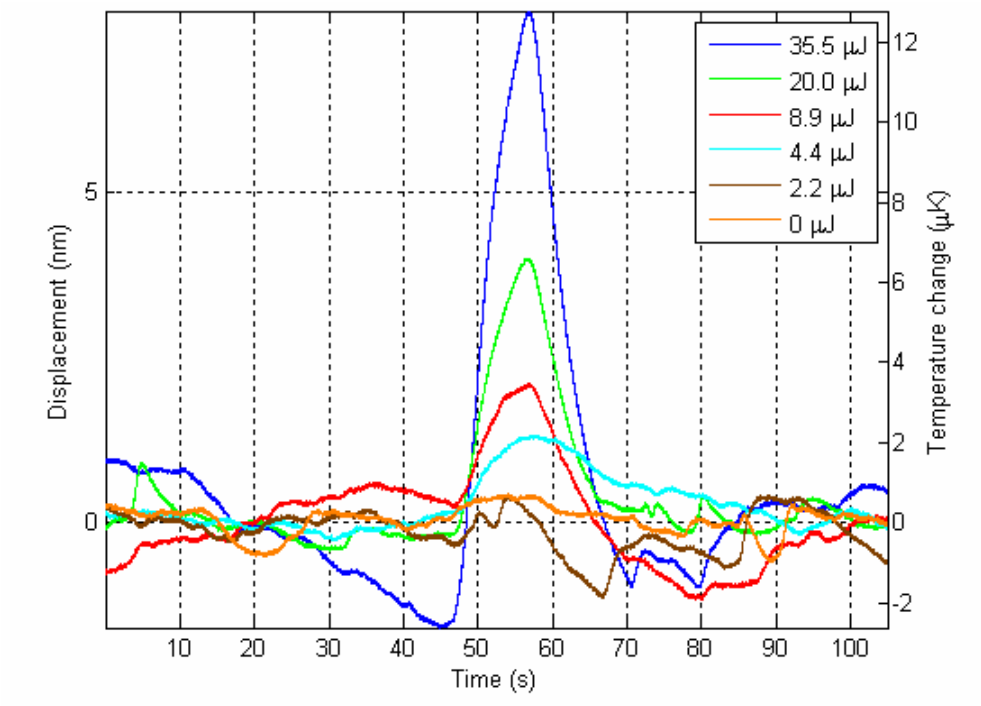


**Figure 27.** Fifth set of thermometer data.

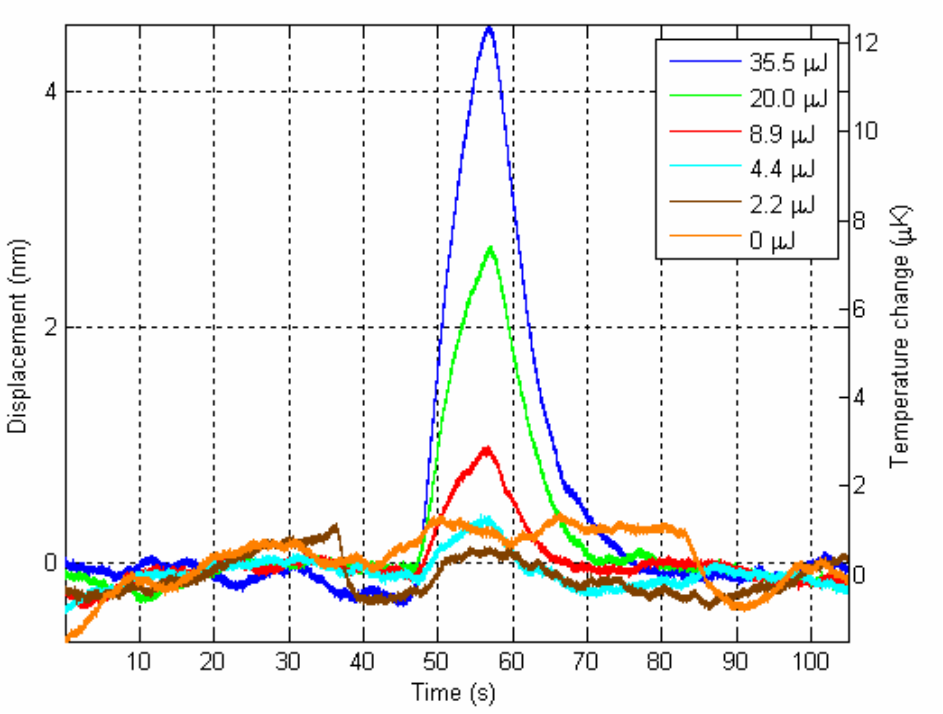


**Figure 28.** Sixth set of thermometer data. A different capillary was used for this set.

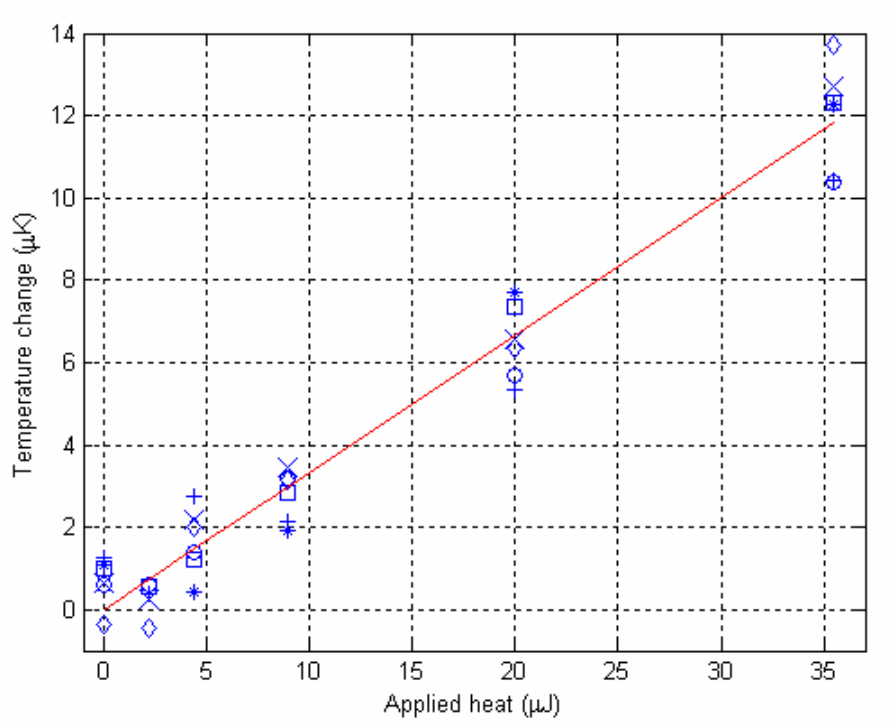


**Figure 29.** Temperature change at 57 s from all six experiments, with a fitted line.

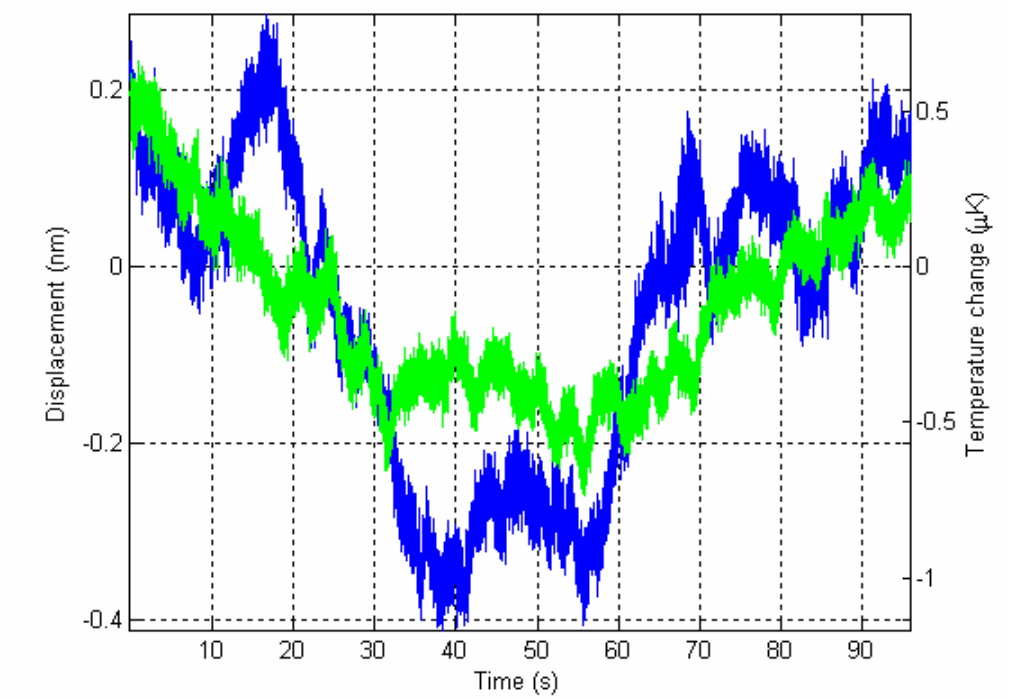


**Figure 30.** Two runs of data showing temperature resolution using a shorter capillary. No heat was applied.

After the data in Figures 23 to 28 were taken, it was discovered that passage of the laser beam through the glass walls of the capillary above the meniscus was deteriorating the signal (see Figure 8 in Section 4.1). Subsequent capillaries were cut closer to the neck to eliminate this problem. Improved data using one of these capillaries are shown in Figure 30.

## 5.3 Calorimeter

An analytical model was used in order to understand the heat transfer expected from the reaction drops in the calorimeter. Since the capillary was long and thin, with a Biot number of about 0.01, the temperature was assumed uniform in the cross-section. For simplicity, a single material was used to represent both glass and water, with values for thermal conductivity $k$ and volumetric heat capacity $\rho c$ averaged over the capillary cross-section. Using symmetry (see Figure 17 in Section 4.5), only half the capillary (with one reaction drop) was analyzed. The boundary conditions were adiabatic at the center of the capillary, and isothermal ($T = 0$) at the end, where it met the copper mount.

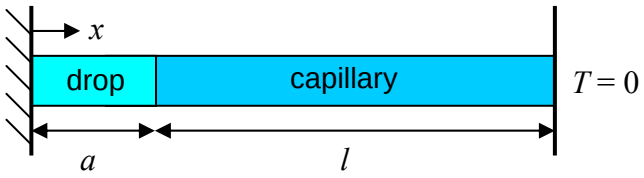


**Figure 31.** Diagram of capillary in heat loss model.

The geometry, illustrated in Figure 31, was adjusted to fit a solution available in the literature [155]. The same averaged material properties were used for the drop as for the capillary. Since mixing was fast, in the region representing the drop the initial temperature was set to $\Delta T_i$. Along the capillary itself, the initial temperature was 0, and heat was lost from the surface by convection and radiation with equivalent heat transfer coefficient $h$. Heat lost to the pipette tip was negligible due to its high thermal resistance.

The resulting temperature of the modeled capillary was [155]

$$\Delta T(x,t) = \frac{2\,\Delta T_i}{l} \exp\left(-\frac{4ht}{\rho c d}\right) \cdot \sum_{n=0}^{\infty} \left[ \exp\left(-\frac{\beta^2 kt}{\rho c}\right) \cdot \cos(\beta x) \cdot \int_0^a \cos(\beta x')\,dx' \right],$$

where $d$ is the capillary diameter, $t$ is time, and $\beta = (2n+1)\pi / 2l$. The fraction of the reaction energy contained in the capillary was

$$E(t) = \frac{1}{a \cdot \Delta T_i} \int_a^l \Delta T(x,t)\,dx\,, \tag{14}$$

shown plotted in Figure 32. As seen there, the model predicted a peak response 6 s after the drops were mixed, with 40% heat loss. The heat loss was a lower estimate due to the changed geometry, and the Teflon tape on the capillary. These extra thermal resistances were later approximated by increasing the lower limit of the integral in Equation 14, resulting in an estimated 60% heat loss at a peak 8 s after mixing.

Data from the calorimeter are shown in Figures 33 and 34. Data from some experiments, in which insufficient time elapsed for vapor equilibrium, the oil seal broke, the drops coalesced on their own, the drops did not mix due to poor alignment, or oil seeped into and soaked the Teflon tape on the capillary, were discarded. These problems were gradually eliminated with experience.

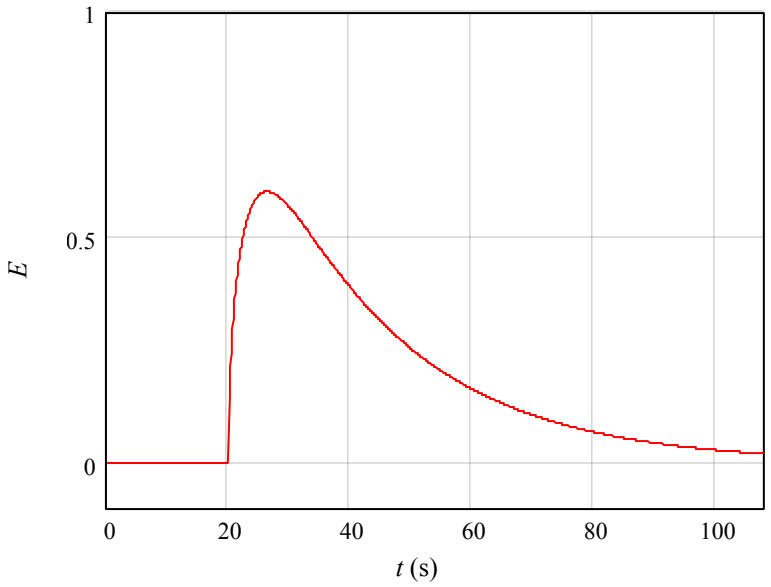


**Figure 32.** Fraction of reaction energy present in the modeled capillary. Time is shifted so that the reaction occurs at $t = 20$ s, as in the experiments. The drop volume was 1 µL, with $d = 1.5$ mm, $l - a = 5$ mm, $k = 1.05$ W/m·K, $\rho c = 2.39$ MJ/m$^3$·K, and $h = 12$ W/m$^2$·K [156].

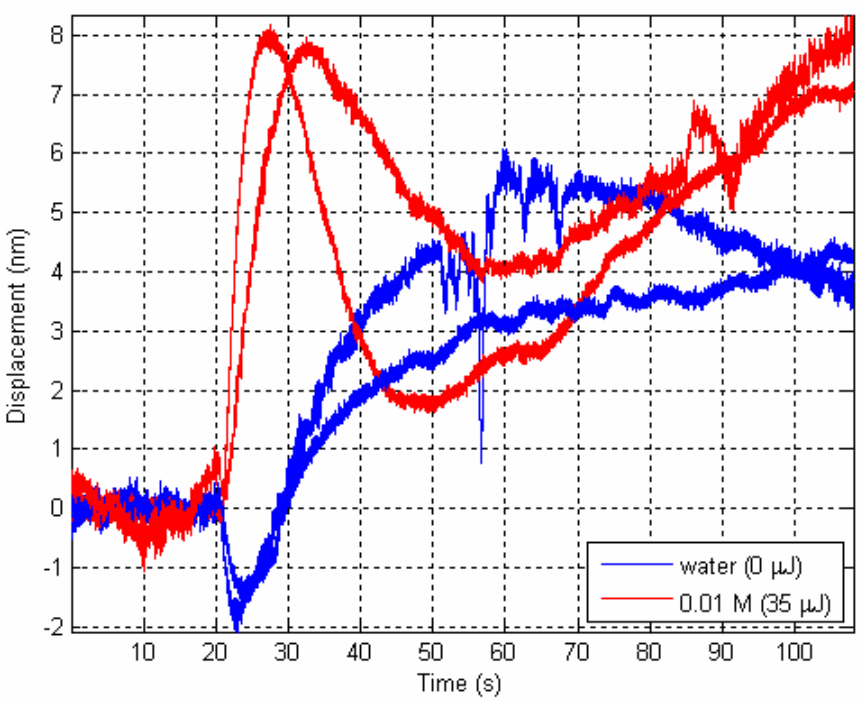


**Figure 33.** Data from four experiments with the calorimeter. At 20 s, 1 µL of water was mixed with 1 µL of either water or 0.01 M sulfuric acid. The data were detrended over the first 20 s. In one experiment, not shown, a jump probably due to contact line pinning occurred at 20 s, obscuring the signal.

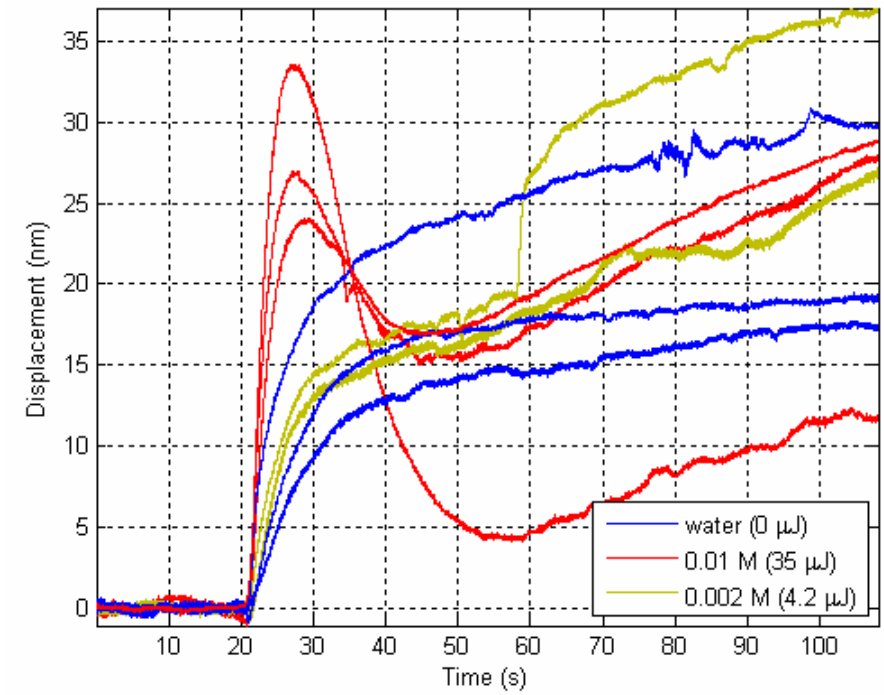


**Figure 34.** Data using a more sensitive capillary. The jump at 58 s in one of the yellow traces was probably due to contact line pinning. The higher peak and lower final level in one of the 0.01 M traces may have been due to a larger surface area for the merged drop in that experiment.

The resolution for the data in Figure 33 appeared to be below 10 μJ. The rising temperature at the end of each run was due to reduced evaporation from the merged drop, caused by its having a smaller surface area than the individual drops. The dip in the control traces after mixing may have been caused by evaporation of a small film of water left by the motion of the drops. The capillary used in these runs had a relatively large diameter neck, reducing its sensitivity, and was several months old, increasing the noise due to contact angle pinning. In experiments with a newer, more sensitive, capillary, the data were not as reproducible, but the 35 μJ signal was still easily distinguishable (Figure 34).

The data were in qualitative agreement with the shape of the model result (Figure 32). A calculation, shown in Table 6, gave the expected response of the calorimeter using the capillary in Figure 33. Heat lost to evaporation was estimated using the temperature dependence of the vapor pressure of water, and the volume of air surrounding the drops ($4.71 \times 10^{-7}$ $m^3$). The actual response was about half the predicted response. A possible reason was additional heat lost to evaporation, since the decrease in drop volume over several hours during the experiments evidenced that vapor was

condensing on other surfaces near the drops, at a rate corresponding to heat loss on the order of 30 μW.

| | |
|---|---|
| Enthalpy of reaction | 35 μJ |
| Heat lost to evaporation | 29 μJ |
| 60% heat loss | 12 μJ |
| Divided by heat capacity of drops + capillary | 0.16 mK |
| Times estimated capillary sensitivity | 15 nm |

**Table 6.** Calculation of expected peak calorimeter response for dilution of 0.01 M sulfuric acid.

# Chapter 6.
# Conclusion

## 6.1 Summary

In this thesis, a novel microcalorimeter was designed and built. It was based on a miniature liquid expansion thermometer.

The thermometer was capable of sub-microKelvin resolution about room temperature. The exact resolution depended on the measurement bandwidth. From Figure 30, in a bandwidth of 0.01 to 0.3 Hz, resolution was approximately 1 μK, while in a narrower bandwidth of 0.1 to 0.3 Hz, it was approximately 0.2 μK. Values for resolution in the literature are rarely given with a specified bandwidth; however, most probably correspond to the narrower bandwidth, as noise at frequencies below 0.1 Hz is often considered "drift". To our knowledge, no temperature measurement with equal resolution near room temperature has been reported in the literature; see Table 7. (This listing excludes a measurement of 2 μK temperature changes using a bimetallic microcantilever [126], since these variations were specifically imposed at 155 Hz and measured with lock-in detection.) Applications for high resolution thermometers include, besides calorimetry, critical point studies [161,162], and, as listed in [160], electronic noise measurement, standard cell enclosures, separation of isotopes, and metallurgical investigations.

The dominant noise sources in the thermometer were ambient temperature fluctuations and building vibrations. Ambient pressure fluctuations were possibly also significant, and in certain cases contact angle hysteresis was as well.

In the second part of this thesis, the setup was adapted to measure heat evolved during a dilution of sulfuric acid. The microcalorimeter achieved resolution of approximately 10 μJ.

| Resolution (μK) | Sensor | Reference |
|---|---|---|
| 0.5 | thermistor | [157] |
| 1 | quartz resonator | [93][a] |
| 1.2 | thermopile | [60][b] |
| 1.8 | thermistor | [158][b,c] |
| 2.3 | thermistor | [159] |
| 3.5 | thermistor | [160] |
| 3.8 | quartz resonator | [94] |

**Table 7.** High resolution temperature measurements in the literature. Resolution is expressed as three standard deviations or half of peak-to-peak noise, where possible. [a] Spassov reported resolution that Smith and Spencer had obtained, citing a reference written by A.G. Smagin in Russian. [b] These were measurements of a temperature difference between adjacent points, rather than an absolute temperature. [c] This result was disputed in [90].

While the goal of microKelvin resolution for the thermometer was realized, the energy resolution of the calorimeter was compromised by factors neglected in the simple calculation in Section 1.5. These included heat loss, disturbances due to evaporation and mixing, and the large heat capacity of the sensor.

In the next, final, section, two directions of future work will be discussed – improvements in the calorimeter resolution, and a proposed design for a high throughput instrument.

## 6.2 Future Work

Heat loss in the calorimeter is unavoidable and probably cannot be drastically reduced. However, the results of Torres et al. [64] exemplify improvements that may be made in other areas.

More work is needed to establish consistency in the mixing process and the environment surrounding the drops. Side-by-side sample and control reactions will also reduce evaporation disturbances. The benefit of the very low noise temperature sensor cannot be realized until these other noise sources no longer dominate. In [64], a twin setup was used and energy resolution was in fact limited by noise in the temperature sensor.

Room for improvement also exists in the minimization of the sensor's heat capacity. Using smaller drops and a sensor with a much smaller heat capacity, Torres et

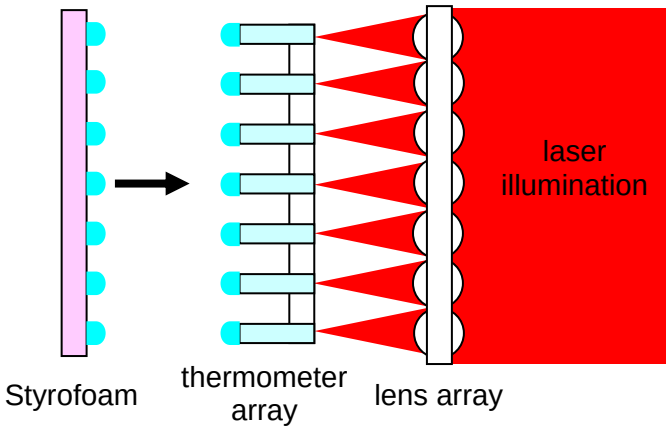


**Figure 35.** Design for a high throughput instrument.

al. [64] achieved a better energy resolution (0.5 μJ) with a much inferior temperature resolution (0.25 mK). Heat capacity may be reduced by a further miniaturization of the capillary using a different manufacturing process (see below), or by replacing water with a gas as the thermometric fluid [163].

An optical transducer was used in the microcalorimeter in order to facilitate the eventual goal of the project, which is a high throughput instrument. A proposed parallel design is illustrated in Figure 35. In it, the reaction takes place outside the capillaries, as was done in this thesis. This has the advantage of not requiring refilling and resealing of the capillaries between experiments. Still, for the purposes of improving the energy resolution and time constant, a design with the reaction occurring inside the capillaries may also merit consideration.

The thermometer array is made of glass, and the individual thermometers are thermally isolated from each other by air spaces. Such arrays may be most easily obtained as a custom order from a microtiter plate manufacturer (e.g., Grace Vydac[8] makes similar glass arrays). At the right ends, the wells are initially closed, and laser drilling may be used to create narrow diameter capillaries. Tapered holes of appropriate diameters are available from, e.g., Oxford Lasers[9].

After the capillaries have been filled, sealing the left ends using a flame, as was done in this thesis, would likely not be practical. Two possible alternatives are an epoxy seal and a silicone seal – in [164], 300 kPa seals were created in a silicone microfluidic

[8] www.grom.de/plates.htm.
[9] www.oxfordlasers.com/applications/laser_drilling.htm.

device by puncturing it with steel needles. In either case, the initial opening at the left end should be narrow, to minimize the seal area.

A uniform meniscus level across the whole array would be necessary in order to image all of the menisci at once. This might be achieved by heating the entire array uniformly to overflow all of the wells; removing the overflowed fluid; immersing the array in mineral oil while lowering the temperature; and finally, removing the oil at a specific temperature and allowing the array to cool further to ambient temperature. The depth of focus in the single well calorimeter was about 0.2 mm, which is a realistic goal for the meniscus height uniformity across a whole array.

The mixing design used in this thesis would also need to be modified in a parallelized instrument. Instead, as shown in the design in Figure 35, a drop of one reactant is placed on the back end of each capillary, with arrayed drops of the other reactant on a Styrofoam plate with a hydrophobic coating (e.g., parylene or Teflon). Mixing is initiated by bringing the plate close enough to the array that each pair of drops, but not the plate and capillaries, comes into contact.

Some capillaries are reserved for control reactions for subtraction of common mode noise. Steps must also be taken to minimize evaporation, as discussed in Section 4.5. Monomolecular surface films [165] have been suggested to retard evaporation; such films would need to allow mixing, re-form after mixing, and not interfere with reagents. Screening compounds with high vapor pressure may be difficult if the sealed volume is too large; minimizing the time required for thermal equilibrium will be essential.

The displacement of the menisci is detected using a parallel Michelson interferometer. A lens array would replace the objective used in the single well instrument, and a CCD or CMOS camera would replace the photodiode. Somewhat similar parallel setups have been described in [166,167], and a parallel fluorescence imager for capillary electrophoresis is currently under development in the MIT Bioinstrumentation Lab.

With conventional Michelson interferometer optics, the sensitivity is high only in the linear portions of the sine wave. In order to measure all meniscus heights in the array simultaneously with equal sensitivity, polarization optics may be used to record phase as well as intensity, as described in [168].

Heat loss would be an important issue for any parallel design. Since the drops are small and mixing is fast, the reaction can be modeled as an instantaneous energy source. We will also assume that the epoxy or silicone sealing the capillary is thin enough to be neglected.

Heat may be lost into the Styrofoam plate. If we approximate the capillary and Styrofoam as semi-infinite bodies, the temperature change of each is described by

$$\Delta T(x,t) = \frac{E}{\sqrt{\pi k \rho c_P t}} \exp\left( -\frac{\rho c_P x^2}{4kt} \right), \tag{15}$$

where $E$ is the energy entering each body, $k$ is its thermal conductivity, $\rho$ is its density, $c_P$ is its specific heat, $x$ is distance, and $t$ is time [169]. If we consider the merged drop to be isothermal, then the capillary and Styrofoam would have equal values of $\Delta T(0,t)$. It then follows from Equation 15 that the ratio of energy entering each body would be equal to the ratio of the respective values of $\sqrt{k \rho c_P}$, meaning that only 3% of the reaction heat would be lost into the Styrofoam. We can therefore consider the Styrofoam to be an adiabatic surface.

The above calculation neglected lateral heat flow in the Styrofoam. However, heat loss from the capillary is expected to be greater, which would increase the proportion of heat flowing into the capillary.

If the connecting glass on the right ends of the capillaries in Figure 35 is thick enough to be treated as a heat sink, then the model solution for heat loss from Section 4.5 applies to this design too. It might be used to optimize the dimensions of the capillary.

The heat loss solution can also be used to calculate thermal cross-talk between the capillaries. For capillaries of diameter 1.5 mm and length 5 mm, the model predicts that 37% of heat loss is via convection and radiation, with the remaining heat conducted along the capillary's entire length. If, by symmetry, the lost heat is assumed to be absorbed in equal parts by the four nearest capillaries in the array, the false positive signal is at most 9%. It is also likely to appear with a distinctly different profile in time.

# Appendix

Following is the code for the computer program described in Section 4.4:

```
Option Explicit

Dim m1 As New Motor, slp As New sleep
Dim mode As String, path As String
Dim i As Long, datapoints As Long
Dim volt1 As Double, volt2 As Double, volt3 As Double, volt4 As Double, volt5 As Double
Dim volt6 As Double, volt7 As Double, volt8 As Double
Dim temp1 As Double, temp2 As Double, temp3 As Double, temp4 As Double, temp5 As Double
Dim temp6 As Double, temp7 As Double, temp8 As Double
Dim sumtemp1 As Double, sumtemp2 As Double, sumtemp3 As Double, sumtemp4 As Double
Dim sumtemp5 As Double, sumtemp6 As Double, sumtemp7 As Double, sumtemp8 As Double
Dim ambtemp As Double, captemp As Double
Dim temp_timer_index As Long
Dim A As Double, B As Double
Dim motor_position As Double
Dim stop_recording As Boolean
Dim data() As Double


Private Sub Form_Load()
  path = "c:\Robert\data\"
  mode = ""
  A = 0.003908          'constants for RTD fit (Callendar-Van Dusen) for alpha = 0.00385
  B = -0.0000005775
  stop_recording = False
  motor_position = 0
  Call m1.init(Motorport)
  Call m1.Shut
End Sub


Private Sub Start_T_ctl_Click()
  Dim Junk As String

  If Not MSComm4.PortOpen Then MSComm4.PortOpen = True
  If Not DAQ.PortOpen Then DAQ.PortOpen = True
  If Not MSComm6.PortOpen Then MSComm6.PortOpen = True
  If Not MSComm7.PortOpen Then MSComm7.PortOpen = True

  Junk = DAQ.Input
  Call slp.SleepMS(200)
  DAQ.Output = "*RST" & vbCrLf          'factory reset
  Call slp.SleepMS(500)
```

```
  volt1 = 0: volt2 = 0: volt3 = 0: volt4 = 0: volt5 = 0: volt6 = 0: volt7 = 0: volt8 = 0
  temp_timer_index = 0      'cycles through reading temperature from each RTD
  T_ctl_timer.Enabled = True
End Sub


Private Sub Stop_T_ctl_Click()
  T_ctl_timer.Enabled = False
End Sub


Private Sub T_ctl_timer_Timer()
  Dim x As String, j As Long, d As Double

  'plastic
  If temp_timer_index = 0 Then
    DAQ.Output = "MEAS:FRES? AUTO,MIN,(@105)" & vbCrLf
    templabel1.ForeColor = &HFF&
  ElseIf temp_timer_index = 14 Then
    templabel1.ForeColor = &H80000012
    x = DAQ.Input
    If Len(x) = 17 Then
      temp1 = (-100 * A + Sqr(10000 * A ^ 2 - 400 * B * (100 - CDbl(x)))) / (200 * B)
      temptext1.Text = temp1
      If ramp.Value Then set_temp1.Text = CStr(CDbl(set_temp1.Text) + ramptext.Text)
      sumtemp1 = i_sum1.Text + (set_temp1.Text - temp1)
      If sumtemp1 > 10 Then sumtemp1 = 10
      If sumtemp1 < 0 Then sumtemp1 = 0
      i_sum1.Text = Round(sumtemp1, 6)
      volt1 = (set_temp1.Text - temp1) * p1.Text + (sumtemp1 * i1.Text)
      If volt1 < 0 Then volt1 = 0
      If volt1 > 3 Then volt1 = 3
      MSComm6.Output = "APPL P25V, " & volt1 & vbCrLf
    End If

  'objective
  ElseIf temp_timer_index = 15 Then
    DAQ.Output = "MEAS:FRES? AUTO,MIN,(@102)" & vbCrLf
    templabel2.ForeColor = &HFF&
  ElseIf temp_timer_index = 29 Then
    templabel2.ForeColor = &H80000012
    x = DAQ.Input
    If Len(x) = 17 Then
      temp2 = (-100 * A + Sqr(10000 * A ^ 2 - 400 * B * (100 - CDbl(x)))) / (200 * B)
      temptext2.Text = temp2
      If ramp.Value Then set_temp2.Text = CStr(CDbl(set_temp2.Text) + ramptext.Text)
      sumtemp2 = i_sum2.Text + (set_temp2.Text - temp2)
      If sumtemp2 > 10 Then sumtemp2 = 10
      If sumtemp2 < 0 Then sumtemp2 = 0
      i_sum2.Text = Round(sumtemp2, 6)
      volt2 = (set_temp2.Text - temp2) * p2.Text + (sumtemp2 * i2.Text)
```

```
    If volt2 < 0 Then volt2 = 0
    If volt2 > 3 Then volt2 = 3
    MSComm7.Output = "APPL P25V, " & volt2 & vbCrLf
  End If

'under box
ElseIf temp_timer_index = 30 Then
  DAQ.Output = "MEAS:FRES? AUTO,MIN,(@103)" & vbCrLf
  templabel3.ForeColor = &HFF&
ElseIf temp_timer_index = 44 Then
  templabel3.ForeColor = &H80000012
  x = DAQ.Input
  If Len(x) = 17 Then
    temp3 = (-100 * A + Sqr(10000 * A ^ 2 - 400 * B * (100 - CDbl(x)))) / (200 * B) + 0.088
    temptext3.Text = temp3
    If ramp.Value Then set_temp3.Text = CStr(CDbl(set_temp3.Text) + ramptext.Text)
    sumtemp3 = i_sum3.Text + (set_temp3.Text - temp3)
    If sumtemp3 > 10 Then sumtemp3 = 10
    If sumtemp3 < 0 Then sumtemp3 = 0
    i_sum3.Text = Round(sumtemp3, 6)
    volt3 = (set_temp3.Text - temp3) * p3.Text + (sumtemp3 * i3.Text)
    If volt3 < 0 Then volt3 = 0
    If volt3 > 3 Then volt3 = 3
    MSComm7.Output = "APPL P6V, " & volt3 & vbCrLf
  End If

'motor
ElseIf temp_timer_index = 45 Then
  DAQ.Output = "MEAS:FRES? AUTO,MIN,(@108)" & vbCrLf
  templabel4.ForeColor = &HFF&
ElseIf temp_timer_index = 59 Then
  templabel4.ForeColor = &H80000012
  x = DAQ.Input
  If Len(x) = 17 Then
    temp4 = (-100 * A + Sqr(10000 * A ^ 2 - 400 * B * (100 - CDbl(x)))) / (200 * B) + 0.018
    temptext4.Text = temp4
    If ramp.Value Then set_temp4.Text = CStr(CDbl(set_temp4.Text) + ramptext.Text)
    sumtemp4 = i_sum4.Text + (set_temp4.Text - temp4)
    If sumtemp4 > 10 Then sumtemp4 = 10
    If sumtemp4 < 0 Then sumtemp4 = 0
    i_sum4.Text = Round(sumtemp4, 6)
    volt4 = (set_temp4.Text - temp4) * p4.Text + (sumtemp4 * i4.Text)
    If volt4 < 0 Then volt4 = 0
    If volt4 > 3 Then volt4 = 3
    MSComm6.Output = "APPL N25V, -" & volt4 & vbCrLf
  End If

'box
ElseIf temp_timer_index = 60 Then
  DAQ.Output = "MEAS:FRES? AUTO,MIN,(@101)" & vbCrLf
  templabel5.ForeColor = &HFF&
```

```
ElseIf temp_timer_index = 74 Then
  templabel5.ForeColor = &H80000012
  x = DAQ.Input
  If Len(x) = 17 Then
    temp5 = (-100 * A + Sqr(10000 * A ^ 2 - 400 * B * (100 - CDbl(x)))) / (200 * B) + 0.03
    temptext5.Text = temp5
    If ramp.Value Then set_temp5.Text = CStr(CDbl(set_temp5.Text) + ramptext.Text)
    sumtemp5 = i_sum5.Text + (set_temp5.Text - temp5)
    If sumtemp5 > 10 Then sumtemp5 = 10
    If sumtemp5 < 0 Then sumtemp5 = 0
    i_sum5.Text = Round(sumtemp5, 6)
    volt5 = (set_temp5.Text - temp5) * p5.Text + (sumtemp5 * i5.Text)
    If volt5 < 0 Then volt5 = 0
    If volt5 > 3 Then volt5 = 3
    MSComm7.Output = "APPL N25V, -" & volt5 & vbCrLf
  End If

'behind box
ElseIf temp_timer_index = 75 Then
  DAQ.Output = "MEAS:FRES? AUTO,MIN,(@109)" & vbCrLf
  templabel6.ForeColor = &HFF&
ElseIf temp_timer_index = 89 Then
  templabel6.ForeColor = &H80000012
  x = DAQ.Input
  If Len(x) = 17 Then
    temp6 = (-100 * A + Sqr(10000 * A ^ 2 - 400 * B * (100 - CDbl(x)))) / (200 * B) + 0.073
    temptext6.Text = temp6
    If ramp.Value Then set_temp6.Text = CStr(CDbl(set_temp6.Text) + ramptext.Text)
    sumtemp6 = i_sum6.Text + (set_temp6.Text - temp6)
    If sumtemp6 > 10 Then sumtemp6 = 10
    If sumtemp6 < 0 Then sumtemp6 = 0
    i_sum6.Text = Round(sumtemp6, 6)
    volt6 = (set_temp6.Text - temp6) * p6.Text + (sumtemp6 * i6.Text)
    If volt6 < 0 Then volt6 = 0
    If volt6 > 3 Then volt6 = 3
    MSComm6.Output = "APPL P6V, " & volt6 & vbCrLf
  End If

'peltier
ElseIf temp_timer_index = 90 Then
  DAQ.Output = "MEAS:FRES? AUTO,MIN,(@107)" & vbCrLf
  templabel7.ForeColor = &HFF&
ElseIf temp_timer_index = 104 Then
  templabel7.ForeColor = &H80000012
  x = DAQ.Input
  If Len(x) = 17 Then
    temp7 = (-100 * A + Sqr(10000 * A ^ 2 - 400 * B * (100 - CDbl(x)))) / (200 * B)
    If temp7 < 15 Then temp7 = 15
    temptext7.Text = temp7
    sumtemp7 = i_sum7.Text + (set_temp7.Text - temp7)
    If sumtemp7 > 0 Then sumtemp7 = 0
```

```
    If sumtemp7 < -10 Then sumtemp7 = -10
    i_sum7.Text = Round(sumtemp7, 6)
    volt7 = (set_temp7.Text - temp7) * p7.Text + (sumtemp7 * i7.Text)
    If volt7 < 0 Then volt7 = 0
    If volt7 > 4 Then volt7 = 4
    MSComm4.Output = "APPL P6V, " & volt7 & vbCrLf
  End If

'laser
ElseIf temp_timer_index = 105 Then
  DAQ.Output = "MEAS:FRES? AUTO,MIN,(@110)" & vbCrLf
  templabel8.ForeColor = &HFF&
ElseIf temp_timer_index = 119 Then
  templabel8.ForeColor = &H80000012
  x = DAQ.Input
  If Len(x) = 17 Then
    temp8 = (-100 * A + Sqr(10000 * A ^ 2 - 400 * B * (100 - CDbl(x)))) / (200 * B)
    temptext8.Text = temp8
    sumtemp8 = i_sum8.Text + (set_temp8.Text - temp8)
    If sumtemp8 > 10 Then sumtemp8 = 10
    If sumtemp8 < 0 Then sumtemp8 = 0
    i_sum8.Text = Round(sumtemp8, 6)
    volt8 = (set_temp8.Text - temp8) * p8.Text + (sumtemp8 * i8.Text)
    If volt8 < 0 Then volt8 = 0
    If volt8 > 3 Then volt8 = 3
    MSComm4.Output = "APPL N25V, -" & volt8 & vbCrLf
  End If

'capillary
ElseIf temp_timer_index = 120 Then
  DAQ.Output = "MEAS:FRES? AUTO,MIN,(@104)" & vbCrLf
  caplabel.ForeColor = &HFF&
ElseIf temp_timer_index = 134 Then
  caplabel.ForeColor = &H80000012
  x = DAQ.Input
  If Len(x) = 17 Then
    captemp = (-100 * A + Sqr(10000 * A ^ 2 - 400 * B * (100 - CDbl(x)))) / (200 * B) + 0.106
    captext.Text = captemp
  End If

'ambient
ElseIf temp_timer_index = 135 Then
  DAQ.Output = "MEAS:FRES? AUTO,MIN,(@106)" & vbCrLf
  amblabel.ForeColor = &HFF&
ElseIf temp_timer_index = 149 Then
  amblabel.ForeColor = &H80000012
  x = DAQ.Input
  If Len(x) = 17 Then
    ambtemp = (-100 * A + Sqr(10000 * A ^ 2 - 400 * B * (100 - CDbl(x)))) / (200 * B)
    ambtext.Text = ambtemp
  End If
```

```
  End If

  temp_timer_index = temp_timer_index + 1
  If temp_timer_index = 150 Then temp_timer_index = 0

  If mode = "monitor" And temp_timer_index Mod 10 = 0 Then
    d = 0
    For j = 1 To 200
      d = d + ADC(0)  'National Instruments DAQ card
    Next j
    d = d / 200
    Open path & "monitor.txt" For Append As #2
    Print #2, temp1, temp2, temp3, temp4, temp5, temp6, temp7, temp8, captemp, ambtemp, _
          set_temp2, d
    Close #2
  End If

  If volt1 > 3.5 Or volt2 > 3.5 Or volt3 > 3.5 Or volt4 > 3.5 Or volt5 > 3.5 Or volt6 > 4.5 Or _
     volt7 > 3.5 Or volt8 > 3.5 Or temp1 > 30 Or temp2 > 30 Or temp3 > 30 Or temp4 > 30 Or _
     temp5 > 30 Or temp6 > 30 Or temp7 > 30 Or temp8 > 30 Then
    T_ctl_timer.Enabled = False
    Call AddText("Too hot!")
    MSComm6.Output = "APPL P6V, 0.0" & vbCrLf
    MSComm6.Output = "APPL P25V, 0.0" & vbCrLf
    MSComm6.Output = "APPL N25V, -0.0" & vbCrLf
    MSComm7.Output = "APPL P6V, 0.0" & vbCrLf
    MSComm7.Output = "APPL P25V, 0.0" & vbCrLf
    MSComm7.Output = "APPL N25V, -0.0" & vbCrLf
  End If
End Sub


Private Sub Start_Click()
  RichTextBox1.Text = ""
  stop_recording = False
  If Option13.Value Then
    mode = "heat"
    Call Heat
  ElseIf Option3.Value Then
    mode = "monitor"
    Call Monitor
  End If
End Sub


Private Sub Record()
  Dim j As Long

  For i = 0 To datapoints
    If stop_recording Then Exit For

    If mode = "heat" And i = Text2.Text Then
```

```
      Call m1.Move(dist.Text, vel.Text)
      Call m1.Move(-dist.Text, vel.Text)
    End If

    data(i) = 0
    For j = 1 To 25
      data(i) = data(i) + ADC(0)  'National Instruments DAQ card
    Next j
    data(i) = data(i) / 25
  Next i

  If mode = "heat" Then
    Open path & "signal.txt" For Output As #1
    For j = 0 To datapoints - 1
      Print #1, data(j)
    Next j
    Close #1
    Call AddText("Heat done.")
    Beep
  End If
End Sub


Private Sub Heat()
  If Not MSComm4.PortOpen Then MSComm4.PortOpen = True
  If Not DAQ.PortOpen Then DAQ.PortOpen = True
  If Not MSComm6.PortOpen Then MSComm6.PortOpen = True
  If Not MSComm7.PortOpen Then MSComm7.PortOpen = True
  datapoints = Text1.Text
  ReDim data(datapoints)
  Call Record
End Sub


Private Sub Monitor()
  Call AddText("Monitoring...")
  Open path & "monitor.txt" For Output As #2   'clear the file
  Close #2
End Sub


Private Sub Stop_Click()
  stop_recording = True
  mode = ""
  Call AddText("Stopped.")
End Sub


Private Sub Form_Unload(Cancel As Integer)
  Text3.Text = 0
  If Motorport.PortOpen Then Motorport.PortOpen = False
  If MSComm4.PortOpen Then MSComm4.PortOpen = False
  If DAQ.PortOpen Then DAQ.PortOpen = False
```

```
  If MSComm6.PortOpen Then MSComm6.PortOpen = False
  If MSComm7.PortOpen Then MSComm7.PortOpen = False
End Sub


Private Sub AddText(s As Variant)
  RichTextBox1.Text = RichTextBox1.Text & CStr(s) & Chr(10)
End Sub


Private Sub Check2_Click()
  If Check2.Value Then
    Call m1.UnShut
    Check2.ForeColor = &HFF&
  Else
    Call m1.Shut
    Check2.ForeColor = &H80000012
  End If
End Sub


Private Sub Command3_Click()
  Call m1.UnShut
  Call m1.Move(Text3.Text - motor_position, vel.Text)
  motor_position = Text3.Text
  Call m1.Shut
End Sub


Private Sub Command5_Click()
  motor_position = 0
  Text3.Text = "0"
End Sub
```

# References


1. Pharmaceutical Researchers and Manufacturers of America. "The Value of Medicines." www.phrma.org (2001).
2. Pharmaceutical Researchers and Manufacturers of America. "Pharmaceutical Industry Profile 2003." www.phrma.org (2003).
3. J.A. DiMasi, R.W. Hansen, H.G. Grabowski. "The price of innovation: new estimates of drug development costs." *Journal of Health Economics* 22: 151 (2003).
4. M.A. Lindsay. "Target discovery." *Nature Reviews Drug Discovery* 2: 831 (2003).
5. J. Drews. "Drug discovery: a historical perspective." *Science* 287: 1960 (2000).
6. B.K. Shoichet. "Virtual screening of chemical libraries." *Nature* 432: 862 (2004).
7. W.P. Walters, M. Namchuk. "Designing screens: how to make your hits a hit." *Nature Reviews Drug Discovery* 2: 259 (2003).
8. J.A. DiMasi. "The value of improving the productivity of the drug development process: faster times and better decisions." *Pharmacoeconomics* 20 (Suppl. 3): 1 (2002).
9. C. Dalvit, E. Ardini, G.P. Fogliatto, N. Mongelli, M. Veronesi. "Reliable high-throughput functional screening with 3-FABS." *Drug Discovery Today* 9: 595 (2004).
10. A. Dove. "Screening for content – the evolution of high throughput." *Nature Biotechnology* 21: 859 (2003).
11. M. Bruchez Jr., M. Moronne, P. Gin, S. Weiss, A.P. Alivisatos. "Semiconductor nanocrystals as fluorescent biological labels." *Science* 281: 2013 (1998).
12. W.C.W. Chan, S. Nie. "Quantum dot bioconjugates for ultrasensitive nonisotopic detection." *Science* 281: 2016 (1998).
13. M. Ozkan. "Quantum dots and other nanoparticles: what can they offer to drug discovery?" *Drug Discovery Today* 9: 1065 (2004).
14. A.S. Verkman. "Drug discovery in academia." *American Journal of Physiology – Cell Physiology* 286: C465 (2004).
15. J. Ireson, private communication.
16. K.D. Pavey, C.J. Olliff, F. Paul. "Quartz crystal resonant sensor (QCRS) model for label-free, small molecules—receptor studies." *Analyst* 126: 1711 (2001).
17. R. Macarrón, R.P. Hertzberg. "Design and implementation of high throughput screening assays." In: W.P. Janzen, ed. "High Throughput Screening: Methods and Protocols." Humana Press (2002).
18. M. Vaschetto, T. Weissbrod, D. Bodle, O. Guner. "Enabling high-throughput discovery." *Current Opinion in Drug Discovery & Development* 6: 377 (2003).
19. C. Dickey. "Protein and binding event detection without labels." *Drug Discovery & Development* (August 2003).

20. J. Homola. "Present and future of surface plasmon resonance biosensors." *Analytical and Bioanalytical Chemistry* 377: 528 (2003).

21. M.A. Cooper. "Optical biosensors in drug discovery." *Nature Reviews Drug Discovery* 1: 515 (2002).

22. P. Englebienne, A. Van Hoonacker, M. Verhas. "High-throughput screening using the surface plasmon resonance effect of colloidal gold nanoparticles." *Analyst* 126: 1645 (2001).

23. M. Piliarik, H. Vaisocherová, J. Homola. "A new surface plasmon resonance sensor for high-throughput screening applications." *Biosensors & Bioelectronics* 20: 2104 (2005).

24. J. Homola, H. Vaisocherová, J. Dostálek, M. Piliarik. "Multi-analyte surface plasmon resonance biosensing." *Methods* 37: 26 (2005).

25. M.A. Cooper. "Label-free screening of bio-molecular interactions." *Analytical and Bioanalytical Chemistry* 377: 834 (2003).

26. P.A. van der Merwe. "Surface plasmon resonance." In: S.E. Harding, B.Z. Chowdhry, eds. "Protein-ligand Interactions: Hydrodynamics and Calorimetry." Oxford University Press (2001).

27. J.-C. Peter, J.-P. Briand, J. Hoebeke. "How biotinylation can interfere with recognition: a surface plasmon resonance study of peptide-antibody interactions." *Journal of Immunological Methods* 274: 149 (2003).

28. P. Pattnaik. "Surface plasmon resonance – applications in understanding receptor-ligand interaction." *Applied Biochemistry and Biotechnology* 126: 79 (2005).

29. D.G. Myszka. "Analysis of small-molecule interactions using Biacore S51 technology." *Analytical Biochemistry* 329: 316 (2004).

30. Biacore. "Biacore S51 Product Information." www.biacore.com (2005).

31. P.Y. Li, B. Lin, J. Gerstenmaier, B.T. Cunningham. "A new method for label-free imaging of biomolecular interactions." *Sensors and Actuators B – Chemical* 99: 6 (2004).

32. D.A. Markov, K. Swinney, D.J. Bornhop. "Label-free molecular interaction determinations with nanoscale interferometry." *Journal of the American Chemical Society* 126: 16659 (2004).

33. J.C. Latham, D.A. Markov, H.S. Sorensen, D.J. Bornhop. "Photobiotin surface chemistry improves label-free interferometric sensing of biochemical interactions." *Angewandte Chemie – International Edition* 45: 955 (2006).

34. K.A. Marx. "Quartz crystal microbalance: a useful tool for studying thin polymer films and complex biomolecular systems at the solution-surface interface." *Biomacromolecules* 4: 1099 (2003).

35. B. Godber, K.S.J. Thompson, M. Rehak, Y. Uludag, S. Kelling, A. Sleptsov, M. Frogley, K. Wiehler, C. Whalen, M.A. Cooper. "Direct quantification of analyte concentration by resonant acoustic profiling." *Clinical Chemistry* 51: 1962 (2005).

36. K.D. Pavey, C.J. Olliff, F. Paul. "Development of novel liquid phase QCRS sensor technology." *Journal of Thermal Analysis and Calorimetry* 71: 83 (2003).

37. W.U. Wang, C. Chen, K.H. Lin, Y. Fang, C.M. Lieber. "Label-free detection of small-molecule–protein interactions by using nanowire nanosensors." *Proceedings of the National Academy of Sciences of the United States of America* 102: 3208 (2005).

38. W.A. Korfmacher. "Principles and applications of LC-MS in new drug discovery." *Drug Discovery Today* 10: 1357 (2005).

39. K. Benkestock, C.K. Van Pelt, T. Akerud, A. Sterling, P.O. Edlund, J. Roeraade. "Automated nano-electrospray mass spectrometry for protein-ligand screening by noncovalent interaction applied to human H-FABP and A-FABP." *Journal of Biomolecular Screening* 8: 247 (2003).

40. K. De Vriendt, K. Sandra, T. Desmet, W. Nerinckx, J. Van Beeumen, B. Devreese. "Evaluation of automated nano-electrospray mass spectrometry in the determination of non-covalent protein-ligand complexes." *Rapid Communications in Mass Spectrometry* 18: 3061 (2004).

41. H. Zehender, F. Le Goff, N. Lehmann, I. Filipuzzi, L.M. Mayr. "SpeedScreen: the "missing link" between genomics and lead discovery." *Journal of Biomolecular Screening* 9: 498 (2004).

42. M.W. Pantoliano, A.W. Rhind, F.R. Salemme. US6020141 (2000).

43. M.W. Pantoliano, E.C. Petrella, J.D. Kwasnoski, V.S. Lobanov, J. Myslik, E. Graf, T. Carver, E. Asel, B.A. Springer, P. Lane, F.R. Salemme. "High-density miniaturized thermal shift assays as a general strategy for drug discovery." *Journal of Biomolecular Screening* 6: 429 (2001).

44. M.-C. Lo, A. Aulabaugh, G. Jin, R. Cowling, J. Bard, M. Malamas, G. Ellestad. "Evaluation of fluorescence-based thermal shift assays for hit identification in drug discovery." *Analytical Biochemistry* 332: 153 (2004).

45. D. Matulis, J.K. Kranz, F.R. Salemme, M.J. Todd. "Thermodynamic stability of carbonic anhydrase: measurements of binding affinity and stoichiometry using ThermoFluor." *Biochemistry* 44: 5258 (2005).

46. F. Eggers, U. Kaatze. "Broad-band ultrasonic measurement techniques for liquids." *Measurement Science & Technology* 7: 1 (1996).

47. T.V. Chalikian. "Volumetric properties of proteins." *Annual Review of Biophysics and Biomolecular Structure* 32: 207 (2003).

48. D.N. Dubins, R. Filfil, R.B. Macgregor, T.V. Chalikian. "Role of water in protein-ligand interactions: volumetric characterization of the binding of 2'-CMP and 3'-CMP to ribonuclease A." *Journal of Physical Chemistry B* 104: 390 (2000).

49. A.P. Sarvazyan, D.P. Kharakoz. "Small-volume differential manometer for ultrasonic velocity and absorption measurements." *Instruments and Experimental Techniques* 24: 782 (1981).

50. V. Buckin, B. O'Driscoll, C. Smyth. "Ultrasonic spectroscopy for material analysis. Recent advances." *Spectroscopy Europe* 15: 20 (2003).

51. S. Gaisford, G. Buckton. "Potential applications of microcalorimetry for the study of physical processes in pharmaceuticals." *Thermochimica Acta* 380: 185 (2001).

52. G.A. Holdgate, W.H.J. Ward. "Measurements of binding thermodynamics in drug discovery." *Drug Discovery Today* 10: 1543 (2005).

53. H.W. Linde, L.B. Rogers, D.N. Hume. "Automatic thermometric titrations." *Analytical Chemistry* 25: 404 (1953).

54. J.J. Christensen, J.W. Gardner, D.J. Eatough, R.M. Izatt, P.J. Watts, R.M. Hart. "An isothermal titration microcalorimeter." *Review of Scientific Instruments* 44: 481 (1973).

55. C.H. Spink, I. Wadsö. "Calorimetry as an analytical tool in biochemistry and biology." In: D. Glick, ed. "Methods of Biochemical Analysis." Vol. 23, John Wiley & Sons (1976).

56. I.R. McKinnon, L. Fall, A. Parody-Morreale, S.J. Gill. "A twin titration microcalorimeter for the study of biochemical reactions." *Analytical Biochemistry* 139: 134 (1984).

57. T. Wiseman, S. Williston, J.F. Brandts, L.-N. Lin. "Rapid measurement of binding constants and heats of binding using a new titration calorimeter." *Analytical Biochemistry* 179: 131 (1989).

58. E. Freire, O.L. Mayorga, M. Straume. "Isothermal titration calorimetry." *Analytical Chemistry* 62: 950A (1990).

59. E.K. Merabet, H.K. Yuen, W.A. Grote, K.L. Deppermann. "A high sensitivity titration calorimeter using pyroelectric sensor." *Journal of Thermal Analysis* 42: 895 (1994).

60. A. Velázquez-Campoy, O. López-Mayorga, M.A. Cabrerizo-Vílchez. "Development of an isothermal titration microcalorimetric system with digital control and dynamic power Peltier compensation. I. Description and basic performance." *Review of Scientific Instruments* 71: 1824 (2000).

61. E. Hitt. "Label-free methods are not problem free." *Drug Discovery & Development* (September 2004).

62. Y.S.N. Day, C. Baird, R.L. Rich, D.G. Myszka. "Direct comparison of binding equilibrium, thermodynamic, and rate constants determined by surface- and solution-based biophysical methods." *Protein Science* 11: 1017 (2002).

63. P.C. Weber, F.R. Salemme. "Applications of calorimetric methods to drug discovery and the study of protein interactions." *Current Opinion in Structural Biology* 13: 115 (2003).

64. F.E. Torres, P. Kuhn, D. De Bruyker, A.G. Bell, M.V. Wolkin, E. Peeters, J.R. Williamson, G.B. Anderson, G.P. Schmitz, M.I. Recht, S. Schweizer, L.G. Scott, J.H. Ho, S.A. Elrod, P.G. Schultz, R.A. Lerner, R.H. Bruce. "Enthalpy arrays." *Proceedings of the National Academy of Sciences of the United States of America* 101: 9517 (2004).

65. B. Xie, K. Ramanathan, B. Danielsson. "Mini / micro thermal biosensors and other related devices for biochemical / clinical analysis and monitoring." *Trends in Analytical Chemistry* 19: 340 (2000).

66. B. Xie, U. Harborn, M. Mecklenburg, B. Danielsson. "Urea and lactate determined in 1-μL whole-blood samples with a miniaturized thermal biosensor." *Clinical Chemistry* 40: 2282 (1994).

67. A.W. van Herwaarden. "Overview of calorimeter chips for various applications." *Thermochimica Acta* 432: 192 (2005).

68. P. Bataillard, E. Steffgen, S. Haemmerli, A. Manz, H.M. Widmer. "An integrated silicon thermopile as biosensor for the thermal monitoring of glucose, urea and penicillin." *Biosensors & Bioelectronics* 8: 89 (1993).

69. B. Xie, M. Mecklenburg, B. Danielsson, O. Öhman, F. Winquist. "Microbiosensor based on an integrated thermopile." *Analytica Chimica Acta* 299: 165 (1994).

70. J.M. Köhler, M. Zieren. "Chip reactor for microfluid calorimetry." *Thermochimica Acta* 310: 25 (1998).

71. J. Lerchner, A. Wolf, G. Wolf. "Recent developments in integrated circuit calorimetry." *Journal of Thermal Analysis and Calorimetry* 57: 241 (1999).

72. E.A. Johannessen, J.M.R. Weaver, L. Bourova, P. Svoboda, P.H. Cobbold, J.M. Cooper. "Micromachined nanocalorimetric sensor for ultra-low-volume cell-based assays." *Analytical Chemistry* 74: 2190 (2002).

73. J. Lerchner, A. Wolf, R. Hüttl, G. Wolf. "Direct monitoring of biochemical processes using micro-structured heat power detectors." *Chemical Engineering Journal* 101: 187 (2004).

74. Y. Zhang, S. Tadigadapa. "Calorimetric biosensors with integrated microfluidic channels." *Biosensors & Bioelectronics* 19: 1733 (2004).

75. E.B. Chancellor, J.P. Wikswo, F. Baudenbacher, M. Radparvar, D. Osterman. "Heat conduction calorimeter for massively parallel high throughput measurements with picoliter sample volumes." *Applied Physics Letters* 85: 2408 (2004).

76. V. Baier, R. Födisch, A. Ihring, E. Kessler, J. Lerchner, G. Wolf, J.M. Köhler, M. Nietzsch, M. Krügel. "Highly sensitive thermopile heat power sensor for micro-fluid calorimetry of biochemical processes." *Sensors and Actuators A – Physical* 123-124: 354 (2005).

77. I. Wadsö. "Isothermal microcalorimetry in applied biology." *Thermochimica Acta* 394: 305 (2002).

78. K. Verhaegen, K. Baert, J. Simaels, W. Van Driessche. "A high-throughput silicon microphysiometer." *Sensors and Actuators A – Physical* 82: 186 (2000).

79. Vivactis. "MiDiCal-II brochure." www.vivactis.com (2006).

80. K. Verhaegen. WO0185901 (2001).

81. D.D. Pollock. "Thermoelectricity: Theory, Thermometry, Tool." ASTM (1985).

82. J. Schieferdecker, R. Quad, E. Holzenkämpfer, M. Schulze. "Infrared thermopile sensors with high sensitivity and very low temperature coefficient." *Sensors and Actuators A – Physical* 46-47: 422 (1995).

83. S. van Herwaarden. "Nanocalorimeters." www.xensor.nl (2006).

84. A. Schaufelbühl, N. Schneeberger, U. Munch, M. Waeliti, O. Paul, O. Brand, H. Baltes, C. Menolofi, Q.T. Huang, E. Doering, M. Loefe. "Uncooled low-cost thermal imager based on micromachined CMOS integrated sensor array." *Journal of Microelectromechanical Systems* 10: 503 (2001).

85. A.W. van Herwaarden, P.M. Sarro, J.W. Gardner, P. Bataillard. "Liquid and gas micro-calorimeters for (bio)chemical measurements." *Sensors and Actuators A – Physical* 43: 24 (1994).

86. P.J. Reilly, L.G. Hepler. "Temperature measurements with positive temperature coefficient thermistors." *Journal of Chemical Education* 49: 514 (1972).

87. J.A. Lynch, J. Jordan. "Ferroelectric temperature sensors for thermometric titrations and enthalpimetric analysis." *Analytica Chimica Acta* 251: 59 (1991).

88. L.D. Bowers, P.W. Carr. "Noise measurement and the temperature resolution of negative temperature coefficient thermistors." *Thermochimica Acta* 10: 129 (1974).

89. L.D. Hansen, R.M. Hart. "The art of calorimetry." *Thermochimica Acta* 417: 257 (2004).

90. P.W. Carr, L.D. Bowers. "On the temperature resolution of thermistors." In: R.S. Porter, J.F. Johnson, eds. "Analytical Calorimetry." Vol. 3, Plenum Press (1974).

91. L.D. Bowers, P.W. Carr. "The sensitivity, linearity and temperature resolution of non-equal arm thermistor Wheatstone bridges near balance." *Thermochimica Acta* 11: 225 (1975).

92. M. Noda. "Uncooled thermal infrared sensors: recent status in microbolometers and their sensing materials." *Sensor Letters* 3: 194 (2005).

93. L. Spassov. "Piezoelectric quartz resonators as highly sensitive temperature sensors." *Sensors and Actuators A – Physical* 30: 67 (1992).

94. W.L. Smith, W.J. Spencer. "Quartz crystal thermometer for measuring temperature deviations in the $10^{-3}$ to $10^{-6}$ °C range." *Review of Scientific Instruments* 34: 268 (1963).

95. N. Miura, H. Minamoto, G. Sakai, N. Yamazoe. "New-type calorimetric gas sensor using temperature characteristics of piezoelectric quartz crystal fitted with noble metal catalyst film." *Sensors and Actuators B – Chemical* 5: 211 (1991).

96. J. He, Z. Chen, J. Lin, J. Dai. "A new low-cost high-performance quartz tuning-fork temperature sensor." *Sensor Review* 23: 134 (2003).

97. L. Spassov, E. Yossiffov, V. Georgiev, L. Vergov. "A rotated Y-cut quartz resonator with a linear temperature-frequency characteristic." *Sensors and Actuators A – Physical* 58: 185 (1997).

98. D. Hauden, S. Rousseau, G. Jaillet, R. Coquerel. "Pressure and temperature measurements with SAW sensors." In *36th Annual Frequency Control Symposium*, IEEE (1982).

99. T.G. Leblois, C.R. Tellier. "Micromachined resonant temperature sensors: theoretical and experimental results." *IEEE Transactions on Ultrasonics, Ferroelectrics, and Frequency Control* 47: 333 (2000).

100. R.J. Dinger. "The torsional tuning fork as a temperature sensor." In *36th Annual Frequency Control Symposium*, IEEE (1982).

101. V.N. Hung, T. Abe, P.N. Minh, M. Esashi. "High-frequency one-chip multichannel quartz crystal microbalance fabricated by deep RIE." *Sensors and Actuators A – Physical* 108: 91 (2003).

102. J.R. Vig, R.L. Filler, Y. Kim. "Microresonator sensor arrays." In *Proceedings of the 1995 IEEE International Frequency Control Symposium*, IEEE (1995).

103. T.W. Kenny, J.K. Reynolds, J.A. Podosek, E.C. Vote, L.M. Miller, H.K. Rockstad, W.J. Kaiser. "Micromachined infrared sensors using tunneling displacement transducers." *Review of Scientific Instruments* 67: 112 (1996).

104. J.-B. Chévrier, K. Baert, T. Slater. "An infrared pneumatic detector made by micromachining technology." *Journal of Micromechanics and Microengineering* 5: 193 (1995).

105. K. Yamashita, A. Murata, M. Okuyama. "Miniaturized infrared sensor using silicon diaphragm based on Golay cell." *Sensors and Actuators A – Physical* 66: 29 (1998).

106. S. Timoshenko, S. Woinowsky-Krieger. "Theory of Plates and Shells." McGraw-Hill (1959), p. 55.

107. M. Tabib-Azar, A. Garcia-Valenzuela. "Sensing means and sensor shells: a new method of comparative study of piezoelectric, piezoresistive, electrostatic, magnetic, and optical sensors." *Sensors and Actuators A – Physical* 48: 87 (1995).

108. T.W. Kenny. Private communication.

109. P.G.A. Madden. "Construction of a Digitally Controlled Scanning Tunneling Microscope." M.Eng. thesis, McGill University (1996).

110. W. Marczak. "Water as a standard in the measurements of speed of sound in liquids." *Journal of the Acoustical Society of America* 102: 2776 (1997).

111. W.T. Yost, J.H. Cantrell, P.W. Kushnick. "Constant frequency pulsed phase-locked-loop instrument for measurement of ultrasonic velocity." *Review of Scientific Instruments* 62: 2451 (1991).

112. G. Horváth-Szabó, H. Høiland, E. Høgseth. "An automated apparatus for ultrasound velocity measurements improving the pulse-echo-overlap method to a precision better than 0.5 ppm in liquids." *Review of Scientific Instruments* 65: 1644 (1994).

113. F. Farahi, P.A. Leilabady, J.D.C. Jones, D.A. Jackson. "Optical-fibre flammable gas sensor." *Journal of Physics E – Scientific Instruments* 20: 435 (1987).

114. S.J. Choquette, L. Locascio-Brown. "Thermal detection of enzyme-labelled antigen–antibody complexes using fiber-optic interferometry." *Sensors and Actuators B – Chemical* 22: 89 (1984).

115. S.L. Tsao, J. Wu, B.C. Yeh. "High-resolution neural temperature sensor using fiber Bragg gratings." *IEEE Journal of Quantum Electronics* 35: 1590 (1999).

116. W.B. Li, P.N. Segrè, R.W. Gammon, J.V. Sengers, M. Lamvik. "Determination of the temperature and concentration dependence of the refractive index of a liquid mixture." *Journal of Chemical Physics* 101: 5058 (1994).

117. G. Abbate, U. Bernini, E. Ragozzino, F. Somma. "The temperature dependence of the refractive index of water." *Journal of Physics D – Applied Physics* 11: 1167 (1978).

118. S.D. Woodruff, E.S. Yeung. "Refractive index and absorption detector for liquid chromatography based on Fabry-Perot interferometry." *Analytical Chemistry* 54: 1174 (1982).

119. D. Markov, D. Begari, D.J. Bornhop. "Breaking the $10^{-7}$ barrier for RI measurements in nanoliter volumes." *Analytical Chemistry* 74: 5438 (2002).

120. J.K. Gimzewski, Ch. Gerber, E. Meyer, R.R. Schlittler. "Observation of a chemical reaction using a micromechanical sensor." *Chemical Physics Letters* 217: 589 (1994).

121. J.R. Barnes, R.J. Stephenson, C.N. Woodburn, S.J. O'Shea, M.E. Welland, T. Rayment, J.K. Gimzewski, Ch. Gerber. "A femtojoule calorimeter using micromechanical sensors." *Review of Scientific Instruments* 65: 3793 (1994).

122. R. Berger, Ch. Gerber, J.K. Gimzewski, E. Meyer, H.J. Güntherodt. "Thermal analysis using a micromechanical calorimeter." *Applied Physics Letters* 69: 40 (1996).

123. J. Fritz, M.K. Baller, H.P. Lang, H. Rothuizen, P. Vettiger, E. Meyer, H.J. Güntherodt, C. Gerber, J.K. Gimzewski. "Translating biomolecular recognition into nanomechanics." *Science* 288: 316 (2000).

124. S.J. O'Shea, M.E. Welland, T.A. Brunt, A.R. Ramadan, T. Rayment. "Atomic force microscopy stress sensors for studies in liquids." *Journal of Vacuum Science & Technology B* 14: 1383 (1996).

125. V. Tabard-Cossa, M. Godin, L.Y. Beaulieu, P. Grütter. "A differential microcantilever-based system for measuring surface stress changes induced by electrochemical reactions." *Sensors and Actuators B – Chemical* 107: 233 (2005).

126. J. Lai, T. Perazzo, Z. Shi, A. Majumdar. "Optimization and performance of high-resolution micro-optomechanical thermal sensors." *Sensors and Actuators A – Physical* 58: 113 (1997).

127. H.L. Horton, ed. "Ingenious Mechanisms for Designers and Inventors." Vol. 3, Industrial Press (1951), p. 493.

128. J. Dixon. "Radiation thermometry." *Journal of Physics E – Scientific Instruments* 21: 425 (1988).

129. D.P. DeWitt, G.D. Nutter, eds. "Theory and Practice of Radiation Thermometry." John Wiley & Sons (1988).

130. A. Rogalski. "Infrared detectors: status and trends." *Progress in Quantum Electronics* 27: 59 (2003).

131. V. Batagelj, J. Bojkovski, J. Drnovek, I. Pusnik. "Automation of reading liquid-in-glass thermometers." *IEEE Transactions on Instrumentation and Measurement* 50: 1594 (2001).

132. R. Saarimaa, P. Wallin. "Electronic liquid-in-glass thermometer." *Review of Scientific Instruments* 47: 195 (1976).

133. Y. Gao, Y. Bando, Z. Liu, D. Golberg, H. Nakanishi. "Temperature measurement using a gallium-filled carbon nanotube nanothermometer." *Applied Physics Letters* 83: 2913 (2003).

134. A. Deficis. US4036060 (1977).

135. J. DeMaria. GB2040131 (1980).

136. C.R. Tilford. "Three and a half centuries later – the modern art of liquid-column manometry." *Metrologia* 30: 545 (1994).

137. G. Joly, J.M. Buisine. "Thermodilatometric measurements on small samples of liquid crystals." *Journal of Thermal Analysis* 37: 2483 (1991).

138. B.A. Grzybowski, S.T. Brittain, G.M. Whitesides. "Thermally actuated interferometric sensors based on the thermal expansion of transparent elastomeric media." *Review of Scientific Instruments* 70: 2031 (1999).

139. S.U. Pickering. "On delicate calorimetric thermometers." *Proceedings of the Physical Society of London* 8: 8 (1886).

140. S.U. Pickering. "On delicate thermometers." *Proceedings of the Physical Society of London* 8: 229 (1886).

141. C.E. Guillaume. "Traité Pratique de la Thermométrie de Précision." Gauthier-Villars et fils (1889). In French.

142. J.A. Hall, V.M. Leaver. "The design of mercury thermometers for calorimetry." *Journal of Scientific Instruments* 36: 183 (1959).

143. T.E. Mumley, C.J. Radke, M.C. Williams. "Kinetics of liquid/liquid capillary rise: I. Experimental observations." *Journal of Colloid and Interface Science* 109: 398 (1986).

144. E.B. Dussan V. "On the spreading of liquids on solid surfaces: static and dynamic contact angles." *Annual Review of Fluid Mechanics* 11: 371 (1979).

145. B.B. Sauer, T.E. Carney. "Dynamic contact angle measurements on glass fibers: influence of fiber diameter on hysteresis and contact line pinning." *Langmuir* 6: 1002 (1990).

146. E. Schäffer, P. Wong. "Contact line dynamics near the pinning threshold: a capillary rise and fall experiment." *Physical Review E* 61: 5257 (2000).

147. E.L. Decker, S. Garoff. "Using vibrational noise to probe energy barriers producing contact angle hysteresis." *Langmuir* 12: 2100 (1996).

148. Z.M. Zorin, N.V. Churaev. "Immiscible liquid-liquid displacement in thin quartz capillaries." *Advances in Colloid and Interface Science* 40: 85 (1992).

149. C.D. Rugge, R.C. Ahlert. "Contact angle hysteresis in chlorinated hydrocarbon-water mixtures." *Journal of Physical Chemistry* 97: 8776 (1993).

150. K. Stoev, E. Ramé, T. Leonhardt, S. Garoff. "The effects of thin films on the hydrodynamics near moving contact lines." *Physics of Fluids* 10: 1793 (1998).

151. C.J.H. Brenan, T.D. Doukoglou, I.W. Hunter, S. Lafontaine. "Characterization and use of a novel optical position sensor for microposition control of a linear motor." *Review of Scientific Instruments* 64: 349 (1993).

152. T. Wilson, A.R. Carlini. "Size of the detector in confocal imaging systems." *Optics Letters* 12: 227 (1987).

153. E. Lange, J. Monheim, A.L. Robinson. "The heats of dilution of aqueous solutions of zinc, cadmium and copper sulfates and sulfuric acid at 25°." *Journal of the American Chemical Society* 55: 4733 (1933).

154. J. Berger, R. Hilt, E. Husmann, S. Nooner, R. Widmer-Schnidrig, M. Zumberge. "An Optical Fiber Infrasound Sensor." www.nemre.nnsa.doe.gov (2000).

155. H.S. Carslaw, J.C. Jaeger. "Conduction of Heat in Solids." 2nd ed., Oxford University Press (1959), p. 144.

156. A.F. Mills. "Heat Transfer." 2nd ed., Prentice Hall (1999), pp. 326, 884.

157. L.D. Hansen, D.J. Eatough. "Comparison of the detection limits of microcalorimeters." *Thermochimica Acta* 70: 257 (1983).

158. L. Lampugnani, L. Meites. "Simple procedure for calibrating cells for calorimetry and related purposes; a new standard of internal consistency in measurements of temperature differences with thermistors." *Thermochimica Acta* 5: 351 (1973).

159. C. Festa. "Thermostat with ±0.5 μK monitoring sensitivity." *Journal of Physics E – Scientific Instruments* 16: 683 (1983).

160. Z. Priel. "Thermostat with a stability of ±3.5 μK." *Journal of Physics E – Scientific Instruments* 11: 27 (1978).

161. R.F. Berg, G.A. Zimmerli, M.R. Moldover. "Measurement of microkelvin temperature differences in a critical-point thermostat." *International Journal of Thermophysics* 19: 481 (1998).

162. D.T. Jacobs, S.M.Y. Lau, A. Mukherjee, C.A. Williams. "Measuring turbidity in a near-critical, liquid-liquid system: a precise, automated experiment." *International Journal of Thermophysics* 20: 877 (1999).

163. I.W. Hunter, private communication.

164. T. Thorsen, S.J. Maerkl, S.R. Quake. "Microfluidic large-scale integration." *Science* 298: 580 (2002).

165. W.D. Garrett. "Retardation of water drop evaporation with monomolecular surface films." *Journal of the Atmospheric Sciences* 28: 816 (1971).

166. H.J. Tiziani, H.-M. Uhde. "Three-dimensional analysis by a microlens-array confocal arrangement." *Applied Optics* 33: 567 (1994).

167. C. Quan, S.H. Wang, C.J. Tay, I. Reading, Z.P. Fang. "Integrated optical inspection on surface geometry and refractive index distribution of a microlens array." *Optics Communications* 225: 223 (2003).

168. R. Smythe, R. Moore. "Instantaneous phase measuring interferometry." *Optical Engineering* 23: 361 (1984).

169. [156], p. 181.